Regulation of T follicular helper cells in the germinal center reaction of chronic graft-versus-host disease

A DISSERTATION
SUBMITTED TO THE FACULTY OF THE
UNIVERSITY OF MINNESOTA
BY

Stephanie Youngki Rhee

IN PARTIAL FULFILLMENT OF THE REQUIREMENTS
FOR THE DEGREE OF DOCTOR OF PHILOSOPHY

Bruce Blazar, M.D.

MAY 2022

Acknowledgements

To Bruce Blazar and colleagues within the Blazar lab, thank you for providing me with the resources to nurture all my projects. My experiences in this lab have taught me invaluable lessons, both about science and the human condition.

To the MSTP and its leadership, I am indebted to you and the MD/PhD program for this opportunity to chase after the physician-scientist-shaped castle in the sky. Thank you for your kindness and support, especially when I stray too close to the sun.

To friends and family who have loved and supported me along the way, this still-incomplete person would be much less whole without you. My gratitude doesn't feel like enough, but when we give one another everything, it's an even trade and each gains all.

Turner, my love for you and the life that we share together is beyond words. Your endless love sustains my forward momentum, and every day is an intrepid adventure into a boundless unknown with you.

Dedication

Ultimately, the dedication of this inelegant elegy is to you, the reader. This is my tribute to the inviolable infinite thing.

Abstract

Chronic graft-versus-host disease (GVHD) is a major complication following allogeneic hematopoietic stem cell transplantation, leading to significant long-term morbidity, mortality, and diminished quality of life. Though improvements in transplantation practices have led to the reduction in the incidence of acute GVHD, the occurrence of chronic GVHD remains unaffected, and additional therapeutic approaches must be investigated to address this unique pathophysiology. The germinal center reaction that produces pathogenic immunoglobulin is a significant contributor to chronic GVHD pathology and we therefore look to regulate the factors that support versus suppress the germinal center reaction in order to treat chronic GVHD. In this work, we explore the modulation of metabolic and co-inhibitory pathways to achieve this end.

Our studies identify a temporal shift in the metabolic pathways used by the T follicular helper cells that support germinal center B cell activity, from initial dependence on glycolysis to later substantial utilization of mitochondrial respiration. This discovery informs future immunometabolic methods to control the germinal center response and validates the use of pharmaceutical agents inhibiting mitochondrial pyruvate transport for the alleviation of chronic GVHD. Our studies also establish PD-1 pathway support for the germinal center reaction, and identify the ITIM, but not ITSM, PD-1 signaling motif as necessary for T follicular helper cell function in assisting B cell-mediated immune responses. We also find that blockade of the PD-1 axis through monoclonal antibody administration or nonfunctional mutation in ITIM results in T follicular helper cells adopting suppressive T follicular regulatory cell characteristics and leads to the attenuation of chronic GVHD. Collectively, this research provides new insights into the biology of the germinal center reaction that enables T cell-dependent humoral immunity and identifies new potential therapeutic means for the treatment of chronic GVHD.

Table of Contents

Abbreviations

ACC1	Acetyl-CoA carboxylase I
AM	Affinity maturation
APC	Antigen presenting cell
aHSCT	Allogeneic hematopoietic stem cell transplantation
ATP	Adenosine triphosphate
BAFF	B cell activating factor
Bcl	B cell lymphoma
BCR	B cell receptor
Blimp-1	B lymphocyte-induced maturation protein-1
BM	Bone marrow
BMT	Bone marrow transplantation
BO	Bronchiolitis obliterans
Breg	B regulatory cell
CCL	Chemokine (C-C motif) ligand
CCR	CC chemokine receptor
CD	Cluster of differentiation
CDR	Complementarity determining region
CSR	Class switch recombination
CTLA-4	Cytotoxic T lymphocyte associated protein 4
CXCL	Chemokine (C-X-C motif) ligand
CXCR	CXC chemokine receptor
Cy	Cyclophosphamide
DAMP	Damage associated molecular pattern
DC	Dendritic cell
DZ	Dark zone
FA	Fatty acid
FAO	Fatty acid oxidation
FDA	Food and Drug Administration
Foxp3	Forkhead box P3
FDC	Follicular dendritic cell
GC	Germinal center
GC B	Germinal center B cell
GITR	Glucocorticoid-induced tumor necrosis factor receptor-related protein

GLUT	Glucose transporter
GSEA	Gene set enrichment analysis
GVHD	Graft versus host disease
GVL	Graft versus leukemia
HSC	Hematopoietic stem cell
HVR	Hypervariable region
ICOS	Inducible T cell costimulator
IFN	Interferon
Ig	Immunoglobulin
IL	Interleukin
ITIM	Immunoreceptor tyrosine-based inhibitory motif
ITSM	Immunoreceptor tyrosine-based switch motif
Klf2	Kruppel-like factor 2
KO	Knockout, -/-
LZ	Light zone
mAb	Monoclonal antibody
MFI	Mean fluorescence intensity
MHC	Major histocompatibility antigen
MiHA	Minor histocompatibility antigen
MCT	Monocarboxylate transporter
MPC	Mitochondrial pyruvate carrier
NF-κB	Nuclear factor kappa B
NP-OVA	4-hydroxy-3-nitrophenylacetyl hapten conjugated to ovalbumin
OXPHOS	Oxidative phosphorylation
PAMP	Pathogen associated molecular pattern
PC	Plasma cell
PDGF	Platelet derived growth factor
PD-1	Programmed cell death protein 1
PD-L	PD-1 ligand
PI3K	Phosphoinositide-3 kinase
PFT	Pulmonary function test
PNA	Peanut agglutinin
RNA	Ribonucleic acid
SH2	Src homology 2
SHM	Somatic hypermutation

SHP-1	Src homology region 2 domain-containing phosphatase-1
SHP-2	Src homology region 2 domain-containing phosphatase-2
SLE	Systemic lupus erythematosus
SLO	Secondary lymphoid organ
STAT	Signal transducer and activator of transcription
TBI	Total body irradiation
TCA	Tricarboxylic acid
Tcon	T conventional cell
TCR	T cell receptor
TEC	Thymic epithelial cells
Teff	T effector cell
TFH	T follicular helper cell
TFR	T follicular regulatory cell
TH17	Type 17 helper T cell
TIGIT	T cell immunoreceptor with Ig and ITIM domains
TIM-3	T cell immunoglobulin and mucin domain-containing protein 3
Treg	T regulatory cell
Tg	Transgenic
TGF	Transforming growth factor
TNF	Tumor necrosis factor
WT	Wild type

List of Figures

Chapter I

Chapter II

Chapter III

List of Tables

Chapter I: General Introduction

Allogeneic hematopoietic stem cell transplantation

As a scientific discipline, immunology is relatively young. Put in perspective, the foundations of innate and adaptive immunity were only established at the end of the 19th century, one hundred years after the invention of the electric battery. However, the field's rapid and continual expansion has created a deep and detailed sandbox system in which to explore, and humankind's predilection to tinker and transform has kept pace. Of these developments, allogeneic hematopoietic stem cell transplantation (aHSCT) has been especially impactful.

HSCT is a powerful and potentially curative treatment for a wide range of different pathologies, including hematologic malignancies and disorders, immunodeficiencies, and heritable metabolic storage diseases. Furthermore, for a number of these pathologies, disease progression or lack of alternative therapies can mean that HSCT may be the only treatment option available to patients. In this procedure, patients undergo a myeloablative conditioning regimen, commonly radio- and/or chemotherapy, to deplete their own hematopoietic stem cells (HSC) and receive a stem cell infusion from a major histocompatibility (MHC), or human leukocyte antigen (HLA), matched donor. The engrafted donor stem cells then repopulate the patient's entire hematopoietic repertoire, functionally resetting the immune system.

The first successful attempt at aHSCT in humans was performed at the University of Minnesota by Dr. Robert Good in 1968, in a procedure transplanting bone marrow donated by a healthy sibling into an infant with an immunodeficiency syndrome. More than fifty years later, aHSCT has been a curative option for many other patients since then, with over 30,000 allogeneic transplants performed worldwide each year[1]. However, despite the success of aHSCT for many patients, others can develop severe complications such as graft-versus-host disease (GVHD).

Acute graft-versus-host disease

Occurring in up to 70% of aHSCT patients, and with a fatality rate of nearly 20%, GVHD is an iatrogenic condition in which immune cells from the donor stem cell graft initiate a destructive alloreactive response against host tissues[2,3]. The two main clinical presentations of GVHD, acute GVHD (aGVHD) and chronic GVHD (cGVHD), result from the presence of mature T cells in the donor graft, which can become activated upon recognition of recipient antigen, principally MHC or minor histocompatibility antigen (MiHa) molecules, as foreign. This etiology underscores the criticality of MHC matching for aHSCT, as MHC mismatch is one of the most significant and consistently reported risk factors for the development of GVHD[4]. Other meaningful risk factors include the degree of injury sustained by host tissues during pre-HSCT conditioning, which releases inflammatory signals such as damage-associated molecular patterns (DAMPs) and pathogen-associated molecular patterns (PAMPs) that prime innate immune cells toward activation.

In aHSCT, donor immune cells are introduced to an already highly inflammatory environment after pre-transplant conditioning and can become activated via direct allorecognition[5,6], recognition by alloreactive donor T cells against MHC on recipient antigen presenting cells (APC), or via indirect allorecognition[7–9], recognition by alloreactive donor T cells against recipient MHC-derived peptides presented by donor APCs. Now indoctrinated against recipient antigen, these alloreactive T cells migrate to GVHD target tissues, re-encounter cognate antigens, and rapidly proliferate and produce inflammatory cytokines that activate innate immune cells and mediate further injury. The resulting damage to host tissues potentiates additional release of inflammatory factors, amplifying alloreactive T cell response with the continual delivery of signals 1, 2 and 3 required for T cell activation, and perpetuates tissue damage in an aggressive positive feedback cycle.

Chronic graft-versus-host disease

Because the pathology of aGVHD is relatively well understood, improvements in donor selection, MHC matching, and reduced intensity conditioning protocols have resulted in a significant reduction in the incidence of aGVHD[10]. However, the incidence of cGVHD has increased in recent years[2,11]. While aGVHD is characterized by severe inflammatory disease fueled by unchecked T cell activation and cytokine production, cGVHD is characterized by the addition of fibrotic features and is based in a more complex pathophysiology. The initiation of cGVHD is still rooted in early inflammation caused by tissue injury and is dependent upon dysregulated alloreactive T cell response, but the observation of autoimmune attributes in the presentation of cGVHD suggests more extensive defects in immune regulation (**Figure 1**).

An established conceptual model of cGVHD divides pathogenesis into three phases[12]. In the first phase, soluble inflammatory elements released by tissue damage sustained during pre-transplant conditioning or aGVHD lead to the upregulation of costimulatory molecules and increased antigen presentation by APCs. In the next phase, these activated APCs shape the adaptive immune response, activating allo- and autoreactive B and T cells, which expand and differentiate into effector populations. Of note, levels of B cell activating factor (BAFF) are significantly increased in the setting of aHSCT and cGVHD[13,14], and promote the survival of B cells with heightened B cell receptor (BCR) responsiveness[15–18]. In addition to functioning as APCs[19], these autoreactive B cells can form germinal centers in secondary lymphoid organs with the support of T follicular helper (TFH) cells, resulting in the generation of long-lived plasma cells (PC) that produce autoantibody[20,21]. Pathogenic allo- and autoantibody deposition in the thymus[22] augments sustained thymic injury from pre-transplant conditioning or aGVHD, and this damage results in the failure to maintain central tolerance. Loss of cortical and medullary thymic epithelial cells (TEC) leads to deficiencies in positive and

negative selection, allowing for the release of potentially pathogenic and autoreactive T cells that have escaped tolerization or deletion[23,24]. Moreover, autoreactive cells also fail to be controlled by peripheral mechanisms; impaired display of tissue-restricted self-antigen in secondary lymphoid organs[25,26] combined with a reduction in the generation and survival of regulatory cell populations, including regulatory T cells (Treg)[27–29] and regulatory B cells (Breg)[30–32] inhibits the efficacy of peripheral tolerance. A chronic inflammatory state is further perpetuated by the secretion of interleukin-17A (IL-17A) by polarized type 17 helper T cells (Th17)[33].

The final phase of cGVHD is characterized by aberrant tissue repair. Transforming growth factor (TGF)-β and platelet-derived growth factor (PDGF)-α secreted by activated macrophages leads to the activation of fibroblasts, which increase the production of extracellular matrix components, including collagen and biglycan, leading to tissue sclerosis[34]. The production of allo- and autoantibodies by PC, while further aiding in the induction of macrophage activation[35], additionally leads to pathogenic immunoglobulin (Ig) deposition throughout tissues, contributing to systemic damage and fibrosis[36,20,22]. Altogether, these events coalesce into a clinical picture that covers a wide spectrum, though typical pathology includes sclerotic or fibrotic manifestations, usually observed throughout the skin, mouth, eyes, gastrointestinal tract, liver, lungs, genital tract, and fasciae or joints[37,12].

Standard first-line therapy for cGVHD is broad immunosuppression with corticosteroids. However, patient response can be variable and graft-versus-leukemia effects are diminished, indicating a need for more targeted therapies. Excitingly, pre-clinical and clinical research efforts have recently yielded the addition of three other FDA-approved agents for cGVHD: ibrutinib, targeting Bruton's tyrosine kinase (BTK) and interleukin-2-inducible T-cell kinase (ITK), was approved in August 2017[38]; belumosudil, targeting Rho-associated coiled-coil-containing kinase 2 (ROCK2), was approved in July

2021[39]; and ruxolitinib, targeting Janus kinase 1 (JAK1) and 2 (JAK2), was approved in September 2021[40]. The sanctioning of these therapies provides recognition for the struggles and endurance of past cGVHD patients, hopeful possibilities for current and future cGVHD patients, and validation for the hard work of many researchers and clinicians. The work described here aspires to continue in this same spirit.

Preclinical modeling of cGVHD

As cGVHD has emerged as the primary cause of morbidity and mortality following aHSCT, better preclinical models are needed to advance our incomplete understanding of disease pathogenesis in the search for new therapeutics. Commonly used murine models of cGVHD are generally categorized by recapitulated phenotypes and their underlying immune mechanisms: the sclerodermatous models driven by fibrotic mechanisms; and the bronchiolitis obliterans (BO) model driven by germinal center responses.

In the scleroderma models of cGVHD, donor and recipient mice are normally MHC matched but MiHa mismatched, similar to cGVHD in human patients in the majority of clinical contexts[41]. Recipients are conditioned with lethal doses of irradiation, and graft compartments include high dose T cell-depleted bone marrow and high dose whole spleens. Donor-derived T cells and macrophages are activated by tissue damage after irradiation and release inflammatory cytokines that propagate injury. These models faithfully reproduce the cutaneous sclerodermatous symptoms observed in 7-15%[42–44] of human patients, which are generally refractive to therapy. However, the reproduction of clinical disease ends there, falling short of the multi-organ involvement that is typical of cGVHD.

Comparatively, the hallmark of the BO model is the development of systemic disease that involves the spleen, colon, liver, lung, thymus and tongue[45]. In this model, where donor and recipient mice are mismatched for MHCI, MHCII and MiHa, clinically relevant pre-transplant conditioning procedures are incorporated, with the administration of cyclophosphamide and sublethal irradiation before transplant with T cell-depleted bone marrow and purified splenic T cells (**Figure 2**). Significant among the wide spectrum of clinically observed manifestations of disease in the BO model is the development of bronchiolitis obliterans in the lungs, which is pathognomonic for cGVHD

in human patients. Histologically, lungs of BO cGVHD mice display peribronchiolar and perivascular cuffing, and infiltration of the airway epithelium, in addition to increased collagen deposition around non-obliterated bronchioles, similar to human pathology. The loss of pulmonary function in this model is mediated by donor T cells and B cells, which cooperate in the germinal center reaction to produce antibody that deposits in affected tissues. Preclinical work in this model was instrumental in laying the groundwork for the FDA approval of both ibrutinib and belumosudil in cGVHD[46,47]. The following work also utilizes the BO model to illuminate cGVHD biology and investigate additional therapeutic approaches.

Germinal center reaction

Germinal centers (GC) are transient, highly dynamic specialized structures that form within secondary lymphoid organs (SLO) during the T cell-dependent humoral immune response (**Figure 3**). Antigens enter the SLO from the blood and collect in the T cell areas, where naïve T cells expressing chemokine receptor CCR7 localize to the vicinity of stromal cells and dendritic cells (DC) producing the CCR7 ligands CCL19 and CCL21, and in the B cell follicles, where naïve B cells expressing chemokine receptor CXCR5 localize to the vicinity of stromal cells and follicular dendritic cells (FDC) producing the CXCR5 ligand CXCL13. B cells that encounter and bind cognate antigen presented on FDC or macrophages become activated and upregulate expression of CCR7 and migrate toward the T cell area. Meanwhile, T cells activated by antigen-presenting DC upregulate expression of CXCR5 and migrate toward the B cell follicle. At the follicular border, these antigen-experienced B and T cells that have been activated during the same immune response come in contact and interact with each other. In this encounter, B cells internalize and process the cognate antigen bound by their B cell receptor (BCR) and present MHCII-bound antigen to T cells. If the T cell receptor (TCR) is also specific for the antigen, this linked recognition induces the T cell to deliver pro-survival signals to the B cell, and together they coordinate the GC reaction.

The basis for the production of high affinity and class switched antibody, the GC reaction is organized across distinct compartments within the lymphoid follicle. A perimeter of resting B cells forms the mantle zone around two areas of activated B cells: the dark zone (DZ) and the light zone (LZ). The DZ is densely packed with rapidly proliferating B cells, called centroblasts, expressing CXCR4 and CXCR5. These centroblasts undergo somatic hypermutation (SHM), which introduces single nucleotide substitutions into the hypervariable regions (HVR) of the immunoglobulin (Ig) genes that alter antigen-binding ability. As the centroblasts become less proliferative and enter the

growth phase of the cell cycle, they increase expression of surface Ig and decrease expression of CXCR4. However, the centroblasts still maintain expression of CXCR5, which draws them toward stromal cells producing CXCL13 within the LZ, where they are termed centrocytes.

The LZ contains a network of FDC and T follicular helper cells (TFH), in addition to the CXCR4- centrocytes. Antigen-containing immune complexes bound to the FDCs are captured by the centrocytes, which process and present the antigen on MHCII to nearby TFH. If the TCR of the TFH are able to recognize the antigen:MHCII complex, the TFH continue to provide pro-survival signals to the centrocytes. CD40L expressed on the TFH binds to CD40 on the centrocyte, activating the non-canonical NF-κB pathway and inducing expression of anti-apoptotic molecules. TFH production of the cytokine interleukin (IL)-21 activates STAT3 signaling in centrocytes, enhancing their cellular proliferation and differentiation. Centrocytes with higher antigen-binding affinity as a result of SHM are able to take up more antigen and consequently receive more survival signals from the TFH. These successful centrocytes will re-express CXCR4 and become centroblasts drawn back into the DZ where stromal cells express the CXCR4 ligand CXCL12, while less successful centrocytes that fail to sufficiently engage TFH will become apoptotic.

By this process of migration and cyclic reentry between the DZ and LZ, B cells undergo iterative rounds of mutation and selection in a process called affinity maturation (AM) to select for the survival of GC B cells (GC B) with the highest affinity for specific antigen[48,49]. Additionally, exposure to different TFH-produced cytokines during the GC reaction regulates the isotype of Ig produced by GC B, determining the effector function of the antibodies. In comparison to SHM which affects only the complementarity-determining regions (CDR) of Ig, this process of class switch recombination (CSR) affects only the heavy chain constant regions of the Ig. In CSR, cytokines activate

promoters upstream of switch regions, which themselves are upstream of corresponding constant regions, and initiate deletional recombination across double strand breaks that results in the irreversible excision of the intervening constant regions. IL-4 promotes class switching to IgG1 and IgE; IL-5 promotes class switching to IgA; interferon (IFN)-γ promotes class switching to IgG2a and IgG3; transforming growth factor (TGF)-β promotes class switching to IgG2b and IgA; IL-21 promotes class switching to IgG1 and IgG3. GC B cells that endure through the GC reaction eventually exit the LZ and differentiate into memory B cells or into long-lived antibody-secreting plasma cells (PC).

While GC B are clearly dependent upon TFH support in the GC reaction, it is important to acknowledge the reciprocal nature of their relationship, as TFH depend on GC B in return[50,51]. After the initial priming by DC in the T cell areas of SLO, CD4+ T cells begin to upregulate expression of the lineage-defining transcriptional repressor B cell lymphoma 6 (Bcl6)[52,53], which facilitates the expression of CXCR5 and allows the differentiating TFH to move to the follicular T cell:B cell border. At this interface, interaction between inducible T cell co-stimulator (ICOS) ligand on B cells and ICOS on T cells is necessary for full determination of TFH maturation[54–57]. B cell-dependent ICOS signaling induces a second wave of Bcl6 expression that is required for the follicular T cell program[55,58–60], and inhibits the transcription factors Blimp-1[61,62] and Klf2[63,64], both of which negatively regulate maintenance of the TFH phenotype. Bcl6 further promotes the expression of CXCR5[58,65] in GC-resident TFH and antagonizes alternative T cell effector fates[66,67], though TFH are still capable of acquiring attributes of other effector subsets to generate cytokine-skewed immune responses[50,68,69].

While T follicular regulatory (TFR) cells share expression of CXCR5, ICOS, PD-1 and Bcl6 with TFH, they also express the canonical transcription factor of T regulatory (Treg) cells, Foxp3, and act to negatively regulate the GC reaction[70–72]. In limited circumstances, TFR cells may emerge from peripheral (pTreg)[73,74] or naïve CD4+ T

cells[75], but the far greater majority derive from thymic Treg (tTreg) precursors[70,76]. Similarly to TFH, TFR require contact cues from DC within the SLO as well as from B cells within the follicle[77]. Co-stimulatory signaling from CD28[78] and ICOS[79,80], as well as balanced expression of the transcription factors Bcl6[70,74,81] and Blimp-1[82], which normally act as reciprocal repressors[61], are also necessary for differentiation into TFR. This multi-stage pattern of development allows TFR to assume a dedicated suppressive program that is specific for the regulation of B cell responses, as Treg are unable to suppress B cell class switching to the same extent[83]. Though the exact mechanisms by which TFR exert their suppressive functions are largely unknown, TFR expression of cytotoxic T lymphocyte associated protein (CTLA)-4[84,85] and TGF-β[86] have been acknowledged to contribute to inhibition of GC responses, and TFR immunoregulatory activities are noted to affect both TFH and GC B, inhibiting TFH proliferation and production of IL-21 and IL-4, as well as repressing GC B metabolic activity, CSR, SHM, and antibody secretion[83,84,87,88].

PD-1 signaling in T cells

Programmed cell death protein 1 (PD-1), encoded by the *Pdcd1* gene[89], is a cell surface receptor expressed on a variety of hematopoietic cells in the immune periphery, including T, B, natural killer (NK) and myeloid cells[90,91] (**Figure 4**). PD-1 interacts with its known ligands, PD-L1, broadly expressed on a wide variety of professional APCs and non-hematopoietic cells, and PD-L2, primarily inducibly expressed on professional APCs[92]. In T cells, PD-1 is upregulated upon T cell receptor (TCR) activation and expression remains elevated in the setting of continual antigen stimulation[93].

The structure of PD-1 is composed of an IgV-like extracellular domain, a transmembrane domain, and a cytoplasmic tail with an immunoreceptor inhibitory motif (ITIM) and an immunoreceptor switch motif (ITSM)[92,94,95]. The more distal C-terminal ITSM motif and the more proximal N-terminal ITIM motif each contain a single tyrosine residue that can be phosphorylated following PD-1 engagement[96–98]. The identity of the kinase or possibly kinases involved in these phosphorylation events have not yet been ascertained, though Lck has been proposed as a potential candidate[99].

The phosphorylated tyrosine residues on ITSM and ITIM are then able to bind to the Src homology 2 (SH2) domains of Src homology region 2 domain-containing phosphatase-2 (SHP-2)[100–102], and recent structural characterization of SHP-2 activity in vitro has indicated that full activation of SHP-2 requires both ITSM and ITIM[103], with ITSM binding enabling SHP-2 recruitment to PD-1, and ITIM binding freeing the catalytic pocket of SHP-2[104]. Other recent in vivo studies have also identified an alternative manner of SHP-2 activation by way of PD-1 dimerization, formed by SHP-2 interaction with two phosphorylated ITSM tyrosine residues on two adjacent PD-1 molecules[105]. While current evidence suggests that the ITSM, rather than ITIM, motif is primarily responsible for the inhibitory effects of PD-1 on T cell proliferation and IL-2 production[97,106], as well as the PD-1-mediated inhibition of phosphoinositide-3-kinase

(PI3K)/Akt signaling[107], different means of SHP-2 activation may result in different activity by SHP-2, or another yet unidentified protein, that alters the intricate interplay between signalosomes.

Interestingly, though ITSM preferentially binds to the SHP-2 tyrosine phosphatase[108,109,99,110,111], it is also able to bind to the structurally related Src homology region 2 domain-containing phosphatase-1 (SHP-1)[97,111,112], which is more than an order of magnitude more abundant than SHP-2 in Teff[113,114]. While SHP-2 is largely considered a positive regulator of T cell activation[115–118] and has been reported to be insufficient for PD-1 inhibition of T cells[119,110], conversely, SHP-1 is recognized as a negative regulator of TCR signaling and activation[120–123] and has been observed to enable PD-1 inhibitory effects in the absence of SHP-2[111]. However, SHP-1 and SHP-2 exist in an amalgam of many other molecular partners and pathways within T cells[124], including the co-stimulatory molecule CD28[99,111], and this variety of affiliations may account for the pleiotropic functions of PD-1.

Figures

Figure 1

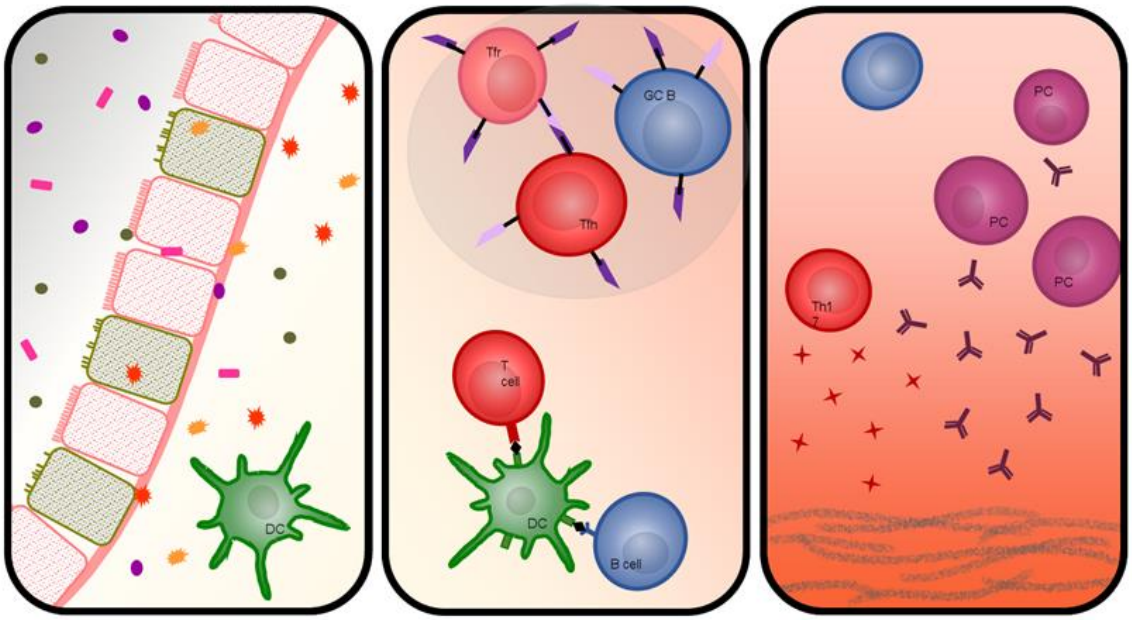

Figure 1. Model of cGVHD pathophysiology

Conceptual model of chronic GVHD pathophysiology, divided into three phases. Release of damage-associated and pathogen-associated molecular patterns activate antigen presenting cells during pre-conditioning or acute GVHD. Activated antigen-presenting cells prime the adaptive immune system, activating T and B cells that expand and polarize into effector populations. Activated fibroblasts secrete extracellular matrix, resulting in organ damage and tissue fibrosis.

Figure 2

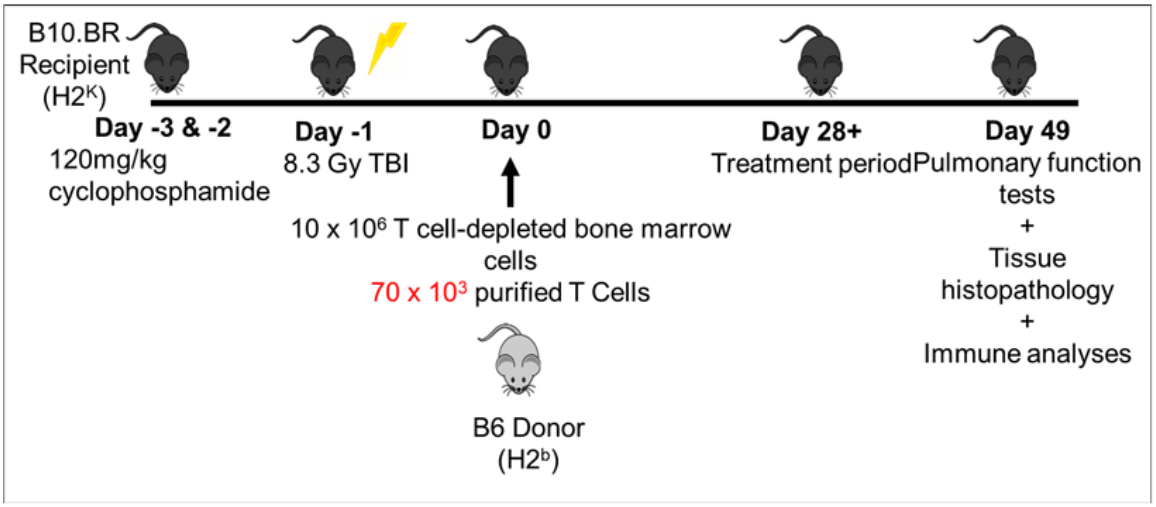

Figure 2. Bronchiolitis obliterans murine model of cGVHD

Transplantation schema of bronchiolitis obliterans chronic GVHD murine model. B10.BR (H2k) recipients receive a conditioning regimen consisting of 120 mg/kg cyclophosphamide on days -3 and -2, and 830 Gy total body irradiation on day -1 before transplantation. On day 0, mice intravenously receive donor graft composed of $1.0x10^6$ T cell-depleted bone marrow, with or without $7.0x10^4$ purified splenic T cells from C57/BL6 (H2b) donors. Prophylactic drug administration is given from day 0-day 28; therapeutic drug administration is given from day 28 until transplant termination.

Figure 3

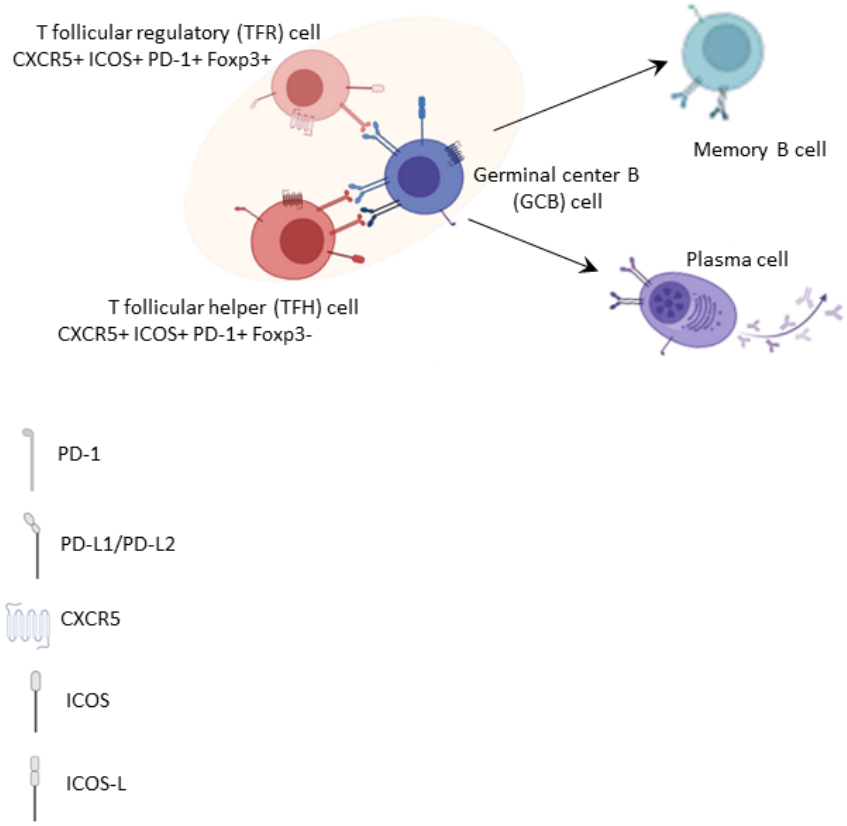

Figure 3. Germinal center reaction

Germinal center reaction enables T cell-dependent humoral immunity. T follicular helper cells provide contact and secreted signals to germinal center B cells to undergo differentiation into memory B cells or antibody-secreting plasma cells. T follicular regulatory cells inhibit this process.

Figure 4

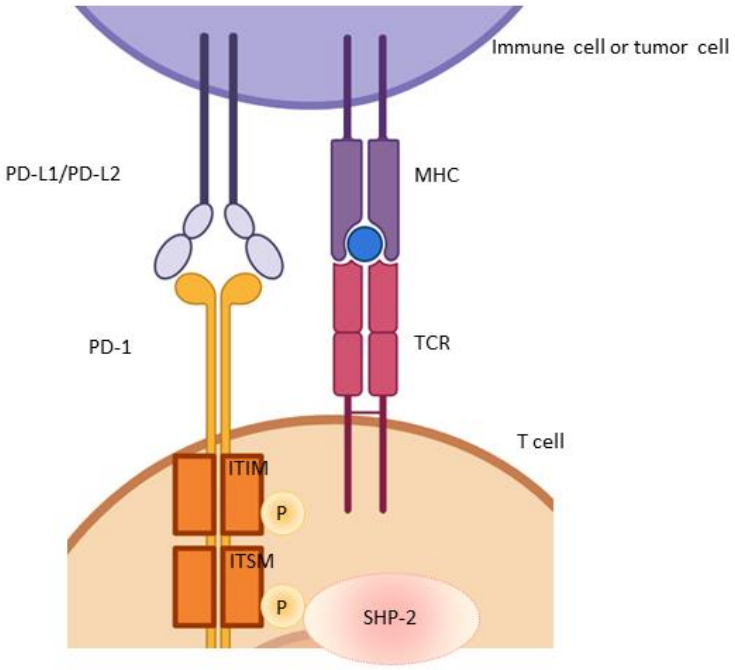

Figure 4. PD-1 pathway

PD-1 is a cell surface receptor that is expressed on a variety of hematopoietic cells, including T cells, and interacts with its known ligands PD-L1 and PD-L2, which are primarily expressed on antigen-presenting cells. In T cells, PD-1 is upregulated upon activation of the T cell receptor (TCR), and PD-1 expression remains high in the setting of continued antigen stimulation.

The structure of PD-1 is composed of an extracellular domain, a transmembrane domain, and a cytoplasmic tail with an ITIM motif and an ITSM motif, which each contain a single tyrosine residue that can be phosphorylated after PD-1 engagement with its ligand. Current understanding of the signaling mechanism of PD-1 is that the phosphatase SHP-2 is then able to bind to these phosphorylated residues and become activated to mediate downstream effects that dampen T cell activation.

Chapter II: Temporal metabolic needs of T follicular helper cells targeted by mitochondrial pyruvate carrier inhibition to treat chronic graft-versus-host disease

OVERVIEW

Chronic graft-versus-host disease (cGVHD) remains the leading cause of late morbidity and mortality following allogeneic hematopoietic stem cell transplantation (allo-HSCT). Immunometabolism has emerged as an area of active investigation in the search for potential therapeutic targets, as our understanding of interactions between metabolic processes and immune responses increases. While alloreactive T cells in the context of acute graft-versus-host disease have previously been demonstrated to preferentially utilize aerobic glycolysis over mitochondrial oxidative phosphorylation, the metabolic activity of cells that mediate cGVHD pathology are less clear.

In this study, we explored the role of glycolysis in the pathogenic germinal center populations of cGVHD and found its use by T follicular helper (TFH) cells to be temporally regulated. Mice receiving grafts comprised of donor T cells deficient in the major glucose transporter GLUT1 did not develop cGVHD, and exhibited minimal germinal center formation, comparable to negative disease control. However, therapeutic administration of 2-deoxyglucose, a non-metabolizable analog of glucose, did not show improvement in cGVHD outcome and we hypothesized this to be due to a shift in TFH metabolic dependency throughout disease progression. Extracellular flux analysis and flow cytometry phenotyping of TFH in early vs late cGVHD showed a switch from glycolysis to oxidative phosphorylation occurring during initial symptomatic presentation. Based on these results, we then investigated the effects of 7ACC2, an inhibitor of mitochondrial pyruvate transport that reduces oxidative phosphorylation, on the germinal center reaction. 7ACC2 reduced TFH support to B cell class switching in vitro and, when tested as a therapeutic agent administered after TFH switch to oxidative phosphorylation, also resulted in the amelioration of cGVHD in vivo. In conclusion, the current work provides evidence for the role of mitochondrial respiration in TFH cells in

cGVHD and validates the importance of consideration for temporal changes in further investigations of immunometabolic therapies.

INTRODUCTION

The curative potential of allogeneic hematopoietic stem cell transplantation is limited by development of chronic graft versus host disease (cGVHD) and metabolic regulation of immune cells is a promising therapeutic target. A central component of the pathophysiology of cGVHD is the germinal center (GC) reaction, in which T follicular helper (TFH) cells aid germinal center B (GC B) cells in class switching and somatic hypermutation, and results in the production of alloreactive class-switched antibodies that attack host tissues, leading to multi-organ damage and tissue fibrosis. In this study, we attempt to metabolically regulate TFH cells to limit cGVHD pathogenesis.

Different T cell subsets have been found to demonstrate different metabolic signatures, dependent upon the context of their activation. Naïve T cells maintain a metabolically quiescent state, minimally engaging in nutrient uptake and predominantly using oxidative phosphorylation as the primary means of energy production[125,126]. Upon antigen encounter, T cell receptor signaling promotes metabolic reprogramming, as metabolic activity must increase to meet increased cellular needs[127–130]. To do this, T effector cells are widely understood to preferentially use glycolysis[131–136], in which glucose is metabolized, producing a net gain in adenosine triphosphate (ATP), and yields pyruvate, which can then enter the tricarboxylic acid (TCA) cycle to generate intermediate metabolites and electron carriers that fuel oxidative phosphorylation. However, context of this metabolic activity still matters[137]. Th1 cells rely on glycolysis and glutaminolysis in order to support proliferation and function[138–140], yet pathogenicity by inflammatory IFNγ cytokine production has been found to be dependent on fatty acid metabolism in the setting of autoimmune encephalomyelitis[141]. In models of cancer and in clinical studies, amino acids such as arginine, serine and tryptophan have been found to be critical for anti-tumor effector T cell responses[142–146]. Single chain fatty acids (SCFAs), while typically associated with immunosuppressive activity and regulatory T

cells, have been found to amplify Th2 cytokine secretion[147], and blockade of lipid metabolism has been found to reduce Th2 production of IL-5 and IL-13 in airway allergy models[148]. All of this is to say that there is still much to study to improve our understanding of the metabolism of immune cells in executing cell-specific functions in different environmental circumstances.

TFH cells are specialized CD4+ helper T cells that provide essential assistance to GC B cells through co-stimulation via CD154/CD40 ligand binding and the secretion of GC-supporting cytokines such as IL-21 and IL-4[50,149]. The germinal center light zone, where these B:T cell interactions take place, is reported to be a hypoxic environment, which invariably affects the metabolism of resident cells. Notably, hypoxia-induced transcription factors (HIF) have been shown to enhance TFH differentiation and activity[150], and are also linked to changes in metabolic programming that result in increased aerobic glycolysis. Additional studies from colleagues have further validated this finding, showing that the differentiation of TFH cells requires the ability to utilize glycolysis[151–153]. Considering this literature, we set out to confirm a TFH metabolic profile within the context of cGVHD.

Using an in vivo cGVHD model, we found that while TFH generation may initially be dependent upon the ability of T cells to undergo glycolysis, a temporal shift in TFH metabolism toward oxidative phosphorylation rendered glycolysis a poor therapeutic target. During oxidative phosphorylation, the reduced electron carriers nicotinamide adenine dinucleotide (NADH) and flavin adenine dinucleotide ($FADH_2$), generated from upstream cellular respiration steps, transfer electrons to the electron accepting mitochondrial complexes I and II, which pass the electron down the electron transport chain, building the proton gradient across the inner mitochondrial membrane that drives ATP synthesis. The significance of this metabolic alteration toward oxidative phosphorylation is demonstrated by the therapeutic efficacy of the mitochondrial

pyruvate carrier inhibitor 7ACC2 in attenuating cGVHD. Furthermore, the observation of a decrease in TFH Bcl6 expression with 7ACC2 administration reveals new potential avenues for exploration in future efforts to discover additional metabolic targets in the germinal center populations, which all require the lineage-defining transcription factor Bcl6[59,81,61,67].

MATERIALS AND METHODS

Mice

C57BL/6 (B6; H2b) mice were purchased from the National Cancer Institute (NCI). B10.BR (H2k) mice were purchased from Jackson Laboratories. B6 *CD4*^{Cre} *GLUT1*$^{fl/fl}$ (GLUT1KO T) mice were provided courtesy of Dr. Jeffrey Rathmell. All mice used in these studies were between 8-14 weeks of age. Co-housed littermates were used as controls when applicable. All mice were maintained in specific pathogen-free facilities. All studies were conducted in accordance with University of Minnesota Institutional Animal Care Committee approval (IACUC protocol # 2103-38904A).

Immunization

For immunization experiments, 7–12-week-old female C57Bl/6 (B6; H2b) (National Cancer Institute) mice were immunized via bilateral subcutaneous inguinal injection with 100ug of NP-OVA (Biosearch Technologies) emulsified in solution with CFA (BD Bioscience). At day 7 post-immunization, draining lymph nodes were harvested for further analysis.

Bone marrow transplantation and induction of cGVHD

For bronchiolitis obliterans cGVHD transplantation experiments, 11–14-week-old female B10.BR (H2k) (Jackson Laboratory) recipients underwent pre-transplant conditioning regimen (cyclophosphamide - 120 mg/kg/day intraperitoneally at days -3, -2; total body irradiation – 8.3Gy at day -1). Transplantation grafts were composed of $1.0x10^6$ C57/BL6 T cell-depleted bone marrow cells for BM only groups (non-disease control), or $1.0x10^6$ C57/BL6 T cell-depleted bone marrow + $7.0x10^4$ T cells (C57/BL6 or, where specified, *CD4*^{Cre} *GLUT1*$^{fl/fl}$) for the induction of chronic GVHD. To generate bone marrow graft

compartment, donor bone marrow was depleted with anti-CD4 (NCI) and anti-CD8 (NCI) monoclonal antibody followed by rabbit complement (Pel-Freez Biologicals). To generate T cell graft compartment, T cells were purified from donor spleens by negative selection using biotin-labeled anti-CD19, anti-B220, anti-CD11b, anti-CD11c, anti-NK1.1, anti-γδTCR, and anti-TER119 (Miltenyi Biotec), followed by streptavidin RapidSpheres deletion with EasySep magnet (StemCell Technologies). Grafts were administered in PBS to recipient mice via intravenous administration at day 0. Prophylactic administration of pharmaceutical agents was executed between day1-day28 post-transplantation. Therapeutic administration of pharmaceutical agents was executed after day28 until terminal endpoint. Mice were monitored daily for survival and weighed twice weekly until terminal endpoint in week 8 post-transplantation.

Pharmaceutical agents

Glucose inhibitor 2-deoxy-glucose (2-DG) was given via IP at 40 mg/kg, daily, with a vehicle control of PBS, for in vivo studies[154].

Mitochondrial pyruvate carrier inhibitors 7ACC1 and 7ACC2 were given via IP at 1.0 mg/kg, daily, with a vehicle control of 5% DMSO, 45% PBS, 50% HPβCD, for in vivo studies. Dr. Venkatram Mereddy provided synthesized 7ACC1 and 7ACC2 for all studies[155].

Pulmonary function tests

Mice were anesthetized using 50 mg/kg pentobarbital, administered using intraperitoneal injection. Mice were then intubated and ventilated, and measures of pulmonary resistance, elastance and compliance were obtained using whole-body plethysmography on the Flexivent system (SCIREQ).

Antibodies and flow cytometry reagents

Anti-GLUT1 (EPR3915), anti-LDH (EP1566Y), and anti-LDH-B (60H11) antibodies were purchased from Abcam. Anti-CD4 (RM4-5), and anti-FAS (Jo2) antibodies were purchased from BD Biosciences. Anti-IgG1 (RMG1-1), anti-GITR (DTA-1), anti-IA/IE (M5/114.15.2), and anti-PD-1 (29F.1A12) antibodies were purchased from BioLegend. Anti-IgG2c (STAR135) antibody was purchased from Bio-Rad. Anti-Bcl6 (BCL-DWN), anti-CD19 (1D3), anti-CXCR5 (SPRCL5), anti-Foxp3 (FJK-16s), anti-ICOS (C398.4A), anti-GL7 (GL7), and fixable viability dye antibodies were purchased from eBioscience. 2-NBDG (2-(N-(7-nitrobenz-2-oxa-1,3-diazol-4-yl)amino)-2-deoxyglucose, CellRox and MitoSOX were purchased from Invitrogen.

Flow cytometry and analysis

Single cell suspensions of immune cells isolated from spleen or lymph nodes were generated and stained for surface markers with conjugated antibodies in FACS buffer (PBS with 2% FBS + 2mM EDTA). Intracellular staining was performed following fixation and permeabilization using the intracellular fixation and permeabilization buffer kit from eBioscience according to manufacturer instructions.

All flow cytometry was conducted on a LSRFortessa flow cytometer (BD Biosciences). Flow cytometry standards were run regularly to ensure instrument stability. All resulting FCS3.0 files were analyzed using FLowJo V10 (Tree Star).

Fluorescence-activated cell sorting

Immune cells were isolated from harvested spleen or lymph nodes and enriched for B and T lymphocytes by negative selection using biotin-labeled anti-CD11b, anti-CD11c, anti-NK1.1, anti-γδTCR, and anti-CD49b (Miltenyi Biotec), followed by streptavidin RapidSpheres deletion with EasySep magnet (StemCell Technologies). Lymphocytes

were then stained for surface markers (B cells – CD19+ CD4-; TFH cells – CD19- CD4+ CXCR5+ ICOS+ GITR-; TFR cells – CD19- CD4+ CXCR5+ ICOS+ GITR+) with conjugated antibodies in FACS buffer.

All sorting was conducted on FacsAria II (BD Biosciences) machines, maintained by the University Flow Cytometry Resource (UFCR).

Class switch assay

For in vitro assessment of B cell class switching, lymphocytes harvested from the draining lymph nodes of wildtype (WT) B6 mice were immunized with NP-OVA and enriched for B and T cells by negative selection using biotin-labeled anti-CD11b, anti-CD11c, anti-NK1.1, anti-γδTCR, and anti-CD49b (Miltenyi Biotec), followed by streptavidin RapidSpheres deletion with EasySep magnet (StemCell Technologies). CD19+ B cells, CXCR5+ ICOS+ GITR- TFH cells, and CXCR5+ ICOS+ GITR+ TFH cells were isolated via FACS. Cells were then plated at concentrations of 50,000 B cells/well, 30,000 TFH cells/well and 3,000 TFR cells/well, and co-cultured together in RPMI 1640 media (Invitrogen) supplemented with 10% FBS, 2mM L-glutamine, 10mM HEPES, 1% penicillin/streptomycin and 50 μM β-mercaptoethanol, as well as the addition of soluble 2.0 μg/mL anti-CD3 and 5 μg/mL anti-IgM. Cell cultures were maintained without media change for 6 days at 37˚C. Hypoxia studies were conducted at oxygen concentrations of 1% O2, 5% O2 and 21% O2. After 6 days of culture, supernatant was separated and analyzed for IgG concentration using ELISA, while cells were separated and analyzed for presence of CD19+ IA+/IE- GL7+ IgG+ B cells.

ELISA

IgG in culture supernatant was quantified using indirect ELISA. 96 well plates were coated overnight with 1 μg anti-mouse Ig (Rockland) per well, blocked with 1% bovine

serum albumin, and culture supernatants were added at 1:50 dilution. Total IgG was quantified using pan-IgG capture antibody (Tonbo Biosciences) and alkaline phosphatase-conjugated pan-IgG detection antibody (Tonbo Biosciences). Standard curve was generated using mouse IgG standard in the linear range of detection using a Spectramax plate reader (Molecular Devices).

Metabolism flux analysis

For functional metabolism assays, lymphocytes were harvested from spleens of transplanted mice and enriched for T cells by negative selection using biotin-labeled anti-CD19, anti-B220, anti-CD11b, anti-CD11c, anti-NK1.1, anti-γδTCR, and anti-CD49b (Miltenyi Biotec), followed by streptavidin RapidSpheres deletion with EasySep magnet (StemCell Technologies). CXCR5+ ICOS+ GITR- TFH cells were isolated via FACS, spun onto XF96 cell culture microplates (Agilent) coated with Cell-Tak (Corning), and allowed to acclimate for one hour in Seahorse XF media (modified DMEM supplemented with 25mM glucose, 2mM glutamine, and 1mM sodium pyruvate – Agilent).
Oxygen consumption rate (OCR) and extracellular acidification rate (ECAR) were measured using extracellular flux analysis on the XF-96 Extracellular Flux Analyzer system (Agilent). For OCR studies, cells were analyzed under basal conditions, and in response to 1.0 μM oligomycin (inhibition of mitochondrial complex V), 1.0 μM fluoro-carbonyl cyanide phenylhydrazone (FCCP) (collapses the proton gradient, uncoupling the gradient from the electron transport chain, resulting in the induction of maximal oxygen consumption by mitochondrial complex IV), and 2 μM rotenone (inhibition of mitochondrial complex I) + 100 nM antimycin A (inhibition of mitochondrial complex III). For ECAR studies, cells were analyzed under basal conditions, and in response to 5.5 mM glucose (induction of glycolysis), 1.0 μM oligomycin (inhibition of mitochondrial ATP

production results in maximal glycolysis), and 100 mM 2-DG (competitive inhibition of glucose hexokinase confirms ECAR changes due to glycolysis).

Statistical analysis

All statistical analyses were conducted using Prism software (version 9). Linear regression was used for analysis of class switch experiments. Figures are presented as mean ± SEM, with significance determined using unpaired two-tailed Student's t-test. Log-rank (Cox-Mantel) statistical test was used for analysis of survival curves. Significance is denoted by asterisks as follows:

* $p < 0.05$, ** $p < 0.01$, *** $p < 0.001$, **** $p < 0.0001$.

RESULTS

Pathogenic T follicular helper cells require glycolysis for development of cGVHD

To initially explore the baseline activity of the glycolytic pathway and the expression of related markers by TFH, we isolated lymphocytes from draining lymph nodes of B6 mice immunized with NP-OVA in CFA. These were then examined for expression of the major glucose transporter in T cells, GLUT1, as well as active glucose uptake, and TFH cells were found to significantly upregulate both (**Figure 1A-1C**). In contrast, the regulatory and GC-suppressing counterpart to TFH, TFR cells, were observed to have a decrease in glucose uptake (**Figure 1C**). These opening data support the field's current understanding of the metabolic needs of Teff and Treg cells, where the former largely employ glycolysis to fulfil bioenergetic needs, and the latter are more readily reliant on mitochondrial oxidative phosphorylation.

To examine the necessity of glycolysis for the generation of T follicular helper cells in germinal centers, we then repeated the immunization study in *CD4*^{Cre} *GLUT1*$^{fl/fl}$ mice, in which CD4+ T cells were deficient for GLUT1 (**Figure 1D**). As compared to T cells from WT mice, T cells from these mice that were deficient in the GLUT1 receptor, the primary transporter responsible for glucose import on T cells and essential for CD4+ T cell activation, displayed a significant reduction in the development to TFH 7 days post-immunization (**Figure 1E**). Furthermore, the effects of TFH reduction were noted in the context of TFH support to GCB. The frequency of GCB found in the draining lymph nodes of the *CD4*^{Cre} *GLUT1*$^{fl/fl}$ mice were significantly reduced (**Figure 1E**), likely due to the limited presence of supporting TFH. This data suggests that glucose metabolism is required for the full manifestation and support of TFH cells for GCB development.

Interestingly, the frequency of TFR was likewise reduced at this timepoint (**Figure 1E**). At first glance, this data appears to contradict the observations in Figure

1B, as well as the observations of other groups[156,157], which suggest reduced glycolysis utilization by Treg. However, while GLUT1 is not required for the generation and function of Treg[136,138], it is possible that maintenance of a population of follicular T cells, whether TFH or TFR, requires some degree of glycolysis within the germinal center, particularly the light zone of the germinal center where interaction with TFH induce B cell affinity maturation and which has been previously reported[150,158,159] and confirmed by this group to be a hypoxic environment (in vivo data not shown). Moreover, our preliminary data show that in vitro hypoxia favors IgG production (**Supplementary Figure 4**). In a setting of limited O2, it is plausible that T cells may elect to utilize aerobic glycolysis to generate ATP to fuel cellular activities.

For a more complete examination of glycolytic dependency by T cells in the context of cGVHD, we again used the *CD4^{Cre} GLUT1$^{fl/fl}$* mice, this time in the bronchiolitis obliterans mouse model that replicates the multi-system impacts of cGVHD. T cells were isolated from the *CD4^{Cre} GLUT1$^{fl/fl}$* mice, and, along with bone marrow from WT B6 mice, were transplanted into recipient B10.BR mice given chemotherapy and irradiation, and disease progression was monitored until the terminal endpoint of 8 weeks. Recipients given GLUT1 deficient T cells, as opposed to WT T cells, remained healthy, with no signs of characteristic cGVHD such as weight loss, skin/fur changes, or pulmonary dysfunction. Notably, pulmonary function tests of the recipient mice given GLUT1KO T cells were at the same level as that of non-disease control mice (**Figure 2A**), suggesting the failure of cGVHD to commence at all.

Additionally, splenic germinal center population frequencies in this in vivo transplantation model mirrored what was observed in the immunization results of Figure 1E. Frequency of TFH cells in the recipients of the GLUT1 deficient T cells were markedly reduced (**Figure 2E**), as was the frequency of GCB cells (**Figure 2B**). The one departure between the immunization and transplant data concerns the frequency of

TFR. While the TFR frequency decreased in immunized *CD4^{Cre} GLUT1$^{fl/fl}$* mice, no change to TFR frequency was observed in the transplant (**Figure 2D**). An explanation for this discrepancy may be that while all CD4+ cells in the immunization experiment lacked GLUT1, only the TFH cells in the transplant experiment lacked GLUT1 (**2F-G)**, which corresponds with our group's previous investigations into the origins of the follicular T cell subsets (data not shown). While TFH arise from the T cell compartment of the graft given during transplant, TFR emerge from the bone marrow. Overall, the result of transplanted GLUT1 deficient T cells results in an increase to the TFR:TFH ratio in the germinal center (**Figure 2C**), which can be considered as an on/off switch to control the germinal center reaction. These data indicate the necessity of TFH cells to utilize glycolysis for maximal germinal center response, in agreement with findings from others that glycolysis is a requirement for T cell activation and effector function[136,160], and specify the particular need of TFH to be able to undergo glycolysis during the development of cGVHD.

T follicular helper cells change metabolic needs throughout cGVHD progression

While it is helpful to confirm the requirement of T cell glycolysis in the initiation of cGVHD, we also wanted to investigate the metabolic needs of the germinal center populations throughout disease progression. Due to evidence of cGVHD bronchiolitis obliterans pulmonary symptoms and germinal center formation beginning by four weeks post transplantation (**Figure 3A, Figure 4A-B**), we next utilized metabolic flux analysis to outline a profile of TFH metabolic activity during early (day 21 post transplantation) in comparison to late (day 35 post transplantation) disease.

On each day of interest, CXCR5+ ICOS+ GITR- TFH cells were FACS sorted, and oxygen consumption rates (OCR) and extracellular acidification rates (ECAR) were measured (**Figure 3B**). Early in cGVHD, basal respiration and spare respiratory capacity

of cGVHD TFH were both found to be reduced, though not quite reaching significance, as compared to TFH from non-disease control (**Figure 3C**). This data suggests that cGVHD TFH may be less reliant upon oxidative phosphorylation during the early formation of the germinal center reaction central to cGVHD initiation. At this same time point, cGVHD TFH were also found to exhibit a significant increase in glycolytic capacity and glycolytic reserve (**Figure 3D**). These results are in line with the expectation that activated T cells upregulate glycolytic processes.

However, at day 35, after the establishment of cGVHD onset (**Figure 4B**), TFH from disease mice demonstrate a reversal in metabolic preferences. TFH from cGVHD mice exhibited a dramatic increase in basal respiration and spare respiratory capacity, indicating an upsurge in the use of oxidative phosphorylation (**Figure 4C**). Concomitantly, the cGVHD TFH also demonstrate a reduction in glycolytic capacity and reserve (**Figure 4D**). These results, though unexpected, are thought-provoking, and hint at the possibility that the metabolic needs of germinal center TFH may undergo temporal regulation.

To further investigate the degree of TFH dependency upon glycolysis during cGVHD, we tested the performance of 2-deoxyglucose (2-DG), a non-metabolizable analog of glucose, in ameliorating disease. 2-DG was administered therapeutically, after the onset of cGVHD, at a dosing schedule of 40 mg/kg, administered daily until termination of the experiment. Though it would have been reasonable to expect diminished T cell activity and disease severity with this drug, the effects of 2-DG were minimal (**Figure 5A-E**). Pulmonary dysfunction of drug-treated mice did not change, either for better or worse, and cellular frequencies of the germinal center populations also were not seen to shift. Considering our results suggesting a temporal shift in TFH metabolic dependency, it is possible that this inefficacy is in part due to the phase in

which TFH are most reliant upon glycolysis having already mostly passed by the time of 2-DG administration.

Therapeutic administration of inhibitor of mitochondrial pyruvate carrier results in alleviation of cGVHD

Due to the unimpressive results of 2-DG, we sought to find another means of alteration in TFH metabolism to target. As the final product of glycolysis is pyruvate, which can then enter into the mitochondria to participate in the TCA cycle and generate reducing equivalents for oxidative phosphorylation, which we had observed in Figure 4 to be more influential in TFH metabolic activity during the later stages of cGVHD, we decided to further investigate the importance of pyruvate.

We next explored the potential of the pharmaceutical agent 7ACC2 (**Supplementary Figure 2**), an inhibitor of the mitochondrial pyruvate carrier (MPC) protein (**Supplementary Figure 3**), to diminish TFH support of the pathological germinal center reaction that helps to drive cGVHD. WT B6 mice were immunized with NP-OVA in CFA, and B, TFH and TFR cells were isolated and purified from the draining lymph nodes and placed into co-culture with CD3 and IgM (**Figure 6A**). Soluble IgG secreted into the supernatant was quantified and found to be significantly reduced in cultures to which 7ACC2 was added (**Figure 6B**). Additionally, the frequency of class-switched B cells expressing IgG was also observed to be significantly reduced in the presence of 7ACC2 (**Figure 6C**). While one cannot negate the possibility that B cells may also be a target of 7ACC2 and subsequently unable to undergo class switching, regardless of modification to TFH activity, this finding, in light of ours (data not shown) and others' data that germinal center B cells preferentially oxidize fatty acids to meet energy demands[161], seems to indicate that it is the TFH cells in the 7ACC2-laced culture that lose functionality. Additionally, in preliminary studies (data not shown) examining in vitro

B cell class switching with the addition of CD40L and IgM to culture, 7ACC2 did not appear to have a noticeable effect upon the ability of B cells to produce IgG.

To examine the therapeutic potential of 7ACC2 in an in vivo setting, we again conducted bone marrow transplantation studies in the bronchiolitis obliterans cGVHD model, using a 7ACC2 dosing schedule of 1 mg/kg administered daily until termination of the experiment. In confirmation of the metabolic effects of 7ACC2 and in parallel with findings testing 7ACC2 in cell lines in vitro (**Supplementary Figure 1**), mitochondrial reactive oxygen species, and by proxy mitochondrial respiration, were found to be decreased in TFH from mice given 7ACC2 (**Figure 7F**). Mice receiving the 7ACC2 demonstrated a marked improvement in pulmonary function (**Figure 7A**). While the degree of statistical difference between groups is significant, even more striking is the degree of correction of pulmonary function between untreated and treated mice, nearly back down to baseline level in non-disease control. This finding was unusual, as it is highly uncommon for a therapeutically administered pharmaceutical agent in the bronchiolitis obliterans cGVHD model to nearly eliminate pulmonary dysfunction. These data show that 7ACC2 is able to drastically inhibit cGVHD pathogenesis.

In support of the pulmonary function data, the frequencies of the splenic germinal center populations in the transplanted mice parallel the findings in Figure 3C regarding the ability of 7ACC2 to impede the pathological process of cGVHD. Frequency of GCB was significantly lowered in treated mice, on par with non-disease control (**Figure 7B**). This result can be explained by the reduced frequency of TFH with 7ACC2 therapy (**Figure 7E)**. These findings are in accordance with that of the in vitro class-switching assay, wherein the TFH co-cultured with B cells in the presence of 7ACC2 were unable to provide support for production of class-switched antibody, providing further evidence for TFH dependency upon mitochondrial pyruvate transport for functionality. Also notably, the TFR frequency was not seen to change with 7ACC2 (**Figure 7D**), which was

not necessarily expected due to our understanding of regulatory T cell metabolism, which is more dependent on lipid oxidation-fueled oxidative phosphorylation[162–164]. However, though the TFR frequency was minimally impacted, the TFR:TFH ratio demonstrated a dramatic increase due to the significant reduction in TFH frequency (**Figure 7C, E**), indicating a global inhibition of the germinal center reaction with 7ACC2 treatment.

Another noted finding from these transplantation experiments was that with 7ACC2 treatment, Bcl6 expression by both TFH and TFR, was significantly decreased (**Figure 7G**). As Bcl6 is the master lineage-defining transcription factor for follicular T cells[59,81], this outcome is particularly striking as it implicates metabolic alteration in being responsible for cellular identity, and past studies have demonstrated successful elimination of cGVHD by Bcl6 inhibition[165]. Altogether, these data provide strong support for the consideration of 7ACC2 to be used as a therapeutic agent in remedying cGVHD.

DISCUSSION

The necessity of an immune cell to undergo coordinated metabolic changes to fully mount a response to stimuli is the fundamental basis for the examination of metabolic modulation in pursuit of immune modulation. Many studies have previously illustrated the requirement of glycolysis for multiple CD4+ and CD8+ T cell subsets' differentiation and activation in a number of different contexts[127,160,166–169]. However, the metabolic requirements of T follicular helper (TFH) cells within the dynamic germinal center (GC) environment are less well characterized.

Here, we attempt to establish a metabolic profile for TFH cells within the context of chronic graft-versus-host disease (cGVHD). Using an immunization model, we first demonstrate that TFH upregulate expression of their major glucose transporter GLUT1 and increase glucose uptake, and additionally show that GLUT1 deficient CD4+ T cells are unable to support the GC reaction. Then in a bronchiolitis obliterans (BO) cGVHD mouse model, we observe failure to induce cGVHD in recipients given GLUT1 deficient CD4+ T cells in the T cell graft compartment. These results indicate that T cells must use glycolysis in order to initiate development in becoming TFH, and this observation recapitulates those of past studies, which have recognized the necessity of glycolysis for TFH differentiation in other animal models of disease, including spontaneous lupus, induced lupus-like autoimmunity and rheumatoid arthritis[151,152,170–174]. Glycolysis is promoted in part by hypoxia-inducible factor 1-alpha (HIF1α), upregulated in the hypoxic environment of the germinal center, and is associated with increased TFH number and secretion of cytokines IFN-γ and IL-4[150]. In a mouse model of systemic lupus erythematosus, which is characterized by the prevalence of class-switched autoantibodies and in which disease severity typically correlates with TFH presence, inhibition of glucose was found to drastically reduce TFH frequency and number.

However, the authors found that glucose inhibition had minimal consequences to the production of T-cell dependent antibodies[152], though did describe glutaminolysis inhibition to be effective in diminishing TFH and consequent humoral response. More recently, work by another group showed that TFH expression and cell membrane localization of the chemokine receptor CXCR5, considered a defining TFH marker enabling TFH positioning within the B cell follicle[65,175,176], was directly regulated by the cytidine diphosphate (CDP)-ethanolamine pathway that contributes to posttranscriptional programming[177]. These findings that phospholipid metabolism and glutaminolysis are able to direct TFH homing and TFH support to GC B cells, respectively, highlight the importance of examining the role of other non-glycolytic metabolic activity in the context of immune cell activation and operations.

Therefore, after confirming the metabolic processes required for TFH generation, we next investigated the metabolic processes required of TFH cells during the germinal center reaction to create a metabolic profile for TFH functionality. Early in the disease course of cGVHD, during early GC formation and before initial manifestation of characteristic pulmonary dysfunction, at day 21 post-transplantation (data not shown), extracellular flux analysis revealed that, in accordance with our initial findings, TFH significantly employed glycolysis over oxidative phosphorylation. However, two weeks later at day 35 post-transplantation, when the GC reaction fully had been fully established and with clear manifestation of the pulmonary dysfunction that distinguishes bronchiolitis obliterans cGVHD, TFH were found to be far more heavily dependent upon oxidative phosphorylation.

This “switch” in metabolic utilization is important because it has implications for cGVHD therapies that are based on metabolic manipulation. While inhibiting glycolysis may work to prevent the rise of TFH cells, it may not work to alter disease course in the case of a GC B- or TFH-driven pathology where the GC reaction has already been

established. The change in TFH metabolic dependency and its repercussions to disease management were corroborated by the failed results of therapeutic administration of 2-deoxyglucose (2-DG) in the cGVHD mouse model.

2-DG is a glucose analog and can be taken up by glucose transporters, but the 2-hydroxyl group has been replaced by hydrogen, such that it is unable to be acted upon by glucose-6-phosphate-isomerase, which carries out the first committed step of glycolysis, and thus cannot be fully metabolized[178]. Not only did 2-DG in the cGVHD model have negligible effects on pulmonary function, but it also failed to affect either the frequencies of any of the germinal center populations, or the TFR:TFH ratio that determines the balance of the germinal center reaction. A possible alternative explanation for this is that T cells have been found to detect glucose deprivation via AMP-activated protein kinase (AMPK) and then upregulate expression of Bcl6 in response, which is deterministic for TFH differentiation[179]. And under conditions of reduced glucose metabolism with 2-DG treatment, it is conceivable that, despite the impact of glycolytic inhibition, a reactive increase in commitment to Bcl6-driven phenotype led to an overall minimal effect on the germinal center populations. However, Bcl6 itself has been reported to repress cellular programming that increases glycolysis[180], so our current and simpler rationale to account for these results is that the TFH cells' metabolic switch during cGVHD pathogenesis, away from glycolysis and toward oxidative phosphorylation, renders 2-DG therapy ineffectual.

While the presence of this metabolic switch was initially unexpected, additional data from the work of others has provided more supporting evidence to make this case. Other studies have demonstrated that the inhibition of glutamine metabolism, which serves not only as a precursor for amino acid and nucleotide biosynthesis, but also enables efficient energy production in T cells [139,140,181–184], diminishes TFH frequency and the GC reaction[152]. In glutaminolysis, the enzymatic action of glutaminase on glutamine

yields glutamate, which is converted to the tricarboxylic acid (TCA) cycle intermediate α-ketoglutarate[169,185]. As the purpose of the TCA cycle, at the major intersection of cellular metabolism, is to generate the reducing equivalents NADH and $FADH_2$ that carry electrons to fuel mitochondrial respiration, glutaminolysis feeds into oxidative phosphorylation. Furthermore, α-ketoglutarate itself has also been linked to GC B cell differentiation, via epigenetic remodeling of the Bcl6 locus by α-ketoglutarate-dependent histone demethylases[186]. Additionally expression of PD-1, a defining marker of TFH cells, has been reported to inhibit glycolysis and promote fatty acid oxidation[187]. We have also generated data in other experiments (shown in Chapter III) that illustrate an increase in PD-1 expression on T follicular cells with increased time during the germinal center reaction. As higher PD-1 expression by TFH follows a similar time course as the metabolic switch, this correlation may suggest a TFH-specific requirement for oxidative phosphorylation.

With the knowledge of TFH utilization of oxidative phosphorylation during the therapeutic window of cGVHD, we next set out to manipulate this mode of metabolism in TFH. To do this, we turned to a pharmaceutical agent that acts as an inhibitor of the mitochondrial pyruvate carrier (MPC), generously supplied by the Mereddy lab. 7ACC1 and 7ACC2 competitively reduce pyruvate transport across the mitochondrial membrane into the mitochondrial matrix, limiting glucose fueling of the TCA cycle and maximally efficient ATP-generating oxidative phosphorylation. However, the Mereddy lab reports that 7ACC2 (IC50 ~18nM) is far more potent than 7ACC1 (IC50 ~1nM) and so our studies focused on 7ACC2. Preliminary work by our Mereddy lab collaborators characterizing this drug demonstrates a dose-dependent decrease in oxidative phosphorylation with 7ACC2 treatment in the 4T1 cell line. We first examined the effects of 7ACC2 on TFH in an in vitro assay to evaluate GC B cell class switching. In co-cultures of B and TFH cells, introduction of 7ACC2 considerably reduced the B cell class

switching and secretion of IgG. With these results, we pinpoint TFH as the target of 7ACC2, as B cells cultured without TFH cells did not demonstrate a reduction in class switching.

The outcome of the in vitro class switching assay established the premise for attempting 7ACC2 therapy in cGVHD, since TFH support of the GC reaction is fundamental for disease development. Here, we observed 7ACC2 administration to radically reduce pulmonary dysfunction and improve cGVHD severity. 7ACC2 was also found to significantly diminish the germinal center reaction, as the frequencies of TFH and GC B were lowered to nearly that of non-disease control. While the frequency of TFR were not significantly affected, mention should be made for the purpose of discussion that there had been some anticipation that 7ACC2 might have alleviated cGVHD due to the pyruvate transport impedance resulting in increased cytosolic pyruvate and conversion to lactate[188]. Recent studies have presented data to show that not only do regulatory T cells have a survival advantage in a high lactate environment, they possess enhanced suppressive capacity as well[189,190]. However, because TFR frequency is not observed to significantly change with 7ACC2 treatment, we cannot yet identify effects on TFR as an additional mediating factor for the beneficial properties of 7ACC2 in vivo.

Moreover, examination of Bcl6 expression revealed that 7ACC2 treatment greatly decreased expression of this key transcription factor in both TFR and TFH. Bcl6 is the lineage-defining transcription factor that drives the differentiation of GC B and follicular T cells[59,81,61,67], and is critical for the development of humoral immunity[50]. While other studies have demonstrated that increased expression of Bcl6 can be compelled by an increase in oxidative phosphorylation[179,186], this study illustrates the inverse, where metabolic regulation inhibiting oxidative phosphorylation has directed the loss of the phenotype. These links between Bcl6 expression and oxidative phosphorylation, the

presence or absence of one leading to the presence or absence of the other, respectively, insinuate an intimate relationship between the two. However, because changes to pyruvate transport across the mitochondria have many widespread effects in addition to reducing oxidative phosphorylation, further investigation must be conducted. At the time of writing, the author of this study is awaiting the results of a large-scale untargeted metabolomics experiment from samples of TFH harvested from 7ACC2-treated transplantation studies. Once data returns from this experiment, a better understanding of the global effects of 7ACC2 will be revealed. With this data, and from its subsequent studies, we can hopefully acquire a more thorough understanding of the mechanisms behind the therapeutic effects of 7ACC2 in cGVHD.

Figure Legends

Figure 1. T follicular helper cells upregulate glucose transport proteins and glucose uptake during immune activation

C57/BL6 mice were immunized with NP-OVA/CFA and draining lymph nodes were harvested after 7 days. (A) CXCR5+ PD1+ Foxp3- TFH cells and CXCR5+ PD1+ Foxp3+ TFR cells were identified and (B) GLUT1 transporter expression and (C) glucose uptake was assessed by flow cytometry and found to be increased in immunized mice versus naïve controls. (D) GLUT1 deficiency on CD4+ T cells was confirmed by mean fluorescence intensity (MFI) on *CD4^{Cre} GLUT1$^{fl/fl}$* mice, which were immunized with NP-OVA//CFA and draining lymph nodes were harvested after 7 days. Germinal center populations were assessed, and (E) TFR frequency, (F) TFH frequency, and (G) GCB frequency were reduced in *CD4^{Cre} GLUT1$^{fl/fl}$* mice. Data are representative of two experiments, shown with mean ± SEM. * $p < 0.05$, ** $p < 0.01$, *** $p < 0.001$, **** $p < 0.0001$

Figure 2. T cells in donor graft during bone marrow transplantation require GLUT1 transporter for the development of cGVHD in BO mouse model

B10.BR mice were conditioned with cyclophosphamide (120 mg/kg/day, days -3 and -2) and total body irradiation (8.3Gy, day-1), and given bone marrow transplant on day 0. Recipient mice were given $1.0x10^6$ T-cell depleted bone marrow cells alone (BM only), with $7.0x10^4$ purified T cells from C57/BL6 mice (cGVHD) or *CD4^{Cre} GLUT1$^{fl/fl}$* mice (GLUT1 KO T). (A) Pulmonary function tests performed 8 weeks after transplantation show that cGVHD was either radically reduced or not induced in the mice receiving GLUT1 deficient T cells. Splenic germinal center populations were assessed, and (B) GC B cell frequency, (C) TFR:TFH ratio, (D) TFR frequency, and (E) TFH frequency all

indicate an overall inhibition of the germinal center reaction in the mice receiving GLUT1 deficient T cells. Follicular T cell populations were evaluated for expression of GLUT1, and only (F) TFH cells were found to lack GLUT1 in the mice receiving GLUT1 deficient T cells, while (G) TFR cells' expression of GLUT1 was consistent across both cGVHD and GLUT1 KO T groups. Data are representative of three experiments, shown with mean ± SEM. * $p < 0.05$, ** $p < 0.01$, *** $p < 0.001$, **** $p < 0.0001$

Figure 3. Early in cGVHD, at the onset of the germinal center reaction, T follicular helper cells preferentially utilize glycolysis

B10.BR mice were conditioned with cyclophosphamide (120 mg/kg/day, days -3 and -2) and total body irradiation (8.3Gy, day-1), and given bone marrow transplant on day 0. Recipient mice were given $1.0x10^6$ T-cell depleted bone marrow cells alone (BM only), with $7.0x10^4$ purified T cells from C57/BL6 mice (cGVHD). (A) At day 21 post-transplantation, splenic GC populations are beginning to become established. (B) At day 21, T cells from spleens were negatively enriched and (A) CXCR5+ ICOS+ GITR- TFH cells and CXCR5+ ICOS+ GITR+ TFH cells were isolated via sterile FACS for downstream Seahorse analysis. At this timepoint, (C) OCR analysis shows a decrease in oxidative phosphorylation utilization in cGVHD TFH compared to BM only. (D) ECAR analysis shows an increase in glycolytic activity in cGVHD TFH compared to BM only. Temporal bone marrow transplantation data are representative of three experiments, shown with mean ± SEM. Seahorse analysis data are representative of two experiments, shown with mean ± SEM. * $p < 0.05$, ** $p < 0.01$, *** $p < 0.001$, **** $p < 0.0001$

Figure 4. Later in cGVHD, after the establishment of pulmonary dysfunction, T follicular helper cells preferentially utilize oxidative phosphorylation

B10.BR mice were conditioned with cyclophosphamide (120 mg/kg/day, days -3 and -2) and total body irradiation (8.3Gy, day-1), and given bone marrow transplant on day 0. Recipient mice were given $1.0x10^6$ T-cell depleted bone marrow cells alone (BM only), with $7.0x10^4$ purified T cells from C57/BL6 mice (cGVHD). (A-B) At day 35 post-transplantation, splenic GC populations are all fully established, and evidence of pulmonary dysfunction in cGVHD mice can be observed. At day 35, T cells from spleens were negatively enriched and CXCR5+ ICOS+ GITR- TFH cells and CXCR5+ ICOS+ GITR+ TFH cells were isolated via sterile FACS for downstream Seahorse analysis. At this timepoint (C) OCR analysis shows an increase in oxidative phosphorylation in cGVHD TFH compared to BM only. (D) ECAR analysis shows a decrease in glycolytic activity in cGVHD TFH compared to BM only. Temporal bone marrow transplantation data are representative of three experiments, shown with mean ± SEM. Seahorse analysis data are representative of two experiments, shown with mean ± SEM. * $p < 0.05$, ** $p < 0.01$, *** $p < 0.001$, **** $p < 0.0001$

Figure 5. Therapeutic administration of competitive inhibitor of glycolysis 2-DG does not lessen cGVHD severity in BO mouse model

B10.BR mice were conditioned with cyclophosphamide (120 mg/kg/day, days -3 and -2) and total body irradiation (8.3Gy, day-1), and given bone marrow transplant on day 0. Recipient mice were given $1.0x10^6$ T-cell depleted bone marrow cells alone (BM only), with $7.0x10^4$ purified T cells from C57/BL6 mice (cGVHD). 2-deoxyglucose was administered therapeutically after day 28, at a dosing schedule of 40 mg/kg daily (2-DG). (A) Pulmonary function tests performed 8 weeks after transplantation show that cGVHD was not affected in the mice receiving 2-DG. Splenic germinal center populations were assessed, and (B) GC B cell frequency, (C) TFR:TFH ratio, (D) TFR frequency, and (E) TFH frequency all indicate a negligible effect on the germinal center reaction in mice

treated with 2-DG. Data are representative of two experiments, shown with mean ± SEM. * $p < 0.05$, ** $p < 0.01$, *** $p < 0.001$, **** $p < 0.0001$

Figure 6. Mitochondrial pyruvate carrier inhibitor 7ACC2 reduces T follicular helper cell ability to support B cell class switching in vitro

C57/BL6 mice were immunized with NP-OVA/CFA and draining lymph nodes were harvested after 7 days. B and T cells were negatively enriched and CD19+ B cells and CXCR5+ ICOS+ GITR- TFH cells were isolated via sterile FACS for downstream functional assay. (A) 50,000 B cells were plated with 30,000 TFH cells in complete media with the addition of anti-CD3 and anti-IgM and cultured without media change for 6 days at 5% O2, 37˚C. (B) Supernatant from culture was separated and analyzed via ELISA for IgG, and 7ACC2 treatment was found to significantly reduce secreted IgG concentration. (C) Cultured cells were also collected, and 7ACC2 treatment was found to significantly reduce frequency of CD19+ IA+/IE- GL7+ IgG+ B cells. Data are representative of two experiments, shown with mean ± SEM. * $p < 0.05$, ** $p < 0.01$, *** $p < 0.001$, **** $p < 0.0001$

Figure 7. Therapeutic administration of 7ACC2 lessens cGVHD severity in BO mouse model

B10.BR mice were conditioned with cyclophosphamide (120 mg/kg/day, days -3 and -2) and total body irradiation (8.3Gy, day-1), and given bone marrow transplant on day 0. Recipient mice were given $1.0x10^6$ T-cell depleted bone marrow cells alone (BM only), with $7.0x10^4$ purified T cells from C57/BL6 mice (cGVHD). 7ACC2 was administered therapeutically after day 28, at a dosing schedule of 1 mg/kg daily (7ACC2 1mg/kg). (A) Pulmonary function tests performed 7 weeks after transplantation show that cGVHD was significantly improved in the mice receiving 7ACC2. Splenic germinal center populations

were assessed, and (B) GC B cell frequency, (C) TFR:TFH ratio, (D) TFR frequency, and (E) TFH frequency all indicate a substantial decrease in the germinal center reaction in mice treated with 7ACC2. (F) MitoSOX, an indicator of mitochondrial reactive oxygen species that performs as a proxy for mitochondrial respiration, was significantly reduced on TFH and TFR with 7ACC2 administration. (G) Bcl6 expression on TFH cells was significantly suppressed in mice treated with 7ACC2. * $p < 0.05$, ** $p < 0.01$, *** $p < 0.001$, **** $p < 0.0001$

Supplementary Figure 1. 7ACC2 inhibits oxidative phosphorylation in a dose-dependent manner

(A) ATP rate assay indicates 4T1 cell line exhibits preferential oxidative phosphorylation over glycolysis, and readily expresses MPC1 and MPC2 at readily detectable levels. (B-C) Dose titration of 7ACC2 results in inhibitor response of OCR in a concentration-dependent manner; IC_{50} 18 nM.

Supplementary Figure 2. 7ACC2 potently acts to inhibit pyruvate transport across the mitochondrial membrane

Collaborators in the Mereddy lab demonstrate that (A-D) 7ACC2 specifically inhibits pyruvate driven respiration without substantial effects on glutamate or succinate driven respiratory processes. (E-F) Methyl pyruvate reversed the inhibitory capacity of candidate compounds indicating acute MPC inhibition. All experiments are representative of at least three independent experiments, and data represents the mean ± SEM. One-way ANOVA analysis was performed to indicate statistical significance between DMSO and compound-treated cultures. * $p < 0.05$, ** $p < 0.01$, *** $p < 0.001$, **** $p < 0.0001$

Supplementary Figure 3. 7ACC2 inhibits MPC via reversible covalent binding with a mixed mode of inhibition

Collaborators in the Mereddy lab demonstrate that MPC binding characteristics of 7ACC2 are consistent with reversible covalent interactions with amino acids in the pyruvate binding site. (A) Doubly activated olefin of carboxy coumarin template enables reversible covalent bonding with intracellular nucleophiles. (B) Computational modeling and inhibitor docking studies of MPC with 7ACC2 reveal interactions with amino acids in the pyruvate binding site. (C-F) Seahorse XF96 assays illustrate Michaelis-Menten type kinetics of mitochondrial pyruvate uptake, with 7ACC2 demonstrating a “mixed” mode of inhibition based on decreased V_{max} and increased K_m when compared to control cultures.

S**upplementary Figure 4. In vitro B cell class switching is augmented under hypoxic conditions**

C57/BL6 mice were immunized with NP-OVA/CFA and draining lymph nodes were harvested after 7 days. B and T cells were negatively enriched and CD19+ B cells and CXCR5+ ICOS+ GITR- TFH cells were isolated via sterile FACS for downstream functional assay. 50,000 B cells were plated with 30,000 TFH cells in complete media with the addition of anti-CD3 and anti-IgM and cultured without media change for 6 days at varying oxygen levels, 5% O2 and 21% O2. (A) Supernatant from culture was separated and analyzed via ELISA for IgG, and GC B cell production of class-switched IgG antibody was significantly higher at hypoxic 5% O2 conditions compared to normoxic 21% O2 conditions. Data are representative of three experiments, shown with mean ± SEM. * $p < 0.05$, ** $p < 0.01$, *** $p < 0.001$, **** $p < 0.0001$

Supplementary Figure 5. Therapeutic administration of 7ACC1 lessens cGVHD severity in BO mouse model

B10.BR mice were conditioned with cyclophosphamide (120 mg/kg/day, days -3 and -2) and total body irradiation (8.3Gy, day-1), and given bone marrow transplant on day 0. Recipient mice were given $1.0x10^6$ T-cell depleted bone marrow cells alone (BM only), with $7.0x10^4$ purified T cells from C57/BL6 mice (cGVHD). 7ACC1 was administered therapeutically after day 28 at varying dosing schedules, 7ACC1 10 mg/kg, 7ACC1 1 mg/kg, 7ACC1 0.1 mg/kg. (A-B) 7ACC1 administration within the concentrations of the dosing titration do not appear to have adverse toxic effects. (C) Pulmonary function tests performed 7 weeks after transplantation show that cGVHD is improved in mice receiving 7ACC1 at concentrations at or below 1 mg/kg. Splenic germinal center populations were assessed, and (B) GC B cell frequency, (C) TFR:TFH ratio, (D) TFR frequency, and (E) TFH frequency all indicate a substantial decrease in the germinal center reaction in mice treated with 7ACC1 at concentrations at or below 1 mg/kg. * $p < 0.05$, ** $p < 0.01$, *** $p < 0.001$, **** $p < 0.0001$

Supplementary Figure 6. In vivo dosing titration studies indicate maximal therapeutic potential of 7ACC2 administration at 1 mg/kg

B10.BR mice were conditioned with cyclophosphamide (120 mg/kg/day, days -3 and -2) and total body irradiation (8.3Gy, day-1), and given bone marrow transplant on day 0. Recipient mice were given $1.0x10^6$ T-cell depleted bone marrow cells alone (BM only), with $7.0x10^4$ purified T cells from C57/BL6 mice (cGVHD). 7ACC2 was administered therapeutically after day 28 at varying dosing schedules, 7ACC2 10 mg/kg, 7ACC2 1 mg/kg, 7ACC2 0.1 mg/kg. (A-B) 7ACC2 administration within the concentrations of the dosing titration do not appear to have adverse toxic effects. (C) Pulmonary function tests performed 7 weeks after transplantation show that cGVHD is maximally improved in

mice receiving 7ACC2 at 1 mg/kg concentration. Splenic germinal center populations were assessed, and (B) GC B cell frequency, (C) TFR:TFH ratio, (D) TFR frequency, and (E) TFH frequency all indicate a substantial decrease in the germinal center reaction in mice treated with 7ACC1 at concentrations at or above 1 mg/kg. * $p < 0.05$, ** $p < 0.01$, *** $p < 0.001$, **** $p < 0.0001$

Figures

Figure 1

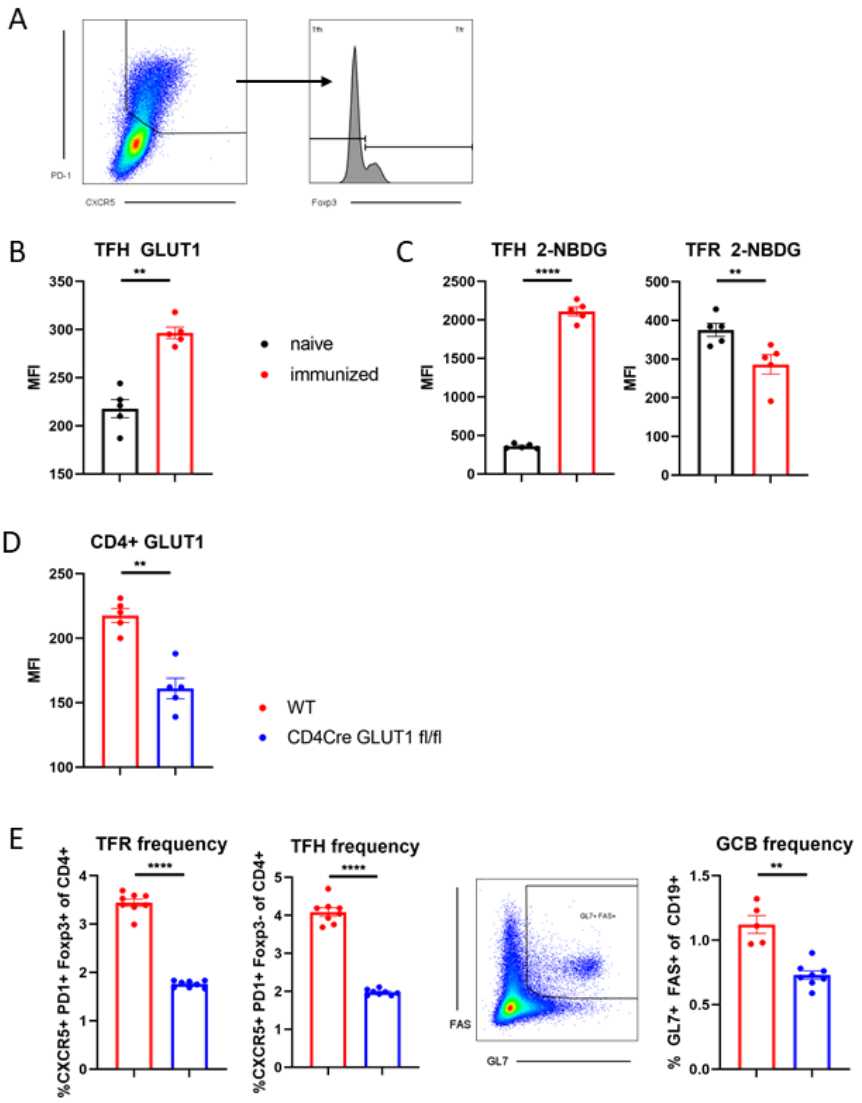

Figure 2

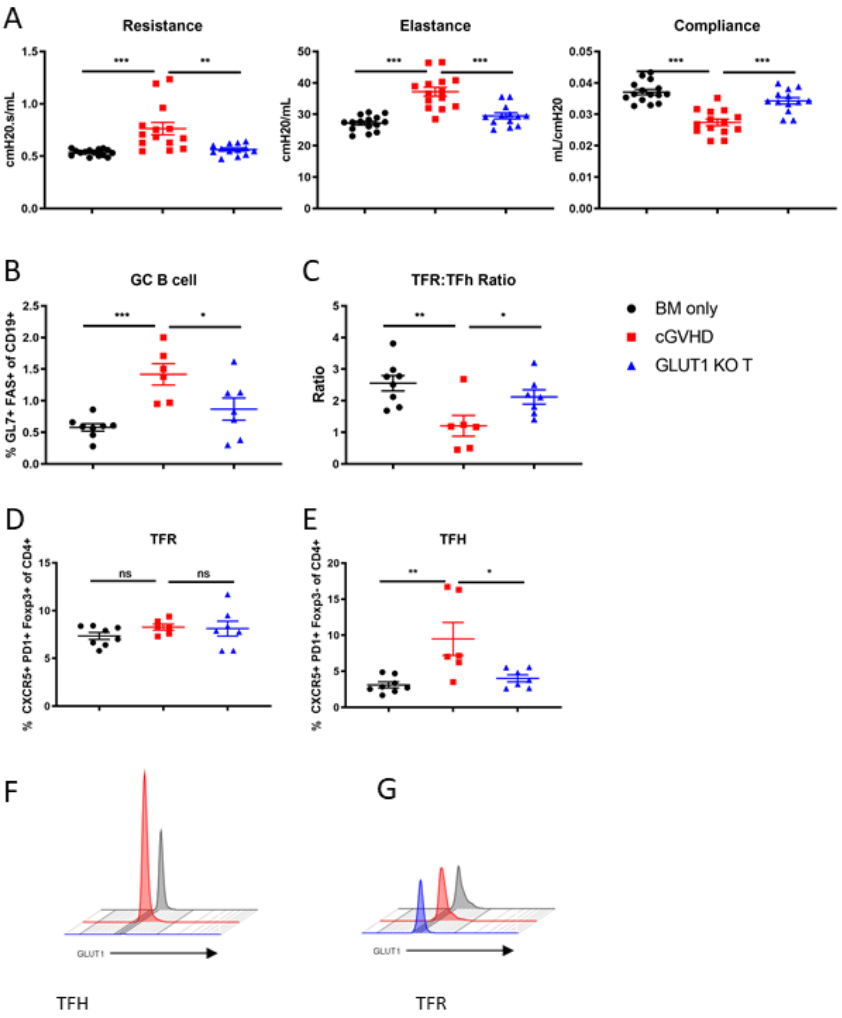
A
Resistance
Elastance
Compliance
cmH20.s/mL
cmH20/mL
mL/cmH20
B
GC B cell
% GL7+ FAS+ of CD19+
C
TFR:TFh Ratio
Ratio
BM only
cGVHD
GLUT1 KO T
D
TFR
% CXCR5+ PD1+ Foxp3+ of CD4+
ns
E
TFH
% CXCR5+ PD1+ Foxp3- of CD4+
F
G
GLUT1
TFH
TFR

Figure 3

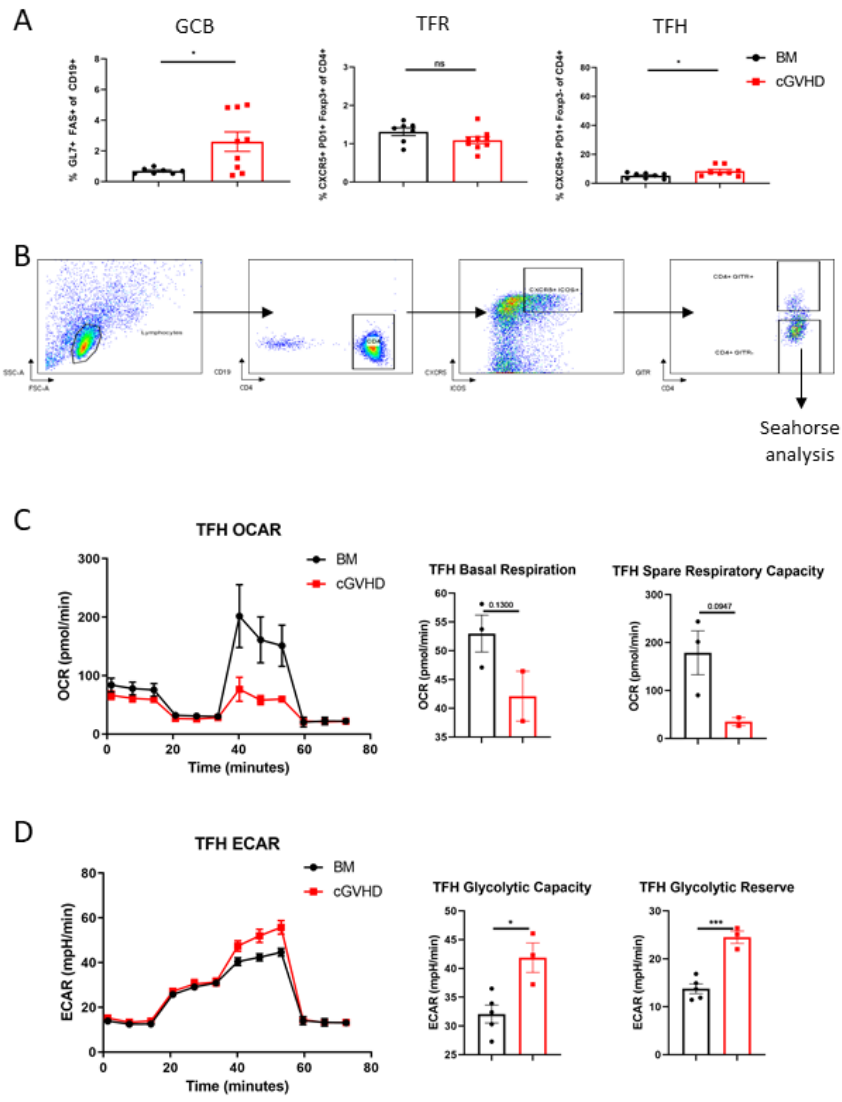
A
GCB
TFR
TFH
BM
cGVHD
% GL7+ FAS+ of CD19+
% CXCR5+ PD1+ Foxp3+ of CD4+
% CXCR5+ PD1+ Foxp3- of CD4+
ns
B
Seahorse analysis
C
TFH OCAR
BM
cGVHD
OCR (pmol/min)
Time (minutes)
TFH Basal Respiration
TFH Spare Respiratory Capacity
0.1300
0.0947
D
TFH ECAR
ECAR (mpH/min)
TFH Glycolytic Capacity
TFH Glycolytic Reserve

Figure 4

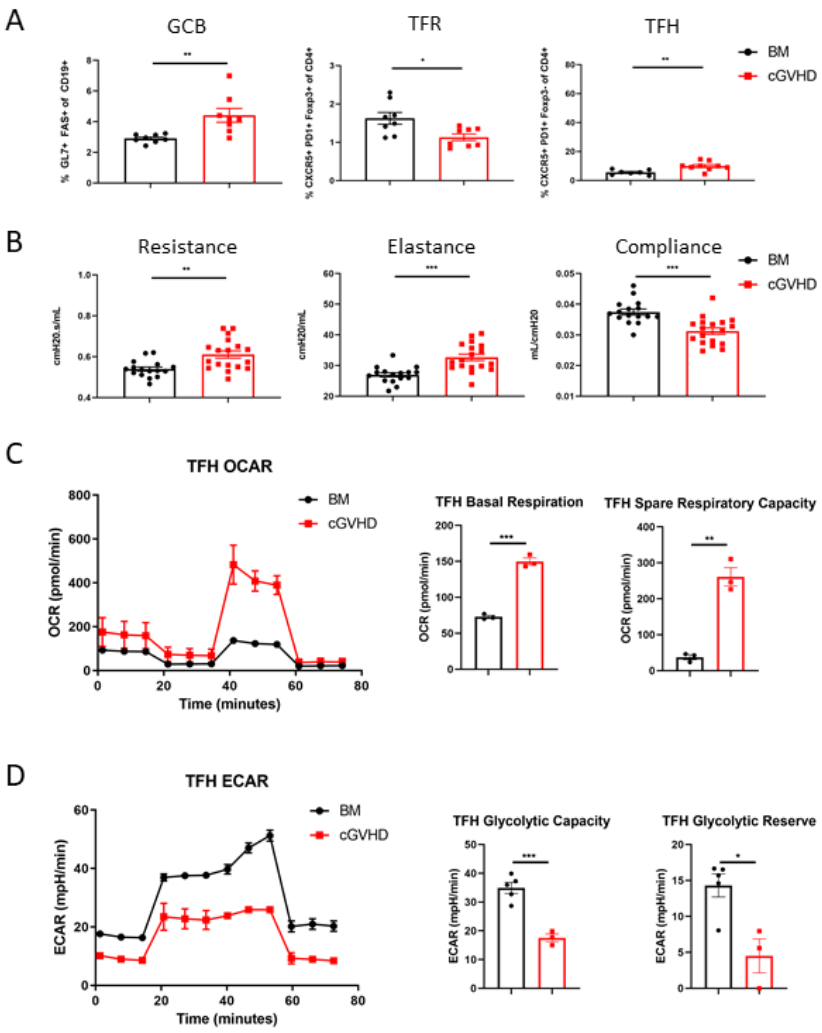
A
GCB
TFR
TFH
BM
cGVHD
% GL7+ FAS+ of CD19+
% CXCR5+ PD1+ Foxp3+ of CD4+
% CXCR5+ PD1+ Foxp3- of CD4+
B
Resistance
Elastance
Compliance
cmH20.s/mL
cmH20/mL
mL/cmH20
C
TFH OCAR
OCR (pmol/min)
Time (minutes)
TFH Basal Respiration
TFH Spare Respiratory Capacity
D
TFH ECAR
ECAR (mpH/min)
TFH Glycolytic Capacity
TFH Glycolytic Reserve

Figure 5

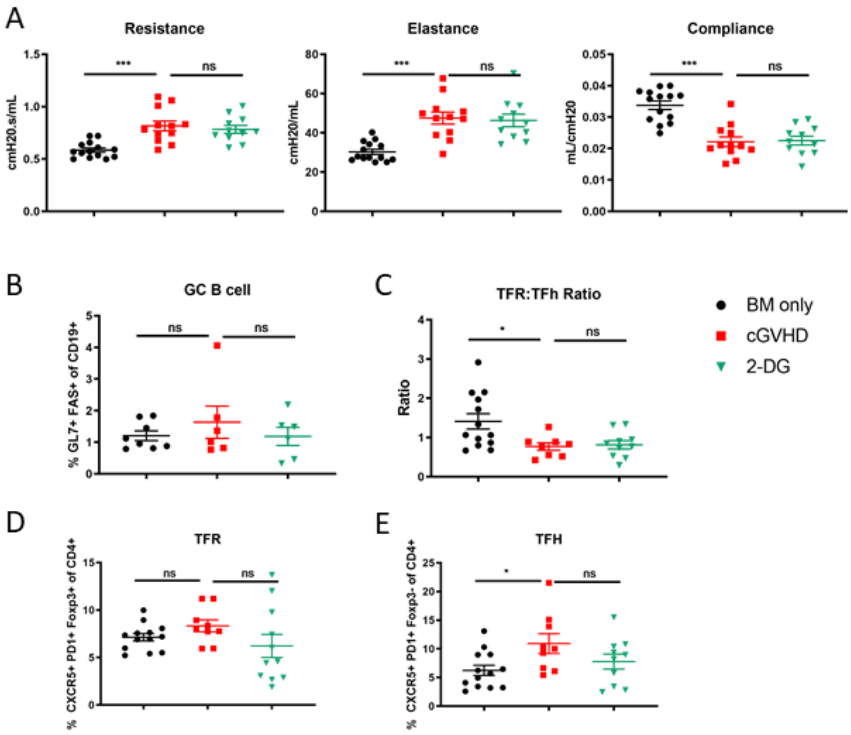
A
Resistance
Elastance
Compliance
cmH20.s/mL
cmH20/mL
mL/cmH20
***
ns
B
GC B cell
% GL7+ FAS+ of CD19+
C
TFR:TFh Ratio
Ratio
*
BM only
cGVHD
2-DG
D
TFR
% CXCR5+ PD1+ Foxp3+ of CD4+
E
TFH
% CXCR5+ PD1+ Foxp3- of CD4+

Figure 6

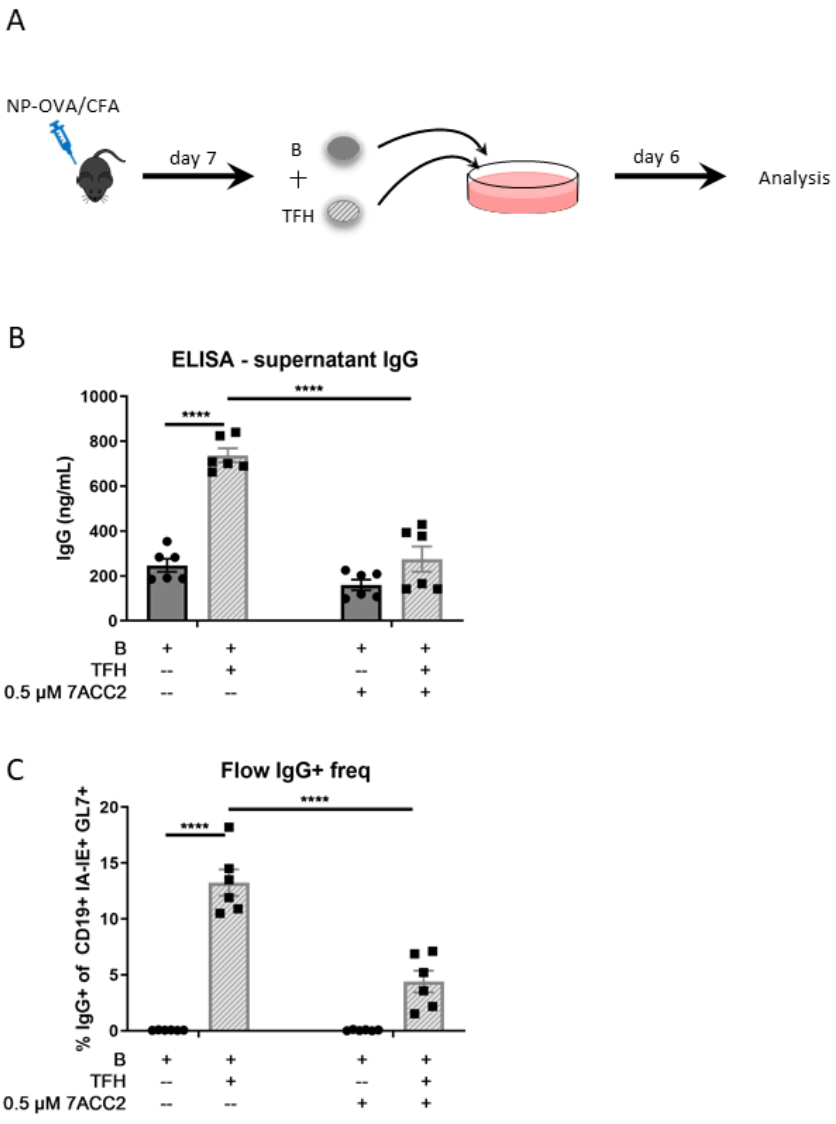
A
NP-OVA/CFA
day 7
B
+
TFH
day 6
Analysis
B
ELISA - supernatant IgG
IgG (ng/mL)
1000
800
600
400
200
0
****
****
B + + + +
TFH -- + -- +
0.5 μM 7ACC2 -- -- + +
C
Flow IgG+ freq
% IgG+ of CD19+ IA-IE+ GL7+
20
15
10
5
0
****
****
B + + + +
TFH -- + -- +
0.5 μM 7ACC2 -- -- + +

Figure 7

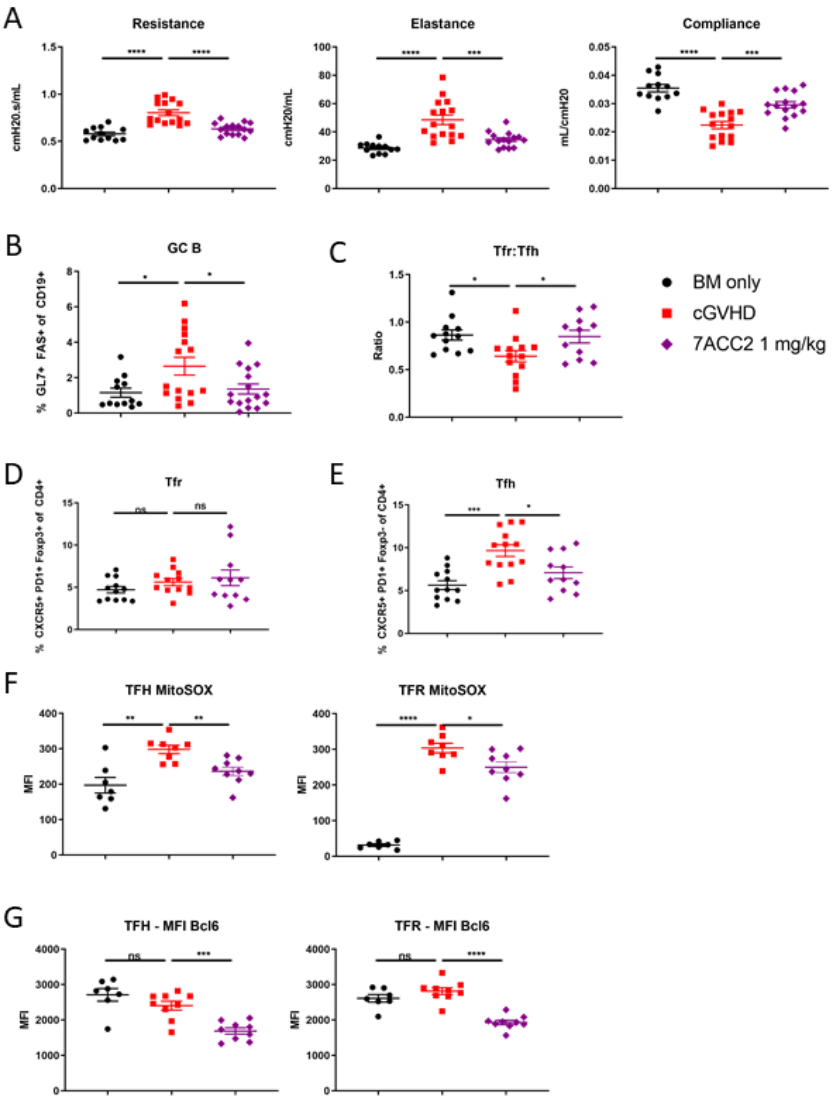
A
Resistance
Elastance
Compliance
cmH20.s/mL
cmH20/mL
mL/cmH20
B
GC B
% GL7+ FAS+ of CD19+
C
Tfr:Tfh
Ratio
BM only
cGVHD
7ACC2 1 mg/kg
D
Tfr
% CXCR5+ PD1+ Foxp3+ of CD4+
E
Tfh
% CXCR5+ PD1+ Foxp3- of CD4+
F
TFH MitoSOX
TFR MitoSOX
MFI
G
TFH - MFI Bcl6
TFR - MFI Bcl6
MFI

Supplementary Figure 1

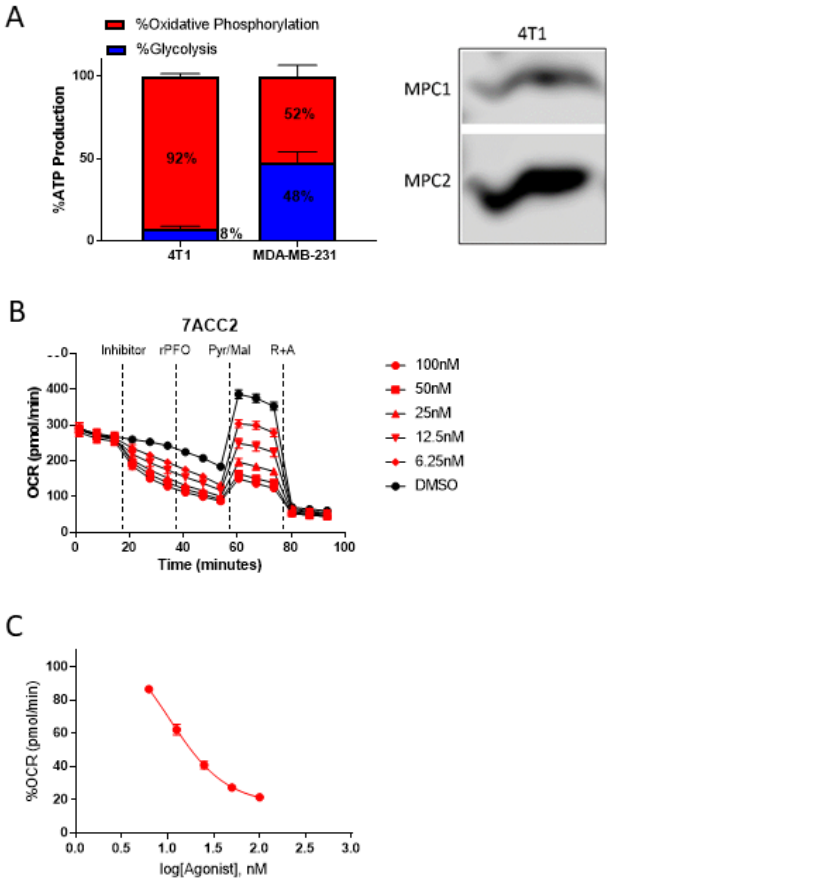

Supplementary Figure 2

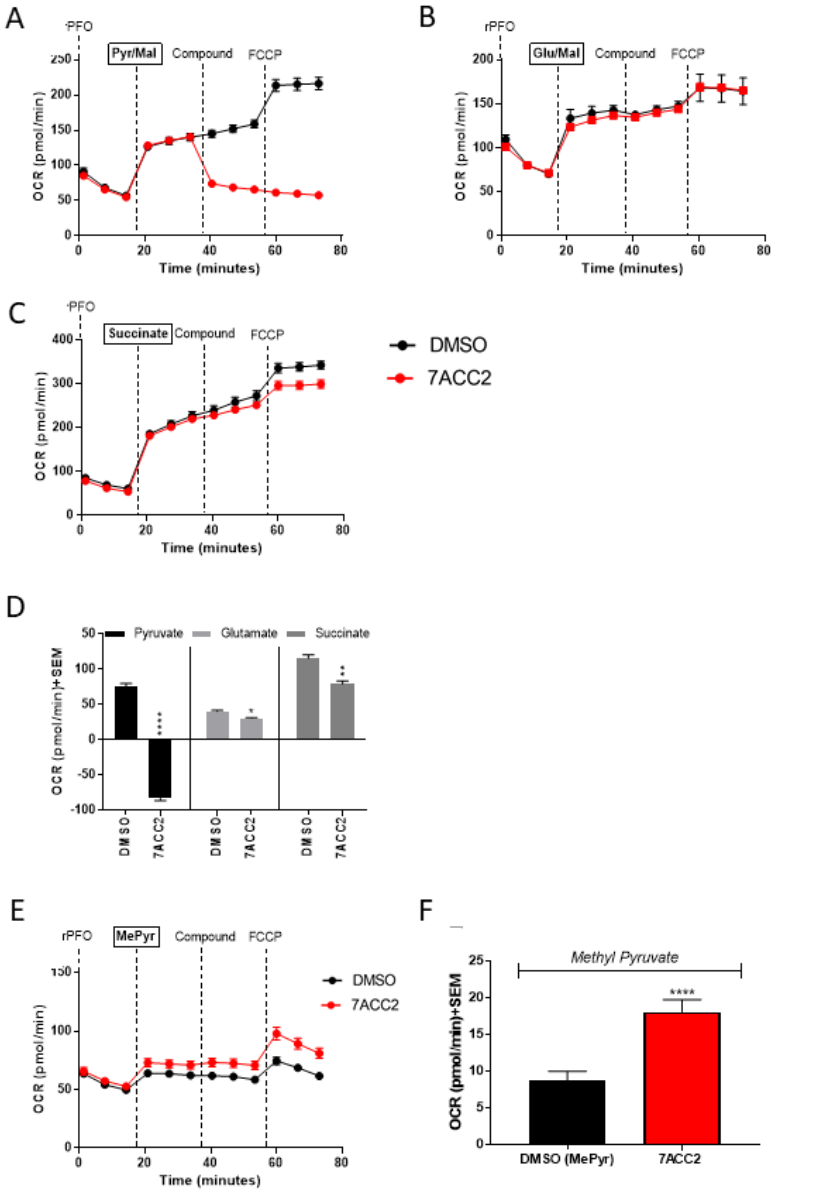

Supplementary Figure 3

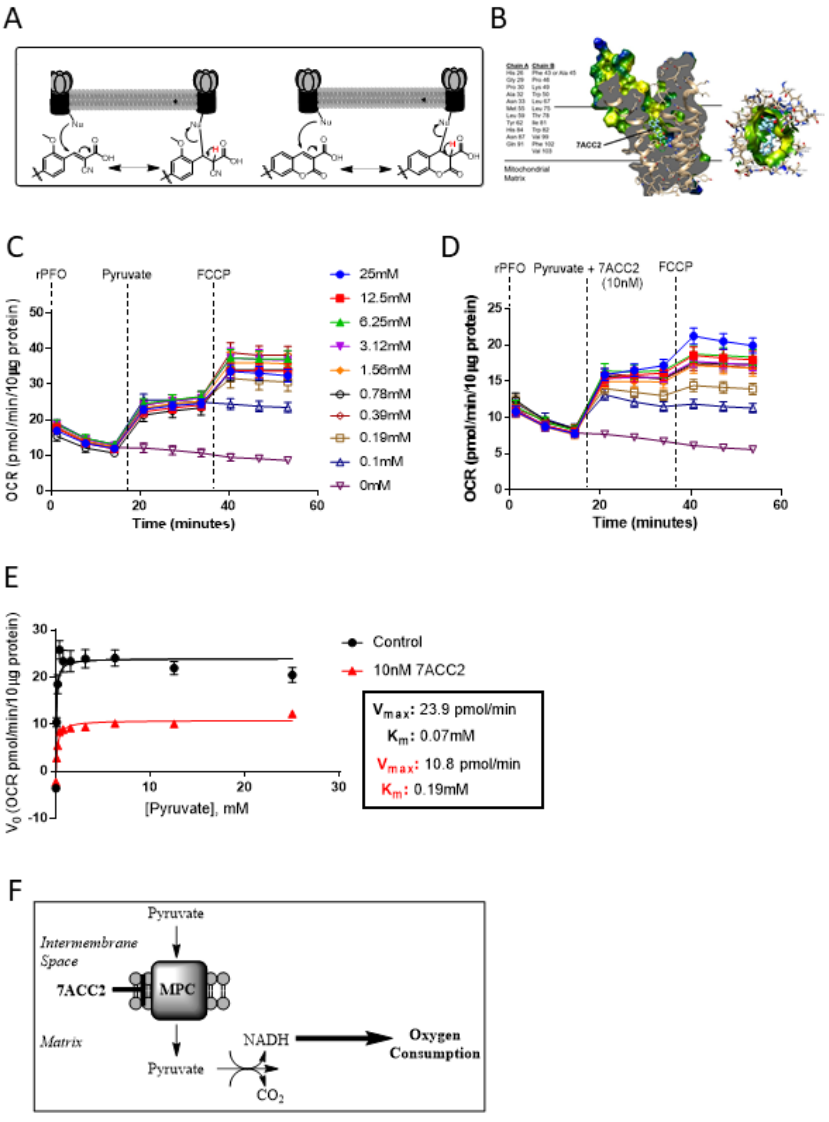

Supplementary Figure 4

A

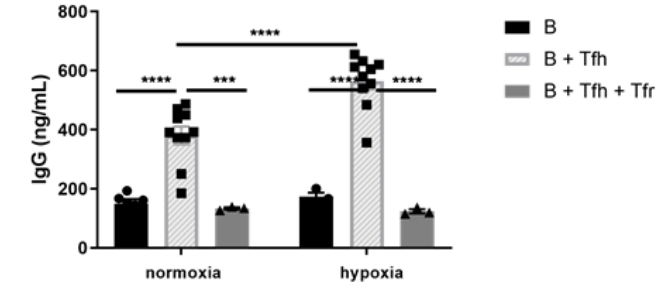

Supplementary Figure 5

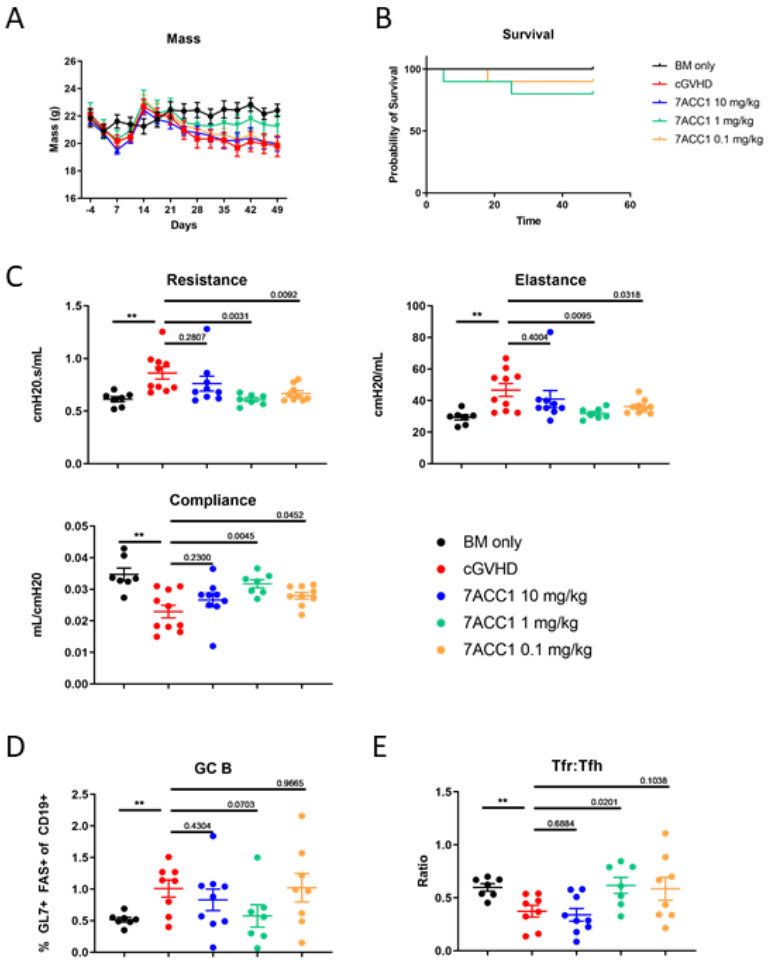

Supplementary Figure 6

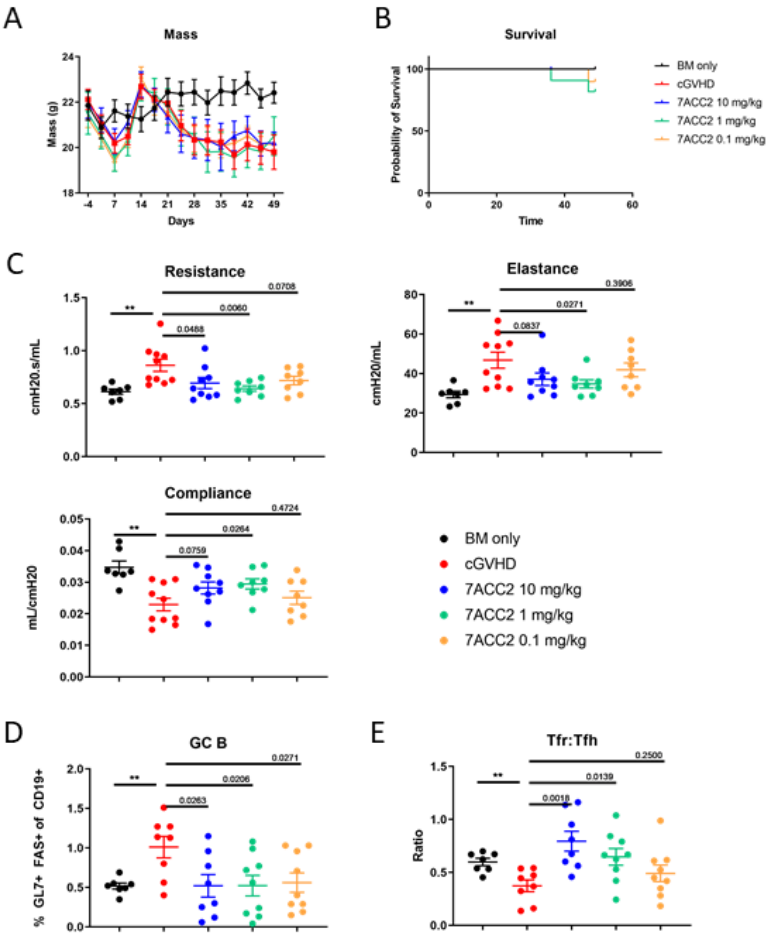

Chapter III: PD-1 blockade and inhibition of PD-1 pathway downstream of ITIM in T follicular helper cells attenuates chronic graft-versus-host disease

OVERVIEW

PD-1 and its ligand PD-L1 are widely appreciated as targets of immune checkpoint blockade. However, as the field continues to examine the PD-1 axis in a variety of immunological environments, it is becoming increasingly apparent that the impact of PD-1 is highly context-dependent. In this study, we sought to investigate the role of the PD-1 pathway within the setting of chronic graft-versus-host disease (cGVHD).

To induce cGVHD, mice are conditioned with chemotherapy and radiation prior to transplantation with MHC disparate bone marrow (BM) and T cells, and develop multi-organ symptoms with bronchiolitis obliterans lung manifestations. Anti-PD-1 mAb given to mice with established cGVHD resulted in disease attenuation assessed by pulmonary function tests (PFTs) as compared to irrelevant mAb controls. PD-1 blockade significantly reduced germinal center (GC)-promoting GC B and T follicular helper (TFH) cell and significantly increased GC-suppressing T-follicular regulatory (TFR) cell frequencies. In vitro studies identified TFH as mediators of the therapeutic effects of PD-1 blockade and implicated the criticality of the PD-1 ITIM, but not the ITSM, motif for the ability of TFH to provide support to GC B class switching. To more closely examine PD-1 signaling in TFH cells we conducted transplants using donor T cells with nonfunctional point mutations in the ITIM or ITSM motifs on the cytoplasmic tail of PD-1. Recipients given ITIM mutant, but not ITSM mutant, donor T cells demonstrated reduced cGVHD lethality with similarly diminished GC reaction as seen in PD-1 blockade. RNA sequencing analysis of anti-PD-1 mAb treated and ITIM mutant TFH cells revealed suppressive TFR-like transcriptomics profiles in the context of cGVHD, and the increased production of anti-inflammatory cytokines by these TFH confirmed a suppressive phenotype. Together, these data provide evidence for PD-1 support of the

GC reaction via the ITIM motif of TFH PD-1 and identifies the PD-1/PD-L1 axis as a potential target for cGVHD therapy.

INTRODUCTION

Chronic graft-versus-host disease (cGVHD) is a major cause of long-term morbidity, mortality and diminished quality of life following allogeneic hematopoietic stem cell transplantation. Current therapies for cGVHD have predominantly been limited to broadly immunosuppressive agents, which are inconsistently effective and associated with relapse, potentially life-threatening infections, and long-term toxicity. While changing practices in GVHD prophylaxis have reduced the incidence and severity of acute GVHD, corresponding statistics for the chronic form remain unchanged, and there is a clear need for the development of new therapeutics to address cGVHD.

Of the cell populations involved in the pathogenic germinal center (GC) reaction in cGVHD, GC B (GCB) cells express the PD-1[89] ligands PD-L1 and PD-L2, while T follicular helper (TFH) cells and T follicular regulatory (TFR) cells are defined by the expression of PD-1[90,91]. The ubiquitous presence of the PD-1/PD-L1 axis across these cells then suggests that modulation of this pathway may be able to regulate T cell-dependent humoral immunity. However, conflicting reports in the literature document both PD-1 pathway inhibition of the GC reaction[191–195], as well as support toward humoral responses[196–198,79,199,200]. Here, we investigate the effects of PD-1 blockade on the GC reaction in the setting of cGVHD.

Though PD-1 serves as a phenotypic marker for both TFH and TFR, its contributions to determining follicular T cell development and functions are not well understood. As TFH must be concentrated in GCs, in close proximity to GC B, in order to provide support for B cell class switching, past studies have examined the role of PD-1 in GC localization. While the PD-1 axis has been shown to negatively regulate the generation of TFH[193], it also appears that PD-1 expression plays an important role in TFH positioning within the follicles of secondary lymphoid organs (SLO)[65,200,201]. PD-1 is

recognized to limit the expression of CXCR3[200], which is upregulated by T cells after TCR stimulation[202]. As CXCR3 is the receptor for chemokines CXCL9 and CXCL10 that are highly expressed by stromal cells immediately external to the follicles[203], T cell expression of CXCR3 is not thought to be congruent with migration to GC and TFH differentiation[204]. Consequently, PD-1-mediated downregulation of CXCR3, via the suppression of phosphoinositode-3 kinase (PI3K) activity downstream of CXCR5[200], facilitates concentration of TFH to the GC.

PD-1, in collaboration with inducible T cell co-stimulator (ICOS), another identifying marker of TFH and TFR, has also been reported to aid in imposing the specific development of TFH within GC. At the same time that PD-1 inhibits phosphoinositide-3-kinase (PI3K) activity downstream of the chemokine receptor CXCR5 and thus reduces cellular motility toward the GC[200,107,205], ICOS promotes TFH PI3K signaling[206–209] and homing to GC areas[58,63,56,55]. In this way, constitutive follicular B cell expression of the PD-1 ligand PD-L1 draws in only PD-1+ T cells with sufficiently high enough expression of ICOS to overcome PD-1-imposed inertia[193,200,65]. This enforces the GC presence of exclusively TFH with significant ICOS expression, which is instrumental for the induction of the lineage-specific transcription factor Bcl6[55,60], TFH differentiation and maintenance[54–57,66,210,211], and the formation of robust T-cell dependent humoral responses[212–215]. Incidentally, ICOS expression and co-stimulation is also reported to induce the upregulation of PD-1[79,216], which further reinforces a CXCR5+ ICOS+ PD-1+ phenotype by TFH within the GC, where GC B express cognate ICOSL.

Once localized in the GC, TFH expression of PD-1 has been found to augment the GC reaction and the generation of immunoglobulin-secreting plasma cells (PC). A key function of TFH in providing support to GCB is the production of IL-21, which not only enhances further TFH differentiation[217–219], but is also essential for PC differentiation and IgG class switching[220–225]. However, along with the expression of

ICOS[218,54], optimal production of IL-21 by TFH requires the expression of PD-1[198,200]. PD-1 additionally assists in maintaining the rigor of GC selection. As PD-1 dampens TCR sensitivity and downstream signaling[109], PD-1:PD-L1 interactions impose a higher selection threshold for GCB, supporting affinity maturation and directing somatic hypermutation toward the generation of higher affinity antibody[201,226,200,227]. With these data as the premise for PD-1 pathway support to the GC reaction, we set out to explore the therapeutic potential of PD-1 blockade in cGVHD.

Within the bronchiolitis obliterans model of cGVHD, we found that inhibition of PD-1 with the use of blocking monoclonal antibody (mAb) resulted in attenuation of disease severity and reduction in the GC reaction. We further identified that the therapeutic activity of anti-PD-1 mAb was mediated by TFH cells and discovered the necessity of intact ITIM motif in TFH PD-1 to inhibit the GC reaction. Additional transplantation studies confirmed that nonfunctional ITIM mutant TFH were unable to support the pathogenic GC reaction in vivo. Transcriptomic analysis of TFH from PD-1 blockade treated and ITIM mutant donor T cell groups at 7 weeks post-transplantation indicated a transformation toward a suppressive TFR-like phenotype, which was supported by the assessment of increased anti-inflammatory cytokine production. Overall, our results indicate PD-1 support of the GC reaction through the PD-1 ITIM motif on TFH and submit the regulation of the PD-1 axis as a viable therapeutic approach for cGVHD.

MATERIALS AND METHODS

Mice

C57BL/6 (B6; H2b) mice were purchased from the National Cancer Institute (NCI). B10.BR (H2k) mice and B6 *CD19*^{Cre} transgenic mice were purchased from Jackson Laboratories. B6 *Pdcd1-/-* (PD-1 KO) mice were obtained courtesy of Dr. Tasuku Honjo. B6 *iFoxp3*^{Cre} *x Pdcd1*$^{fl/fl}$, B6 ITIM mutant (nonfunctional PD-1 ITIM tyrosine motif, generated via site-directed mutation Y→F 225) and B6 ITSM mutant (nonfunctional PD-1 ITSM tyrosine motif, generated via site-directed mutation Y→F 248) mice were obtained courtesy of Dr. Arlene Sharpe. All mice used in these studies were between 8-14 weeks of age. Co-housed littermates were used as controls where applicable. All mice were maintained in specific pathogen-free facilities. All studies were conducted in accordance with University of Minnesota Institutional Animal Care Committee approval (IACUC protocol # 2103-38904A).

Immunization

For immunization experiments, 8–12-week-old female C57Bl/6 (B6; H2b) (National Cancer Institute) mice were immunized via bilateral subcutaneous inguinal injection with 100ug of NP-OVA (Biosearch Technologies) emulsified in solution with CFA (BD Bioscience). At day 7 post-immunization, draining lymph nodes were harvested for further analysis.

Bone marrow transplantation and induction of cGVHD

For bronchiolitis obliterans cGVHD transplantation experiments, 11–14-week-old female B10.BR (H2k) (Jackson Laboratory) recipients underwent pre-transplant conditioning regimen (cyclophosphamide - 120 mg/kg/day intraperitoneally at days -3, -2; total body

irradiation – 8.3Gy at day -1). Transplantation grafts were composed of $1.0x10^6$ C57/BL6 T cell-depleted bone marrow cells for BM only groups (non-disease control), or $1.0x10^6$ C57/BL6 T cell-depleted bone marrow + $7.0x10^4$ T cells (C57/BL6 or, where specified, from genetically modified mice) for the induction of chronic GVHD. To generate bone marrow graft compartment, donor bone marrow was depleted with anti-CD4 (NCI) and anti-CD8 (NCI) monoclonal antibody followed by rabbit complement (Pel-Freez Biologicals). To generate T cell graft compartment, T cells were purified from donor spleens by negative selection using biotin-labeled anti-CD19, anti-B220, anti-CD11b, anti-CD11c, anti-NK1.1, anti-γδTCR, and anti-TER119 (Miltenyi Biotec), followed by streptavidin RapidSpheres deletion with EasySep magnet (StemCell Technologies). Grafts were administered in PBS to recipient mice via intravenous administration at day 0. Prophylactic administration of pharmaceutical agents was executed between day1-day28 post-transplantation. Therapeutic administration of pharmaceutical agents was executed after day28 until terminal endpoint. Mice were monitored daily for survival and weighed twice weekly until terminal endpoint in week 7 post-transplantation.

Inducible deletion of PD-1 in Treg

To inducibly delete PD-1 in *iFoxP3*^{Cre} cells, 5 doses of 1 mg tamoxifen (Sigma) in sunflower oil were given to subjects via intraperitoneal injection for 5 consecutive days beginning at day 28 post-transplantation.

Anti-PD-1 treatment protocol

Therapeutic anti-mouse PD-1 mAb (J43)[228], blocking anti-mouse PD-1 mAb (332.8H3) and depleting anti-mouse PD-1 mAb (332.1H5) were investigated. Prophylactic treatment was administered day1-day28 post-transplantation. Therapeutic treatment was administered after day 28 until transplant termination. All monoclonal antibodies,

including irrelevant IgG isotype control mAb (Abcam), were given intraperitoneally at a dosing schedule of 250 ug, 2x/week.

Pulmonary function tests

Mice were anesthetized using 50 mg/kg pentobarbital, administered using intraperitoneal injection. Mice were then intubated and ventilated, and measures of pulmonary resistance, elastance and compliance were obtained using whole-body plethysmography on the Flexivent system (SCIREQ).

Frozen tissue preparation

Spleens, colons, and livers from mice harvested at day 49 post-transplantation were embedded in optimal cutting temperature compound (OCT), snap frozen in liquid nitrogen, and stored at -80˚C. Lungs were inflated with 1mL of OCT:PBS solution (3:1) and embedded in optimal cutting temperature compound, snap frozen in liquid nitrogen, and stored at -80°C.

Immunofluorescence staining

For all immunofluorescence assays, 6µm cryosections were fixed for 5 minutes in acetone prior to staining. For germinal center quantification assay, spleen sections were stained with PNA-rhodamine and anti-CD4 FITC antibody and mounted in DAPI-containing mounting medium (Vector Laboratories). For PD-1 detection assay, spleen sections were stained with PNA-rhodamine, anti-CD4 BV421 and anti-PD-1 FITC antibodies and mounted in DAPI-free mounting medium (Invitrogen). For Foxp3 detection assay, spleen sections were stained with PNA-rhodamine, anti-CD4 BV521 and anti-Foxp3 FITC antibodies and mounted in DAPI-free mounting medium (Invitrogen). For immunoglobulin deposition assay, lung sections were stained with anti-

mouse IgG-FITC and mounted in DAPI-containing mounting medium (Vector Laboratories). Confocal images were acquired on an Olympus confocal laser scanning microscope at 20X and quantified by ImageJ.

Trichrome staining

6µm cryosections were fixed overnight at room temperature in Bouin's solution and stained with a Masson's trichrome staining kit (Sigma-Aldrich). Confocal images were acquired on an Olympus confocal laser scanning microscope at 20X, and collagen deposition was quantified by ImageJ.

Antibodies

Anti-CD132/IL2Rg (TUGm2), anti-CD4 (RM4-5), and anti-FAS (Jo2) antibodies were purchased from BD Biosciences. Anti-CD126/IL6R (D7715A7), anti-CD130/gp130/IL6ST (4H1B35), anti-CD25/IL2Ra (PC61), anti-CD154/CD40L (MR1), anti-CD223/LAG-3 (C9B7W), anti-CD366/Tim3 (F38-2E2), anti-CD44 (IM7), anti-GITR (DTA-1), anti-IA/IE (M5/114.15.2), anti-IgG1 (RMG1-1), and anti-PD-1 (29F.1A12) antibodies were purchased from BioLegend. Anti-IgG2c (STAR135) antibody was purchased from Bio-Rad. Anti-Bcl6 (BCL-DWN), anti-Blimp-1 (5E7), anti-CD122/IL2Rb (TM-b1), anti-CD19 (1D3), anti-CD3 (145-2C11), anti-CD62L (MEL-14), anti-CD69 (H1.2F3), anti-CXCR5 (SPRCL5), anti-Foxp3 (FJK-16s), anti-GL7 (GL7), anti-ICOS (C398.4A), anti-IL10 (JES5-16E3), anti-IL17 (eBio17B7), anti-IL21 (FFA21), fixable viability dye, anti-TIGIT (GIG57), and anti-PD-L1 (B7-H1) antibodies were purchased from eBioscience. Anti-PD-1 (29F.1A12), anti-PD-1 (332.1F4), anti-PD-1 (332.1H5), anti-PD-1 (332.5E12), anti-PD-1 (332.6D2), anti-PD-1 (332.8H3), anti-PD-1 (2203 – recombinant 332.8H3), anti-PD-L1 (10F.9G2), and phospho-PD-1 (407.6Gs12)[229] antibodies were provided courtesy of Gordon Freeman. Anti-PD-1 (J43)[228] antibody was purchased from the National Cell

Culture Center. Anti-TGFβ (1D11) antibody was purchased from R&D Systems. Anti-GFP antibody was purchased from Rockland.

Flow cytometry and analysis

Single cell suspensions of immune cells isolated from spleen or lymph nodes were generated and stained for surface markers with conjugated antibodies in FACS buffer (PBS with 2% FBS + 2mM EDTA). Intracellular Foxp3 staining was performed following fixation and permeabilization using the intracellular fixation and permeabilization buffer kit from eBioscience according to manufacturer instructions. Phospho-PD1 staining was performed on cells from Foxp3 GFP reporter mice, either transplanted as the donor graft or activated in vitro for 2 hours with anti-CD3, following treatment for 5 minutes at 37˚C with 0.1 mM pervanadate, and by using anti-GFP antibody to boost Foxp3 signal during intracellular staining. Intracellular cytokine staining was performed following stimulation with cell stimulation cocktail in Brefeldin A (BioLegend) for 5 hours in complete RPMI media at 37˚C.

All flow cytometry was conducted on a LSRFortessa flow cytometer (BD Biosciences). Flow cytometry standards were run regularly to ensure instrument stability. All resulting FCS3.0 files were analyzed using FLowJo V10 (Tree Star).

Fluorescence-activated cell sorting

Immune cells were isolated from harvested spleen or lymph nodes and enriched for B and T lymphocytes by negative selection using biotin-labeled anti-CD11b, anti-CD11c, anti-NK1.1, anti-γδTCR, and anti-CD49b (Miltenyi Biotec), followed by streptavidin RapidSpheres deletion with EasySep magnet (StemCell Technologies). Lymphocytes were then stained for surface markers (B cells – CD19+ CD4-; TFH cells – CD19- CD4+

CXCR5+ ICOS+ GITR-; TFR cells – CD19- CD4+ CXCR5+ ICOS+ GITR+) with conjugated antibodies in FACS buffer.

Class switch assay

For in vitro assessment of B cell class switching, lymphocytes harvested from the draining lymph nodes of WT B6 mice were immunized with NP-OVA and enriched for B and T cells by negative selection using biotin-labeled anti-CD11b, anti-CD11c, anti-NK1.1, anti-γδTCR, and anti-CD49b (Miltenyi Biotec), followed by streptavidin RapidSpheres deletion with EasySep magnet (StemCell Technologies). CD19+ B cells, CXCR5+ ICOS+ GITR- TFH cells, and CXCR5+ ICOS+ GITR+ TFH cells were isolated via FACS. Cells were then plated at concentrations of 50,000 B cells/well, 30,000 TFH cells/well and 3,000 TFR cells/well, and co-cultured together in RPMI 1640 media (Invitrogen) supplemented with 10% FBS, 2mM L-glutamine, 10mM HEPES, 1% penicillin/streptomycin and 50 μM β-mercaptoethanol, as well as the addition of soluble 2.0 μg/mL anti-CD3 and 5 μg/mL anti-IgM. Cell cultures were maintained without media change for 6 days at 37˚C. Hypoxia studies were conducted at oxygen concentrations of 1% O2, 5% O2 and 21% O2. After 6 days of culture, supernatant was separated and analyzed for IgG concentration using ELISA, while cells were separated and analyzed for presence of CD19+ IA+/IE- GL7+ IgG+ B cells.

Bulk RNA sequencing experiment and analysis

For RNAseq experiments, lymphocytes harvested from spleens of transplanted mice (groups: negative disease control BM only, cGVHD, anti-PD-1 blockade treated, ITIM mutant T cells) at day 49 post-transplantation were enriched for T cells by negative selection using biotin-labeled anti-CD19, anti-B220, anti-CD11b, anti-CD11c, anti-NK1.1, anti-γδTCR, and anti-CD49b (Miltenyi Biotec), followed by streptavidin RapidSpheres

deletion with EasySep magnet (StemCell Technologies). CXCR5+ ICOS+ GITR- TFH cells were isolated via FACS, collected in Buffer RLT (Qiagen) + 1% β-mercaptoethanol. Within each group, sorted cells from two mice were pooled to create one sample. All samples were kept frozen at -80˚C until RNA extraction, processing, and quality control at the University of Minnesota Genomics Center. Library prep was conducted via Takara/Clontech SMARTer Stranded Total RNA-Seq Kit v2 – Pico Input Mammalian library prep and sequenced via NovaSeq paired-end flow cell sequencing. De-multiplexing was performed using Illumina bcl2fastq v2.20 and resulting FASTQ reads were loaded into ChURP (Collection of Hierarchical UMII/RIS Pipelines) for quality control, Trimmomatic read trimming, and HISAT2 alignment against the GRCm38/mm10 reference genome. Analysis of the resulting count matrix was conducted via DESeq2[230] and ClusterProfiler[231,232].

Statistical analysis

All statistical analyses were conducted using Prism software (version 9). Linear regression was used for analysis of class switch experiments. Figures are presented as mean ± SEM, with significance determined using unpaired two-tailed Student's t-test. Log-rank (Cox-Mantel) statistical test was used for analysis of survival curves. Significance is denoted by asterisks as follows:

* $p < 0.05$, ** $p < 0.01$, *** $p < 0.001$, **** $p < 0.0001$.

RESULTS

In cGVHD, TFH demonstrate increased expression of PD-1 during germinal center reaction, which does not correlate to ITSM phosphorylation

To establish baseline expression of PD-1 and PD-1 signaling in the germinal center populations during cGVHD, we utilized the bronchiolitis obliterans mouse model which reproduces the systemic manifestations of human cGVHD pathology. In this model, damage to the lungs starts to become apparent by day 21 post-transplant (data not shown), and only worsens with disease progression. These changes to tissue pathology parallel the increasing intensity of the GC reaction, and so we examined the temporal patterns of PD-1 expression at day 21 and day 35 post-transplantation. Already by day 21 post-transplant, significantly higher frequencies of GCB and PD-1+ CXCR5+ Foxp3- TFH (**Figure 1B**) were present in the cGVHD mice as compared to non-disease control (data not shown). The establishment of a GC reaction corresponded with higher expression of PD-1 in the cGVHD TFH as compared to the non-disease control TFH at day 21 (**Figure 1A**), and this increase in PD-1 expression remained reproducibly consistent across subsequent timepoints by flow cytometry (**Figure 1C**). Upregulation of PD-1 is understandable considering the increased activation of TFH in the cGVHD state, but surprisingly, cGVHD TFH expression of phospho-PD-1 did not correlate with PD-1 expression at respective timepoints (**Figure 1D**). While TFH phospho-PD-1 expression appeared to increase with time, regardless of disease state, the cGVHD TFH showed a significant decrease in apparent PD-1 signaling. This data was particularly striking as it seemed to contradict the findings regarding PD-1 expression. However, additional studies to illuminate the precise phosphorylation event being captured during phospho-PD-1 staining revealed that phospho-PD-1 expression correlates with the presence of a functional PD-1 ITSM tyrosine motif (**Supplementary Figure 1A**). Staining of CD3-

activated CD4+ T cells from PD-1 ITIM nonfunctional mutant or PD-1 ITSM nonfunctional mutant mice demonstrated phospho-PD-1 signaling only in the ITIM mutant T cells. Based on this observation, it is possible to presume that while the TFH in cGVHD had greater expression of PD-1, PD-1 signaling in these cells was conducted through the ITIM motif to a larger degree compared to the ITSM motif.

Therapeutically-administered PD-1 blockade paradoxically attenuates cGVHD

We next explored the effects of a blocking anti-PD-1 mAb (clone J43) on the pathophysiology of cGVHD. Using the bronchiolitis obliterans (BO) cGVHD model, 250 µg anti-PD-1 mAb was therapeutically administered beginning at day 28 post-transplantation, after the initiation of disease, and given 2x/week until experiment termination at 7 weeks post-transplant. Though mass and survival were not observed to change (**Figure 2A**), Pulmonary dysfunction was found to be significantly decreased in mice receiving therapeutic PD-1 blockade (**Figure 2B**), and immunohistochemical staining of pulmonary tissues depicting immunoglobulin (**Figure 2C**) and collagen deposition (**Figure 2D**) confirm a reduction in pathology.

Analysis of the splenic GC populations was also performed. Because there were concerns regarding the anti-PD-1 mAb potentially affecting PD-1 staining for flow cytometry, our gating strategy for follicular T cells was to identify CD4+ CXCR5+ ICOS+ Foxp3- TFH and CD4+ CXCR5+ ICOS+ Foxp3+ TFR. To examine the possibility of the anti-PD-1 mAb having depleting effects in addition to blocking effects, we assessed absolute cell counts of the GC populations out of $0.5x10^6$ total splenocytes. At day 35, TFH and TFR count were both found to have increased after the first week of anti-PD-1 mAb administration (**Figure 2E**), though TFH count was significantly decreased compared to isotype-treated control two weeks later (**Figure 3A**). From these results, and with findings from other studies confirming high PD-1 expression on both TFH and

TFR in the BO cGVHD model (data not shown), we suspected the depletion effects of the mAb to be minimal. We also surveyed the frequency of splenic GC populations at the end of seven weeks and found that administration of the anti-PD-1 mAb significantly reduced the frequency of GCB and TFH while significantly increasing the frequency of TFR, resulting in a greater TFR:TFH ratio (**Figure 3B-C**). Immunofluorescent staining of splenic sections for GC also showed an inhibition of the GC reaction, as measured by PNA, with GC size and GC frequency decreasing after anti-PD-1 mAb treatment (**Figure 3D-F**). Immunofluorescent staining for Foxp3 in GC also corroborated the increase in TFR frequency, demonstrating a significant increase in the number of Foxp3+ cells per GC with anti-PD-1 mAb administration (**Figure 3G**). These data indicated that therapeutically administered anti-PD-1 mAb attenuated cGVHD through a reduction in TFH, and a shift toward a Foxp3+ phenotype within the pool of follicular T cells.

As the results of the therapeutically administered anti-PD-1 mAb were surprising, we also opted to examine the effects of prophylactically administered anti-PD-1 mAb, given from day 0 to day 28 post-transplantation (**Supplementary Figure 2**). The results of early treatment with PD-1 blockade were not congruent with that of late PD-1 blockade; pulmonary function amongst the group receiving prophylactic anti-PD-1 mAb was decisively unchanged. Notably, the mass of the prophylactic anti-PD-1 mAb group during the period of mAb administration was significantly decreased compared to isotype-treated control and appeared to resemble the pattern seen in recipients given PD-1 KO T cells (**Supplementary Figure 8**). This was likely due to increased disease severity as a result of heightened T cell activation, as would be expected in PD-1 blockade of Tcon cells. Additionally, early PD-1 blockade may have also altered donor T cell development into TFH as PD-1 aids in follicular T cell recruitment, which possibly accounts for the reduced TFH frequency and increased TFR:TFH ratio observed in the prophylactic anti-PD-1 mAb group, despite unimproved lung pathology. This

interpretation suggests that the effects of therapeutically administered anti-PD-1 mAb may be due to particular influence upon the GC reaction, which does not become established until several weeks after transplantation.

To further investigate potential mechanisms for the restorative effects of therapeutic anti-PD-1 mAb, we also conducted supplementary studies with specific blocking (clone 332.8H3) and depleting (clone 332.1H5) mAbs developed and provided courtesy of Gordon Freeman (**Supplementary Figure 3**). Therapeutic administration, from day 28 until experiment termination, of blocking anti-PD-1 mAb, but not depleting anti-PD-1 mAb, resulted in the mitigation of pulmonary dysfunction, as had been observed with the J43 clone. Additionally, PD-1 blockade effects on the GC reaction reduced pathogenic GCB and TFH frequency and increased TFR frequency, comparable with the results from the J43 clone, and elevating, but not significantly increasing, the TFR:TFH ratio. PD-1 depletion was found to reduce GCB, TFH and TFR frequency, with an overall decrease in TFR:TFH ratio. These findings lent further support to our understanding of the J43 clone to primarily possess blocking rather than depleting properties.

Inhibitory effects of PD-1 blockade on germinal center reaction are mediated by TFH with intact ITIM motif

We next wanted to more precisely examine the specific GC populations being affected by PD-1 blockade with the anti-PD-1 J43 clone and utilized an in vitro class switching assay to simulate the GC reaction. WT B6 and PD-1 KO mice were immunized with NP-OVA in CFA, and B and TFH cells were isolated and purified from the draining lymph nodes and placed into co-culture with CD3 and IgM (**Figure 4A**). In co-cultures of WT B and WT TFH, the addition of anti-PD-1 mAb was found to significantly reduce the frequency of class switched IgG+ B cells, in parallel with in vivo findings, and the

inhibitory effect of PD-1 blockade was still apparent in co-cultures of PD-1 KO B and WT TFH. However, in co-cultures of WT B and PD-1 KO TFH, the reduction of class switching with the addition of PD-1 blockade was absent (**Figure 4B**). These in vitro observations suggested that PD-1 blockade effects on the GC reaction were mediated by TFH.

We then sought to corroborate these in vitro findings in the in vivo cGVHD model, using *CD19*^{Cre} *PD-1*$^{fl/fl}$ mice as bone marrow donors (**Supplementary Figure 4**). Interestingly, recipients transplanted with Cre+ bone marrow exhibited a slight increase in TFR frequency at baseline, and because the TFR are generated from the bone marrow compartment in this model, this may be indicative of some function for B cell PD-1 in the development of TFR. However, this elevation in TFR frequency did not appear to affect the generation of GCB, and pulmonary dysfunction was unchanged from that of Cre- bone marrow recipients. Though the already-enhanced TFR frequency of the Cre+ cGVHD group was not further increased with PD-1 blockade, anti-PD-1 mAb administration trended with a decrease in GCB frequency, and significantly reduced pulmonary dysfunction across both Cre- cGVHD and Cre+ cGVHD groups, partially validating the findings from the in vitro class switching assay. Moreover, the PD-1 blockade treatment also resulted in a significant decrease in TFH frequency and subsequent increase in TFR:TFH ratio across both Cre- cGVHD and Cre+ cGVHD groups, analogously to the studies conducted with WT bone marrow. Based on this data, GC reaction inhibition and cGVHD improvement by therapeutic PD-1 blockade did not appear to be dependent upon B cells.

While we were unable to examine PD-1 blockade effects on TFR suppression of the GC reaction in vitro due to logistical difficulties with titrating a consistent TFR dose, we did examine the role of PD-1 on bone marrow-derived Tregs in the in vivo cGVHD model using *iFox*^{Cre} *PD-1*$^{fl/fl}$ mice as bone marrow donors (**Supplementary Figure 5**).

Deletion of PD-1 on Foxp3+ cells was induced beginning at day 28 post-transplant, after GC establishment, and only incompletely deleted due to severe adverse effects of tamoxifen preventing full dosing. While full deletion would have required 10 doses of tamoxifen across 10 days, sustained tamoxifen administration led to an immediate acceleration in mortality in cGVHD mice, so ~85% PD-1 deletion was achieved with 5 doses of tamoxifen across 5 days. Despite tamoxifen toxicity, pulmonary dysfunction was comparable between wt/wt cGVHD and fl/fl cGVHD groups, and therapeutic PD-1 blockade significantly improved lung function across both groups. Fl/fl cGVHD mice also demonstrated a significant reduction in GCB frequency at baseline, even without anti-PD-1 mAb treatment, while TFR frequency remained comparable to that of the wt/wt cGVHD group, suggestive of an increase in TFR suppressive capacity with partial deletion of PD-1 on Foxp3+ cells. However, TFR frequency and TFR:TFH ratio were still significantly increased with administration of anti-PD-1 mAb across both the wt/wt cGVHD and fl/fl cGVHD groups, suggestive of therapeutic PD-1 blockade effects on GC cells other than TFR.

Based on these in vitro and in vivo indications for the role of TFH in mediating PD-1 blockade effects, we next attempted to explore the different PD-1 intracellular tyrosine motifs on TFH in the GC reaction. In vitro co-culture of WT B cells with TFH from ITIM nonfunctional mutant mice resulted in a significant decrease in IgG+ B cell class switching as compared to co-culture with WT TFH, and the addition of anti-PD-1 mAb did not yield further reduction in class switching (**Figure 4C**). This finding suggests that PD-1 blockade acts through inhibition of the ITIM motif in TFH during the GC reaction. To confirm this supposition, we also performed the in vitro class switch assay using TFH from ITSM nonfunctional mutant mice with unaltered and intact ITIM motif (**Figure 4D**). Co-culture of WT B cells with ITSM mutant TFH resulted in IgG+ B cell class switching comparable to co-culture with WT TFH, and the addition of anti-PD-1

mAb was able to significantly inhibit class switching. These results indicated that TFH support to B cell class switching in vitro requires the PD-1 ITIM motif, and that PD-1 blockade interrupts this mechanism.

ITIM motif in donor T cells is necessary for the development of cGVHD

To verify the role of the ITIM versus ITSM motifs in TFH during the GC reaction in vivo, we utilized the mutant mice as T cell donors in the bronchiolitis obliterans cGVHD model. Strikingly, recipients given ITSM mutant donor T cells had extremely poor survival, recapitulating the results of transplantation with PD-1 KO donor T cells, and accelerated disease severity in a resemblance of acute GVHD (**Supplementary Figure 8**). With a nearly 75% fatality rate in the ITSM mutant group, it was not possible to collect meaningful data beyond survival and mass, however, this outcome suggested that in this cGVHD model, the ITSM motif facilitates the canonical PD-1 functionality of restraining T cell activation.

The fate of the recipients given ITSM mutant donor T cells was in clear contrast to the recipients given ITIM mutant donor T cells. In the ITIM mutant T group, survival was observed to be significantly improved over WT T cell recipients (**Figure 5A**). Moreover, pulmonary function was found to be significantly increased in the mice given ITIM mutant T cells (**Figure 5B**), and reduction in lung pathology was corroborated by immunohistochemical staining of lung tissues for immunoglobulin (**Figure 5C**) and collagen deposition (**Figure 5D**).

Our findings are suggestive of a distinct role for the ITIM motif in T follicular cells during cGVHD in this model. While the frequency of PD-1+ TFR was decreased and the frequency of PD-1+ TFH was unchanged in the ITIM mutant donor T cell group (**Figure 6B**), both ITIM mutant TFH and ITIM mutant TFR showed significantly decreased expression of PD-1 (**Figure 6A**). Additionally, assessment of the GC populations also

identified a global reduction in the GC reaction in recipients of ITIM mutant donor T cells. The ITIM mutant T group demonstrated a significant decrease in the frequency of GCB and TFH, and a significant increase in the frequency of TFR, resulting in a greater TFR:TFH ratio (**Figure 6C**). We also verified that the changes in these follicular T cell frequencies were not due to differences in Treg vs Tcon composition within the ITIM mutant donor T cell compartment of the graft. Splenic T cells from naïve ITIM mutant mice did not show a significant change in Foxp3+ Treg or Foxp3- Tcon frequencies as compared to WT (**Supplementary Figure 1B**), though, notably, the percentage of PD-1+ Tregs and the degree of PD-1 expression by Tregs in the ITIM mutant mice was significantly increased as compared to WT (**Supplementary Figure 1C-D**). However, because the frequency of Treg is not changed between ITIM mutant T or WT T cells and therefore the frequency of Treg in the transplanted T cell graft did not change, these results indicate that the observed decrease in TFH cells in the ITIM mutant T group was a result of altered TFH functionality within the GC during cGVHD and was not due to a decrease in transplantation of Foxp3- donor T cells. The reduction in GC reaction was also noticeable in immunofluorescent staining for GC in splenic tissue, as both GC size and frequency were diminished in the recipients given ITIM mutant donor T cells (**Figure 6D-F**). Altogether, these data indicate that both therapeutic PD-1 blockade and ITIM mutant donor T cells lessen cGVHD severity through similar means in which TFH frequency and support to GCB is reduced, resulting in a weaker GC reaction and attenuation of disease.

PD-1 blockade and ITIM mutant T cell graft reshape TFH to suppressive phenotype in cGVHD

In a deeper investigation into the mechanism through which PD-1 blockade treatment and nonfunctional PD-1 ITIM mutation impact TFH, we next explored

transcriptomics analysis of TFH from the bronchiolitis obliterans cGVHD model. Splenic TFH were harvested from transplanted recipients at day 49 and isolated by FACS sorting with a CD19- CD4+ CXCR5+ ICOS+ GITR- gating strategy (**Figure 7A**). Expression of GITR, a marker of functional Treg, was analogous with expression of Foxp3, and CD4+ CXCR5+ ICOS+ GITR- cells were verified to be Foxp3- (**Figure 7B**). Preliminary principal component analysis of log-transformed count data revealed discrete clustering of samples, indicative of unique transcriptomic signatures for the PD-1 blockade treated (J43) and ITIM mutant (ITIM) TFH that were separate from that of negative disease control (BMOnly) or positive disease control (cGVHD) mice (**Figure 7C**). A distinctive insight provided by PCA was the substantial overlap between TFH from ITIM mutant and ITIM mutant therapeutically treated with anti-PD-1 mAb, which supports the results of the in vitro class switching data that demonstrated anti-PD-1 mAb administration replicating nonfunctional ITIM in TFH. Also interestingly, the most significant element of variance that was identified across all groups was between the BMOnly and J43 or ITIM samples across the x-axis, which showed that the latter TFH were not becoming more like those found in disease-free subjects in reducing cGVHD severity but assumed a divergent identity with PD-1 blockade and ITIM mutation. To further examine the transcriptomic profile of reference cGVHD TFH, we conducted gene set enrichment analysis (GSEA) using a set of genes that are conventionally upregulated in TFH as compared to Tcon (**Figure 7D, Supplemental Table 1**). The results of this analysis were unexpected; cGVHD TFH, in relation to BMOnly TFH, did not appear to be enriched for canonical TFH-associated genes, which proposes a model of atypical GC reaction in cGVHD pathology. However, TFH from both J43 and ITIM groups were found to be more enriched for established TFH genes in relation to TFH from BM Only, and to a greater extent than that of cGVHD.

Based on the surprising results of the TFH GSEA and on our previous observations in increased TFR frequency with PD-1 blockade and ITIM mutant T in vivo, we then performed GSEA using a gene set specific for TFR-associated markers. TFH from the J43 and ITIM samples were unexpectedly found to be substantially enriched for TFR-associated genes in relation to those of the cGVHD group, and to a greater degree than that of the non-disease control (**Figure 8A**). This analysis suggested that TFH in the context of cGVHD acquired a more TFR-like phenotype with PD-1 blockade and ITIM nonfunctional mutation, and further examination of the transcription of notable TFR vs TFH genes reinforced this impression (**Figure 8B**). Curiously, anti-PD-1 mAb treated and ITIM mutant TFH both demonstrated significant upregulation of the Treg-defining transcription factor *Foxp3* (**Figure 8C**). While we could not confirm this expression by flow cytometry since TFH are gated as Foxp3- during immune analyses, we were able to observe that PD-1 blockade treated and ITIM mutant TFH showed significantly increased expression of Blimp1, a transcriptional regulator that prevents the destabilization of Foxp3 expression, and that TFR from these groups also significantly increased Foxp3 expression (**Figure 8D-E**). These data then solicited the question of TFH/TFR plasticity and whether anti-PD-1 mAb administration and ITIM mutation are able to transform TFH into suppressive TFR. This investigation is still ongoing as of the writing of this thesis, however, our current data points to this possibility.

Because our evidence implied a shift in TFH identity toward a TFR-like phenotype, we next investigated the transcription of genes involved in the signaling pathways responsive to cytokines in control of Treg differentiation. GSEA assessment of signaling downstream of IL-2 demonstrated PD-1 blockade TFH and ITIM mutant TFH enrichment in genes upregulated by STAT5 in response to IL-2 stimulation (**Figure 9A**). However, because IL-2 is a pleiotropic cytokine that both induces Tcon activation and maintains Treg development, we also confirmed the increased expression of regulatory

T cell-associated high affinity IL-2 receptor on TFH from anti-PD-1 mAb and ITIM mutant T groups (**Figure 9B-D**). Our studies also identified a significant increase in the populations of TFH expressing TIGIT and TIM-3, co-inhibitory markers that correlate with enhanced Treg suppressive activity (**Figure 9E-F**). These findings further suggested that PD-1 blockade and ITIM mutant TFH adopted characteristics typically found in regulatory immune cells such as TFR or Treg.

In addition to IL-2, the cytokine TGF-β is also responsible for the development of Treg, both within the thymus and in the peripheral tissues, by inducing Foxp3 expression that drives Treg differentiation. We then explored the transcriptomics of PD-1 blockade and ITIM mutant TFH in response to TGF-β and found that these TFH were significantly enriched for genes upregulated after TGF-β exposure, and to a greater extent than those from negative disease control (**Figure 10A**). This analysis indicated that TFH from the anti-PD-1 mAb and ITIM mutant T groups were more sensitive to proximate TGF-β. However, because TH17 are another cell type involved in cGVHD pathogenesis and are likewise dependent upon TGF-β for differentiation, we also performed GSEA using a curated collection of TH17-associated markers to examine the possibility of a TH17-like bias (GSE32901[233]). PD-1 blockade treated and ITIM mutant TFH were not found to be enriched for the TH17 phenotype, which was further confirmed by the reduced expression of IL-6 signal transducer, which is required for reactivity to the TH17-determining cytokine IL-6 (**Supplementary Figure 7**). This result strengthened our confidence that TFH from the anti-PD-1 mAb and ITIM mutant T groups are less characteristic of the pathogenic T cells observed in cGVHD.

With these findings suggestive of PD-1 blockade treated and ITIM mutant TFH assuming a suppressive identity, we next explored whether the TFH also assumed suppressive functionality. Analysis of the transcriptomics data determined that the TFH from the anti-PD-1 mAb treated and ITIM mutant T groups had increased transcription of

suppressive cytokines TGF-β and IL-10 (**Figure 10B-C**). Flow cytometry studies additionally confirmed the increased production of the Treg-produced and Treg fate-specifying cytokine TGF-β by these TFR-like TFH (**Figure 10D**). Moreover, the PD-1 blockade TFH and ITIM mutant TFH also demonstrated a dramatic and substantial decrease in the production of the pro-inflammatory cytokines IL-21 and IL-17, which are typically secreted by TFH and TH17, respectively (**Figure 10E-F**). This reduction in secreted pathogenic cytokines corroborated the suppressive transcriptomic profiles detailed thus far and provided complementary understanding of these irregularly restorative TFH. Overall, our data intimate a therapeutic mechanism of action for PD-1 blockade and ITIM nonfunctional mutation during cGVHD in which TFH are altered toward a suppressive phenotype, similar to TFR.

DISCUSSION

The programmed cell death protein 1 (PD-1) axis is essential for the maintenance of T cell tolerance. Our established understanding of PD-1 predominantly concerns its immunoinhibitory function in restraining CD4+ and CD8+ T effector (Teff) cells, as the clinical use of blocking anti-PD-1 monoclonal antibodies (mAb) in the treatment of cancer was a pioneering advancement for the field of checkpoint immunotherapy. However, as this area of research continues to grow, it is increasingly apparent that the impact of PD-1 is highly dependent upon its immunological environment and the cell type in which it is expressed. In this study, we investigated the role of the PD-1 pathway in the context of the pathogenic germinal center (GC) reaction in chronic GVHD (cGVHD).

Using the bronchiolitis obliterans (BO) murine model of cGVHD, we observed that therapeutic administration of blocking anti-PD-1 mAb paradoxically reduced the severity of disease. This finding was initially unexpected, as Teff activity has widely been reported to be enhanced with PD-1 blockade. Additionally, these results seemed to contradict data from earlier studies published by the Blazar lab nearly two decades ago examining PD-1 in a model of acute GVHD[234]. In the setting of aGVHD, PD-1 blockade was found to significantly accelerate GVHD mortality, and enhanced donor T cell production of the pro-inflammatory and pathogenic cytokine interferon-γ (IFNγ). However, a defining feature of cGVHD as compared to aGVHD is the presence of a B cell-mediated component to pathogenesis[235], augmented by T follicular helper (TFH) cell support during the GC reaction[13,20,21]. Our data indicates that the restorative effects of anti-PD-1 mAb in the BO cGVHD model were due to influence upon the GC reaction. Findings from another group examining the PD-1 pathway within a primarily TH17/TH1-driven model of cGVHD found that inhibition of PD-1 exacerbated disease[236]. Internally,

in other cGVHD transplantation experiments conducted using a 7% increase in the number of donor T cells present in the graft, which results in an acute and inflammatory form of cGVHD that is driven by activated T cells rather than the GC reaction, we found that PD-1 blockade worsened disease lethality (data not shown), as seen in the early aGVHD studies. Additionally, our studies investigating the prophylactic administration of the anti-PD-1 mAb, in which treatment dosing is scheduled before the initiation of the GC reaction and established disease, also found that PD-1 blockade was unable to improve disease severity. These findings indicate that the setting and timing of anti-PD-1 therapy are critical for therapeutic effects, as administration of PD-1 blockade in the context of highly activated T cells or without the manifestation of GC reaction fails to improve disease.

Closer examination of the effects of anti-PD-1 mAb administration on the splenic GC reaction demonstrated that PD-1 blockade reduced the frequency of GC reaction-supporting cell populations, GC B and TFH, and increased the frequency of GC reaction-suppressing cell populations, T follicular regulatory (TFR) cells. Notably, while the balance of follicular T cells that supported vs suppressed the GC reaction was shifted toward the latter with anti-PD-1 mAb, the absolute TFH cell count was decreased while the TFR cell count was unchanged. This indicated that the pool of CXCR5+ ICOS+ follicular T cells was reduced overall, but more of the follicular T cells were of the TFR phenotype. One potential explanation for this result is that the blocking anti-PD-1 mAb may have also had depleting properties. However, we do not believe this is a likely cause given that the mAb used in these experiments was from the same bioreactor batch as that used in the early aGVHD studies and did not appear to deplete pathogenic T cells in the aGVHD environment. Furthermore, both TFH and TFR express PD-1 and were conspicuously observed to increase following the first two doses of anti-PD-1 mAb, while only TFH count was reduced by the termination of the experiment. Additional

preliminary testing of exclusively blocking anti-PD-1 mAb also resulted in similar improvements to disease severity and GC population frequencies, while depleting anti-PD-1 mAb did not affect disease severity and decreased both TFH and TFR counts. The increase in the number of Foxp3+ T cells observed in the GC after anti-PD-1 mAb administration is also not accounted for by TFH depletion. The source of these additional TFR is unclear, but we maintain the possibility that the decrease in TFH may be related to the increase in TFR density per GC.

Our next line of inquiry was to determine the GC cell-specific effects of PD-1 blockade. We utilized PD-1 KO B and TFH cells in an in vitro simulation of the GC reaction and found that the inhibitory effects of anti-PD-1 mAb on the GC reaction depended on the expression of PD-1 by TFH, while PD-1 in B cells was not necessary. These findings were corroborated in vivo when we tested anti-PD-1 mAb administration in supplementary transplantation experiments with PD-1 deficient B cells. Recipients given *CD19^{Cre}xPD-1$^{fl/fl}$* bone marrow lacked PD-1 expression in all B cells, including GC B, and in these subjects, PD-1 blockade was still found to mitigate cGVHD severity and diminish the frequencies of the GC B and TFH populations. We also tested anti-PD-1 mAb administration in transplants with PD-1 deficient regulatory T (Treg) cells. Recipients given *iFox^{Cre}xPD-1$^{fl/fl}$* bone marrow lacked PD-1 expression on Treg once deletion was induced after the formation of the GC reaction. Because TFR in the BO cGVHD model principally arise from bone marrow-derived Treg, TFR were thus correspondingly PD-1 deficient. In these subjects, PD-1 blockade was again found to reduce disease, but also resulted in a surprising increase in the frequency of the TFR population. While PD-1 deficiency has previously been reported to promote expansion of both TFH and TFR in the blood[79], in our studies, anti-PD-1 mAb administration expanded TFR which were already severely lacking in PD-1 expression. This finding suggested that PD-1 blockade was acting upon PD-1+ TFH or an undifferentiated

follicular PD-1+ T cell pool to create more TFR. Based on this result, and because anti-PD-1 mAb maintained therapeutic effects and inhibited the GC reaction in disease groups with PD-1-deficient GC B and TFR, we believe the predominant effects of PD-1 blockade to target TFH.

Having identified the role of TFH in mediating PD-1 blockade effects on the GC reaction, we then sought to evaluate the contributions of the different PD-1 tyrosine motifs, immunoreceptor tyrosine-based switch motif (ITSM) and immunoreceptor tyrosine-based inhibitory motif (ITIM), that enable signaling[100,102,105]. Using TFH isolated from mice with nonfunctional ITSM or ITIM mutations for in vitro co-culture GC reaction assays, we found that the ITIM, but not ITSM, mutant TFH demonstrated weaker support to GC B class switching. Moreover, we discovered that the ITSM motif in TFH was dispensable for the inhibitory effects of anti-PD-1 mAb on the GC reaction, though the ITIM motif was required. Given our findings that despite increased PD-1 expression by TFH during cGVHD, phosphorylation of the ITSM motif was observed to decrease during the GC reaction, this data was particularly striking. Together, these results lead us to theorize that signaling through the ITIM motif is responsible for TFH support to GCB through the PD-1 pathway, and that PD-1 blockade disrupts signaling downstream of ITIM.

Our results using nonfunctional ITIM or ITSM mutant donor T cells in the T cell graft component during in vivo cGVHD experiments substantiated this assessment. While transplantation of ITSM mutant T cells was found to phenocopy the worsened lethality seen with transplantation of PD-1 deficient T cells, recipients given ITIM mutant donor T cells demonstrated significantly improved survival and reduced disease severity. Furthermore, the nonfunctional ITIM mutation, though having no significant impact upon the Treg/T conventional (Tcon) cell ratio in the donor T cell graft, also had an inhibitory effect on the GC reaction. As with the recipients of therapeutic anti-PD-1 mAb

administration, subjects receiving ITIM mutant donor T cells demonstrated a significant decrease in splenic GCB and TFH frequencies, and simultaneous increase in TFR frequency. Because TFH in the BO cGVHD model are derived from the T cell compartment of the graft, the decreased efficacy in GC support by the TFH of the recipients receiving ITIM mutant donor T cells is a specific consequence of the nonfunctional ITIM mutation. These findings clearly revealed that the ITSM and ITIM motifs of PD-1 on T cells perform discrete functions in the context of cGVHD; while ITSM appears to maintain conventional T cell tolerance, ITIM appears to support TFH development and function.

We then sought to assess the transcriptomic patterns that occurred in TFH as a result of ITIM nonfunctional mutation and PD-1 pathway inhibition in our cGVHD model. A striking initial finding from our gene set enrichment analysis uncovered the apparent lack of a prototypical TFH-like phenotype by TFH from the cGVHD group, as compared to those of the negative disease control group. One might have expected that TFH from mice with a disease driven by the GC reaction would be more deeply enriched for TFH-associated genes. A possible explanation for this result may be that the immunization environment in which TFH are usually studied is vastly different from the post-transplantation and cGVHD environment from which our TFH were isolated, though the establishment of germinal centers in both settings require IL-21 and TFH expression of ICOS. However, both TFH from the anti-PD-1 mAb treated and ITIM mutant donor T cell groups, in which the GC reaction and disease severity were significantly diminished, did demonstrate a TFH-like phenotype by gene set enrichment analysis as compared to that of the negative disease control. This outcome may be explained by the unexpected finding that these TFH also demonstrated significant enrichment for TFR-associated genes.

While PD-1 blockade has previously been determined to improve Treg suppression and proliferation[237,238] and enhance TFR functionality in suppressing the GC reaction[79,239], it was unanticipated that the transcriptomic signatures of anti-PD-1 mAb treated and ITIM deficient TFH would adopt suppressive characteristics. Nonetheless, principal component analysis identified the largest dimension of variance to be between the negative disease control group and the PD-1 blockade and ITIM mutant groups, which indicates that PD-1 blockade and ITIM mutation did not revert TFH to a state found in non-diseased transplant recipients, but rather induced a new and separate phenotype. The combination of these interpretations then suggests some degree of plasticity between TFH and TFR within the follicular T cell pool.

As TFR are acknowledged to generally arise from Foxp3+ precursors[70,74,240,241], their patterns of gene expression include features of both Treg and TFH[74]. An especially notable finding in our gene set analyses was the significant upregulation of the Treg lineage-defining transcription factor *Foxp3*[242–244] in the TFH of the anti-PD-1 mAb treated and ITIM mutant donor T groups. We had conservatively sorted for TFH versus TFR cells on the basis of glucocorticoid-induced TNF receptor (GITR) expression since our appraisal of GITR and Foxp3 overlap confirmed that GITR^{lo} cells were also Foxp3^{lo}, so to find significant differences in Foxp3 expression was surprising. Previous studies examining the transcriptional profile of TFR have reported that Foxp3 is able to modify the TFH program to induce a TFR-like functional state[245], and other investigations have shown that ectopic Foxp3 expression can induce suppressive function in T cells[242,246–248]. Based on these data, we then speculated on the possibility of TFR arising from the follicular T cell pool[75] in a manner reminiscent of peripheral Treg (pTreg) arising from naïve T cells.

Ptreg, unlike natural or thymic Treg (tTreg), develop upon antigen recognition in the secondary lymphoid tissues, and the principal determinants for the generation of

pTreg are the cytokines interleukin (IL)-2[249–255] and transforming growth factor (TGF)-β[251,256–258,254]. Additional enrichment analysis using curated gene sets[259] revealed that the anti-PD-1 mAb treated and ITIM mutant TFH significantly upregulated the expression of genes associated with IL-2 signaling, as well as TGF-β signaling. Because IL-2 signaling inhibits lineage-specifying Bcl6 expression through the STAT5-mediated upregulation of Blimp-1, a transcriptional regulator that stabilizes Foxp3 expression in inflammatory environments[260], it is generally considered to be incongruent with the development of follicular T cells[261–264]. However, the observed increased sensitivity and upregulation of cellular machinery in response to environmental IL-2 and TGF-β by the PD-1 blockade and ITIM mutant TFH is similar to that of pTreg. We also found the transcription of a number of other genes supplementary to *Foxp3* in promoting pTreg development and maintenance, including *Stat5*[265–267], *Irf4*[268,269], *Prdm1*[270,260], *Batf*[271,272], *Runx1*[273,274], *Satb1*[275–277] and *Nr4a* factors[278–281] to mirror that of pTreg gene expression. Computational network analysis by others has previously demonstrated the high degree of positive and negative feedback that enables the “auto-assembly” of the Treg genetic signature regardless of induction environment, and identified the redundancy of transcriptional cofactors other than *Foxp3* for this regulatory program[282]. In light of these findings that support our working theory regarding PD-1 blockade and ITIM mutation modifying TFH or the T follicular pool toward a TFR phenotype, we also assessed the functional potential of these transformed cells.

Regulatory T cells such as TFR and pTreg exert their immunoregulatory capabilities through a variety of different means, including through cell-cell contact via the expression of co-inhibitory molecules and through the secretion of suppressive cytokines. The transcriptomics data of TFH from anti-PD-1 mAb treated and ITIM mutant T groups showed a significant upregulation of the inhibitory receptors cytotoxic T lymphocyte-associated protein (CTLA)-4[283–286,84], T cell immunoreceptor with Ig and ITIM

domains (TIGIT)[287–289], T cell immunoglobulin and mucin domain-containing protein (TIM)-3[290–292], and lymphocyte-activation gene (LAG)-3[293,294]. Regulatory T cell expression of these co-inhibitory molecules is associated with better suppressive ability by competitive reduction of the co-stimulation signals necessary for full T cell activation[295–298] and increased production of the suppressive cytokines IL-10 and TGF-β[297,299–301]. Interestingly, PD-1 blockade and ITIM mutant TFH also demonstrated higher transcription and expression of inducible T cell co-stimulator (ICOS). While ICOS is a defining marker of follicular T cells and is essential for the development of TFH[212,215,211,63,302], it is also required for Foxp3 stability[303] and Treg survival[304,305], and has been associated with enhanced suppressive capacity[306,307].

Transcriptomic analysis of TFH from the anti-PD-1 mAb and ITIM mutant T groups also exhibited a globally immunosuppressive pattern of cytokine production, which was confirmed by flow cytometry. Production of IL-10 and TGF-β, which have been demonstrated to be reduce Teff activity and promote immune tolerance in diverse contexts[308,309], was increased in PD-1 blockade and ITIM mutant TFH, while the production of the GC-supporting cytokine IL-21[223,224,310–312] and the TH17-secreted cytokine IL-17[33,313,314] was decreased. However, while TGF-β is recognized to reduce the generation of GCB and TFH[315,86] and IL-10 has been shown to limit TFH-dependent immunity[316,317], both TGF-β[318,319] and IL-10[320,321], which is ordinarily secreted by follicular T cell populations[320–322,316,317], have also been determined to promote GCB cell responsiveness. Though these reports seem incongruent, it is possible that threshold levels of TGF-β and IL-10 may differentially influence the equilibrium of the GC reaction, and we are currently planning further experiments to clarify the immunosuppressive function of TFR-like anti-PD-1 mAb treated and ITIM mutant TFH.

Though our data provides strong support for the induction of a suppressive phenotype with PD-1 blockade and nonfunctional ITIM mutation, we wish to continue exploring several avenues to address emerging questions.

- Functional suppression by the PD-1 blockade and ITIM mutant TFH needs to be more thoroughly assessed. To this end, we are conducting in vitro co-culture assays using TFH isolated from transplanted mice given therapeutic anti-PD-1 mAb or ITIM mutant donor T cells and evaluate GC B cell class switching. Reduction of class switching in conditions containing TFR-like TFH will cement our finding that PD-1 blockade and ITIM mutation not only express phenotypic markers characteristics of TFR, but also exhibit reduced support to GC B.
- The source of the expanded TFR repertoire and TFR-like TFH also needs to be elucidated. To uncover the origin of the increased population of TFR and the emerging TFR-like TFH, we are conducting transplantation experiments with mice receiving bone marrow from congenic CD45.2 mice and purified T cells from CD45.1 mice. If the expanded TFR and TFR-like TFH are derived from the TFH or donor T cells, they will express CD45.1 and we will be able to verify whether PD-1 blockade enables the proliferation of bone-marrow-derived TFR or induces a TFR-like state in donor T cell-derived TFH.
- The impact of the nonfunctional ITIM mutation demands deeper investigation. At this time, it is unclear whether the TFR-like characteristics of the ITIM deficient TFH are due to an extrinsic property, possibly the indirect result of an environment in which cGVHD is less severe, or due to an intrinsic property that is a direct result of the ITIM mutation. Transplantation of a T cell graft composed of both WT and ITIM mutant T cells, to ensure a robust cGVHD state, would help to refine the degree of cell-extrinsic vs cell-intrinsic influence of the ITIM mutation. Additionally, while the ratio of CD4+ to CD8+ T cells is not significantly changed in the ITIM mutant mice, it is

possible that the ITIM mutant CD8+ T cells exhibit altered functionality that changes cGVHD pathogenesis. Transplantation of separately isolated CD4+ and CD8+ T cells from WT and ITIM mutant mice would inform this potentially confounding variable. Lastly, the temporal effects of nonfunctional ITIM mutant donor T cells need clarification. Should the requisite strains ever become available, transplantation of T cells with inducible ITIM deletion would aid us in determining whether ITIM mutation prevents TFH generation and skews the TFR:TFH ratio from the beginning of transplantation or if ITIM deficiency enables TFR-like behavior by TFH during the GC reaction.

In summary, this study establishes evidence of PD-1 pathway support for the GC reaction and distinguishes the criticality of the PD-1 ITIM, but not ITSM, motif in TFH. Our data further demonstrates that PD-1 blockade and nonfunctional ITIM mutation shift the follicular T cell balance toward a suppressive phenotype and indicates the fluid nature within the follicular T cell pool. In illuminating these mechanisms underlying the GC, our research identifies potential approaches to modulate T cell-dependent humoral immunity and instructs additional means by which to attenuate cGVHD.

Figure Legends

Figure 1. TFH in cGVHD increase expression of PD-1 but not ITSM phosphorylation during germinal center reaction

B10.BR mice were conditioned with cyclophosphamide (120 mg/kg/day, days -3 and -2) and total body irradiation (8.3Gy, day-1), and given bone marrow transplant on day 0. Recipient mice were given $1.0x10^6$ T-cell depleted bone marrow cells alone (BM only), with $7.0x10^4$ purified T cells from C57/BL6 mice (cGVHD). (A) At day 21 and day 35 post-transplantation, PD-1 (green), PNA (red) and CD4 (blue) expression was confirmed in splenic germinal center populations. (B) TFH were gated as CD4+ CXCR5+ PD1+ Foxp3-, and (C) TFH expression of PD-1 was confirmed to increase with germinal center progression. (D) TFH expression of phospho-PD1, capturing ITSM phosphorylation event, did not increase with germinal center progression. Data are representative of two experiments, shown with mean ± SEM. * $p < 0.05$, ** $p < 0.01$, *** $p < 0.001$, **** $p < 0.0001$

Figure 2. Therapeutically administered PD-1 blockade paradoxically attenuates pathology in cGVHD

B10.BR mice were conditioned with cyclophosphamide (120 mg/kg/day, days -3 and -2) and total body irradiation (8.3Gy, day-1), and given bone marrow transplant on day 0. Recipient mice were given $1.0x10^6$ T-cell depleted bone marrow cells alone (BM only), with $7.0x10^4$ purified T cells from C57/BL6 mice (cGVHD). Blocking anti-PD-1 monoclonal antibody (J43) was administered therapeutically after day 28, at a dosing schedule of 250 µg 2x/week (anti-PD1 mAb); cGVHD mice were administered isotype control at the same dosing schedule. (A) Mass and survival were not shown to improve with therapeutic anti-PD-1 blockade. (B) Pulmonary function tests performed 7 weeks

post-transplantation demonstrated significant improvement in lung dysfunction with therapeutic anti-PD-1 blockade. (C) Ig deposition (green) and (D) collagen deposition (blue) in lung tissues showed reduction in cGVHD pathology with therapeutic anti-PD-1 blockade. (E) Absolute counts of GC populations out of 500,000 total splenocytes were assessed at day 35, and TFR and TFH counts were increased after one week of anti-PD-1 mAb administration. Data are representative of three experiments, shown with mean ± SEM. * $p < 0.05$, ** $p < 0.01$, *** $p < 0.001$, **** $p < 0.0001$

Figure 3. Therapeutically administered PD-1 blockade reduces germinal center reaction in cGVHD

B10.BR mice were conditioned with cyclophosphamide (120 mg/kg/day, days -3 and -2) and total body irradiation (8.3Gy, day-1), and given bone marrow transplant on day 0. Recipient mice were given $1.0x10^6$ T-cell depleted bone marrow cells alone (BM only), with $7.0x10^4$ purified T cells from C57/BL6 mice (cGVHD). Blocking anti-PD-1 monoclonal antibody (J43) was administered therapeutically after day 28, at a dosing schedule of 250 µg 2x/week (anti-PD1 mAb); cGVHD mice were administered isotype control at the same dosing schedule. Absolute counts of GC populations out of 500,000 total splenocytes were assessed, and (A) GCB and TFH counts were reduced at day 49 post-transplantation with therapeutic anti-PD-1 mAb. Splenic germinal center populations were assessed at day 49, and (B) GC B cell frequency, and (C) TFR frequency, TFH frequency, and TFR:TFH ratio all indicated a significant decrease in the germinal center reaction in mice therapeutically treated with anti-PD-1 mAb blockade. (D) Splenic sections were evaluated by immunofluorescence for GC, with colocalization of CD4 (green), B220 (blue), and PNA (red). (E) GC size, measured by area of PNA staining, and (F) GC frequency per mm^2 of spleen section were quantified and found to be reduced with therapeutic anti-PD-1 mAb blockade. (G) TFR frequency per GC was

calculated by dividing measured area of Foxp3 staining by measured area of PNA staining and found to be increased with therapeutic anti-PD-1 mAb. Data are representative of three experiments, shown with mean ± SEM. * $p < 0.05$, ** $p < 0.01$, *** $p < 0.001$, **** $p < 0.0001$

Figure 4. Inhibitory effects of PD-1 blockade on germinal center reaction in vitro are mediated by TFH with intact ITIM

C57/BL6, PD1KO, ITIM mutant, or ITSM mutant mice were immunized with NP-OVA/CFA and draining lymph nodes were harvested after 7 days. B and T cells were negatively enriched and CD19+ B cells and CD4+ CXCR5+ ICOS+ GITR- TFH cells were isolated via sterile FACS for downstream functional assay. (A) 50,000 B cells were plated with 30,000 TFH cells in complete media with the addition of anti-CD3 and anti-IgM and cultured without media change for 6 days at 5% O2, 37˚C. Cultured cells were analyzed by flow cytometry. (B) Anti-PD-1 mAb blockade was found to significantly reduce the frequency of class-switched B cells, though this inhibitory effect was lost in cultures with PD1 KO TFH cells, and PD-1 deficient B cells did not demonstrate reduced capacity for class switching. (C) ITIM mutant TFH were found to significantly reduce the frequency of class-switched B cells, and the addition of anti-PD-1 mAb blockade was not found to reduce class-switching further. (D) ITSM mutant TFH were not found to change the frequency of class-switched B cells, and the addition of anti-PD-1 mAb blockade maintained inhibitory effect on B cell class switching. Data are representative of two experiments, shown with mean ± SEM. * $p < 0.05$, ** $p < 0.01$, *** $p < 0.001$, **** $p < 0.0001$

Figure 5. ITIM mutant donor T cells in T cell graft compartment result in reduced pathology in cGVHD

B10.BR mice were conditioned with cyclophosphamide (120 mg/kg/day, days -3 and -2) and total body irradiation (8.3Gy, day-1), and given bone marrow transplant on day 0. Recipient mice were given $1.0x10^6$ T-cell depleted bone marrow cells alone (BM only), with $7.0x10^4$ purified T cells from C57/BL6 mice (cGVHD) or ITIM mutant mice (ITIM mutant T). (A) Mass was not changed, but survival significantly improved with ITIM mutant donor T cells. (B) Pulmonary function tests performed 7 weeks post-transplantation demonstrate significant reduction in lung dysfunction with ITIM mutant donor T cells. (C) Ig deposition (green) and (D) collagen deposition (blue) in lung tissues show reduction in cGVHD pathology with ITIM mutant donor T cells. Data are representative of three experiments, shown with mean ± SEM. * $p < 0.05$, ** $p < 0.01$, *** $p < 0.001$, **** $p < 0.0001$

Figure 6. ITIM mutant donor T cells in T cell graft compartment lessen germinal center reaction in cGVHD

B10.BR mice were conditioned with cyclophosphamide (120 mg/kg/day, days -3 and -2) and total body irradiation (8.3Gy, day-1), and given bone marrow transplant on day 0. Recipient mice were given $1.0x10^6$ T-cell depleted bone marrow cells alone (BM only), with $7.0x10^4$ purified T cells from C57/BL6 mice (cGVHD) or ITIM mutant mice (ITIM mutant T). Splenic germinal center populations were assessed at transplant termination at day 49, and PD-1 expression and percentage of PD-1+ cells were examined. (A) ITIM mutant TFH showed a slight but significant decrease in PD-1 expression compared to WT TFH, though (B) the number of PD-1+ TFH was unchanged. (C) GC B cell frequency, TFR frequency, TFH frequency and TFR:TFH ratio all indicated a significant decrease in the germinal center reaction in mice transplanted with ITIM mutant donor T cells. (D) Splenic sections were evaluated by immunofluorescence for GC, with colocalization of CD4 (green), B220 (blue), and PNA (red). (E) GC size, measured by

area of PNA staining, and (F) GC frequency per mm^2 of spleen section were quantified and found to be reduced with ITIM mutant donor T cells. Data are representative of three experiments, shown with mean ± SEM. * $p < 0.05$, ** $p < 0.01$, *** $p < 0.001$, **** $p < 0.0001$

Figure 7. TFH in cGVHD have a unique GSEA signature that is similarly changed with therapeutically administered PD-1 blockade and ITIM mutant T cell graft

B10.BR mice were conditioned with cyclophosphamide (120 mg/kg/day, days -3 and -2) and total body irradiation (8.3Gy, day-1), and given bone marrow transplant on day 0. Recipient mice were given $1.0x10^6$ T-cell depleted bone marrow cells alone (BM only), with $7.0x10^4$ purified T cells from C57/BL6 mice (cGVHD) or ITIM mutant mice (ITIM mutant T). Blocking anti-PD-1 monoclonal antibody was administered therapeutically after day 28, at a dosing schedule of 250 µg 2x/week (anti-PD1 mAb); cGVHD mice were administered isotype control at the same dosing schedule. T cells were negatively enriched, and (A) CD4+ CXCR5+ ICOS+ GITR- TFH cells were isolated via sterile FACS for bulk RNA sequencing. (B) Flow cytometry evaluation of CD4+ CXCR5+ ICOS+ GITR- cells demonstrated minimal Foxp3 expression. After alignment and quantification, intersect set of genes was identified and principal component analysis (PCA) was performed. (C) Samples were found to cluster discretely, with the exception of significant overlap between ITIM mutant TFH and the ITIM mutant TFH + anti-PD1 mAb-treatment groups. RNA sequencing data was compared against a gene set specific for TFH versus Tcon, and (D) TFH from cGVHD mice were not found to be more TFH-like than Tcon-like, compared to that of BM only. while anti-PD-1 mAb treated and ITIM mutant TFH were found to be more enriched for TFH-associated genes.

Figure 8. Therapeutically administered PD-1 blockade and ITIM mutant T cell graft reshape TFH to have TFR phenotype in cGVHD

B10.BR mice were conditioned with cyclophosphamide (120 mg/kg/day, days -3 and -2) and total body irradiation (8.3Gy, day-1), and given bone marrow transplant on day 0. Recipient mice were given $1.0x10^6$ T-cell depleted bone marrow cells alone (BM only), with $7.0x10^4$ purified T cells from C57/BL6 mice (cGVHD) or ITIM mutant mice (ITIM mutant T). Blocking anti-PD-1 monoclonal antibody was administered therapeutically after day 28, at a dosing schedule of 250 μg 2x/week (anti-PD1 mAb); cGVHD mice were administered isotype control at the same dosing schedule. RNA sequencing data from flow sorted CD4+ CXCR5+ ICOS+ GITR- TFH cells was compared against a gene set specific for TFR vs TFH cells, and (A) anti-PD-1 mAb treated TFH and ITIM mutant TFH were found to be more significantly enriched for TFR-associated genes than cGVHD TFH, though BM only TFH did not display TFR-like phenotype as compared to cGVHD TFH. (B-C) Upregulated genes of interest in anti-PD-1 mAb treated TFH and ITIM mutant TFH included those encoding for Treg-associated markers such as Foxp3, Blimp1, high affinity IL-2 receptor, CTLA-4, LAG-3, TIGIT, TIM-3, TGF-β and IL-10. (D) Flow cytometry phenotyping demonstrated significantly increased expression of Blimp1 in the anti-PD-1 mAb treated and ITIM mutant TFH. (E) Foxp3 expression was observed to be significantly increased in TFR from anti-PD-1 mAb treated and ITIM mutant donor T cell groups. Flow cytometry data are representative of two experiments, shown with mean ± SEM. * $p < 0.05$, ** $p < 0.01$, *** $p < 0.001$, **** $p < 0.0001$

Figure 9. Therapeutically administered PD-1 blockade and ITIM mutant T cell graft reshape TFH to express Treg-associated markers

B10.BR mice were conditioned with cyclophosphamide (120 mg/kg/day, days -3 and -2) and total body irradiation (8.3Gy, day-1), and given bone marrow transplant on day 0.

Recipient mice were given $1.0x10^6$ T-cell depleted bone marrow cells alone (BM only), with $7.0x10^4$ purified T cells from C57/BL6 mice (cGVHD) or ITIM mutant mice (ITIM mutant T). Blocking anti-PD-1 monoclonal antibody was administered therapeutically after day 28, at a dosing schedule of 250 µg 2x/week (anti-PD1 mAb); cGVHD mice were administered isotype control at the same dosing schedule. RNA sequencing data from flow sorted CD4+ CXCR5+ ICOS+ GITR- TFH cells was compared against a gene set specific for IL-2 and STAT5 signaling, and (A) anti-PD-1 mAb treated TFH and ITIM mutant TFH demonstrated transcriptomic profiles enriched for pathways downstream of IL-2 and were confirmed to have higher transcription of (B-D) high affinity IL-2 receptor subunits. Flow cytometry phenotyping also showed an increase in the populations of (E) TIGIT+ and (F) TIM3+ TFH. Flow cytometry data are representative of two experiments, shown with mean ± SEM. * $p < 0.05$, ** $p < 0.01$, *** $p < 0.001$, **** $p < 0.0001$

Figure 10. Therapeutically administered PD-1 blockade and ITIM mutant T cell graft reshape TFH to secrete suppressive cytokine in cGVHD

B10.BR mice were conditioned with cyclophosphamide (120 mg/kg/day, days -3 and -2) and total body irradiation (8.3Gy, day-1), and given bone marrow transplant on day 0. Recipient mice were given $1.0x10^6$ T-cell depleted bone marrow cells alone (BM only), with $7.0x10^4$ purified T cells from C57/BL6 mice (cGVHD) or ITIM mutant mice (ITIM mutant T). Blocking anti-PD-1 monoclonal antibody was administered therapeutically after day 28, at a dosing schedule of 250 µg 2x/week (anti-PD1 mAb); cGVHD mice were administered isotype control at the same dosing schedule. RNA sequencing data from flow sorted CD4+ CXCR5+ ICOS+ GITR- TFH cells was compared against a gene set specific for TGF-β signaling, and (A-B) anti-PD-1 mAb treated TFH and ITIM mutant TFH were found to significantly upregulate transcription of genes associated with TGF-β signaling, as well as (C) increased transcription of suppressive cytokine IL-10.

Intracellular flow cytometry confirmed the (D) increased production of TGF-β in anti-PD-1 mAb treated and ITIM mutant TFH. (E-F) Production of inflammatory cytokines IL-21 and IL-17 were significantly reduced in anti-PD-1 mAb treated and ITIM mutant TFH. Flow cytometry data are representative of two experiments, shown with mean ± SEM. * $p < 0.05$, ** $p < 0.01$, *** $p < 0.001$, **** $p < 0.0001$

Supplementary Figure 1. T cells from ITIM mutant, but not ITSM mutant, show phospho-PD-1 signal

Splenocytes from naïve C57/BL6, ITIM mutant and ITSM mutant mice were harvested and stained for CD4, Foxp3, PD-1 and phospho-PD1. ITIM mutant and ITSM mutant CD4+ T cells were assessed for phospho-PD1 staining, and (A) ITIM mutant T cells were found to have greater staining than ITSM mutant for phospho-PD1, which has previously been reported to capture the ITSM phosphorylation event. Frequencies of Foxp3- and Foxp3+ cells were analyzed, and (B) ITIM mice were found to have comparable Treg and Tcon levels as WT, though ITSM mice demonstrated significant increase in Treg frequency. Assessment of PD-1 staining in Treg and Tcon showed (C) significantly greater frequency of PD-1+ Treg and Tcon in both ITIM and ITSM mice, as compared to WT. (D) Treg expression of PD-1 was significantly greater in both ITIM and ITSM mice as compared to WT, and (E) Tcon expression of PD-1 was significantly greater in ITSM, though not ITIM, mice. Data are representative of two experiments, shown with mean ± SEM. * $p < 0.05$, ** $p < 0.01$, *** $p < 0.001$, **** $p < 0.0001$

Supplementary Figure 2. Prophylactic administration of PD-1 blockade leads to no improvement in cGVHD

B10.BR mice were conditioned with cyclophosphamide (120 mg/kg/day, days -3 and -2) and total body irradiation (8.3Gy, day-1), and given bone marrow transplant on day 0.

Recipient mice were given $1.0x10^6$ T-cell depleted bone marrow cells alone (BM only), with $7.0x10^4$ purified T cells from C57/BL6 mice (cGVHD) or ITIM mutant mice (ITIM mutant T). Blocking anti-PD-1 monoclonal antibody was administered prophylactically between day 1 and day 28 post-transplantation, at a dosing schedule of 250 µg 2x/week (anti-PD1 mAb); cGVHD mice were administered isotype control at the same dosing schedule. (A) Mass and survival were not shown to change with prophylactic anti-PD-1 blockade. (B) Pulmonary function tests failed to demonstrate improvement in lung dysfunction with prophylactic anti-PD-1 blockade. (C) TFH frequency was reduced and TFR:TFH ratio was increased, but GCB frequency was unaffected by prophylactic anti-PD-1 blockade. Data are representative of two experiments, shown with mean ± SEM. * $p < 0.05$, ** $p < 0.01$, *** $p < 0.001$, **** $p < 0.0001$

Supplementary Figure 3. Therapeutic administration of PD-1 depletion leads to no improvement in cGVHD

B10.BR mice were conditioned with cyclophosphamide (120 mg/kg/day, days -3 and -2) and total body irradiation (8.3Gy, day-1), and given bone marrow transplant on day 0. Recipient mice were given $1.0x10^6$ T-cell depleted bone marrow cells alone (BM only), with $7.0x10^4$ purified T cells from C57/BL6 mice (cGVHD). Blocking anti-PD-1 monoclonal antibody (332.8H3) and depleting anti-PD-1 monoclonal antibody (332.1H5) were administered therapeutically after day 28, at a dosing schedule of 250 µg 2x/week; cGVHD mice were administered isotype control at the same dosing schedule. (A) Mass and survival were not shown to change with blocking or depleting anti-PD-1 mAb administered therapeutically. (B) Pulmonary function tests demonstrated improvement in lung dysfunction with therapeutic blocking anti-PD-1 mAb, but not depleting anti-PD-1 mAb. (C) Therapeutic depleting anti-PD-1 mAb drastically reduced frequencies of all germinal center populations. Data is from one experiment (due to limited availability of

custom antibodies from collaborating lab), shown with mean ± SEM. * $p < 0.05$, ** $p < 0.01$, *** $p < 0.001$, **** $p < 0.0001$

Supplementary Figure 4. PD-1 deficiency on CD19+ B cells in bone marrow compartment of graft does not improve cGVHD

B10.BR mice were conditioned with cyclophosphamide (120 mg/kg/day, days -3 and -2) and total body irradiation (8.3Gy, day-1), and given bone marrow transplant on day 0. Recipient mice were given $1.0x10^6$ T-cell depleted *CD19^{Cre} x PD-1$^{fl/fl}$* bone marrow cells alone (Cre- BM only; Cre+ BM only), with $7.0x10^4$ purified T cells from C57/BL6 mice (Cre- cGVHD; Cre+ cGVHD). Blocking anti-PD-1 monoclonal antibody (J43) was administered therapeutically after day 28, at a dosing schedule of 250 µg 2x/week; cGVHD mice were administered isotype control at the same dosing schedule. (A) Mass and survival were not shown to change with transplantation of Cre+ bone marrow. (B) Pulmonary function tests demonstrated improvement with blocking anti-PD-1 mAb, regardless of Cre- or Cre+ bone marrow graft. (C) CD19+ GL7+ FAS+ GC B cells from Cre+ bone marrow were confirmed to have reduced expression of PD-1. (D) Cre+ bone marrow increased TFR frequency and TFR:TFH ratio but did not reduce GCB frequency. Data is representative of two experiments, shown with mean ± SEM. * $p < 0.05$, ** $p < 0.01$, *** $p < 0.001$, **** $p < 0.0001$

Supplementary Figure 5. PD-1 deficiency on Foxp3+ Treg cells in bone marrow compartment of graft does not improve cGVHD

B10.BR mice were conditioned with cyclophosphamide (120 mg/kg/day, days -3 and -2) and total body irradiation (8.3Gy, day-1), and given bone marrow transplant on day 0. Recipient mice were given $1.0x10^6$ T-cell depleted *iFoxp3^{Cre} x PD-1$^{fl/fl}$* bone marrow cells alone (wt/wt BM only; fl/fl BM only), with $7.0x10^4$ purified T cells from C57/BL6 mice

(wt/wt cGVHD; fl/fl cGVHD). Blocking anti-PD-1 monoclonal antibody (J43) was administered therapeutically after day 28, at a dosing schedule of 250 µg 2x/week; cGVHD mice were administered isotype control at the same dosing schedule. At day 28, all groups were administered 1 mg tamoxifen daily for 5 consecutive days. (A) Mass and survival were both found to be significantly affected by tamoxifen administration, which was observed to have severe toxicity effects. (B) Pulmonary function tests demonstrated improvement with blocking anti-PD-1 mAb, regardless of wt/wt or fl/fl bone marrow graft. (C) CD4+ CXCR5+ ICOS+ Foxp3+ TFR cells from mice receiving fl/fl bone marrow were confirmed to have reduced expression of PD-1. (D) Fl/fl bone marrow reduced TFR frequency and TFR:TFH ratio. Data is representative of two experiments, shown with mean ± SEM. * $p < 0.05$, ** $p < 0.01$, *** $p < 0.001$, **** $p < 0.0001$

Supplementary Figure 6. cGVHD TFH upregulate PD-1 pathway associated genes

B10.BR mice were conditioned with cyclophosphamide (120 mg/kg/day, days -3 and -2) and total body irradiation (8.3Gy, day-1), and given bone marrow transplant on day 0. Recipient mice were given $1.0x10^6$ T-cell depleted bone marrow cells alone (BM only), with $7.0x10^4$ purified T cells from C57/BL6 mice (cGVHD) or ITIM mutant mice (ITIM mutant T). Blocking anti-PD-1 monoclonal antibody was administered therapeutically after day 28, at a dosing schedule of 250 µg 2x/week (anti-PD1 mAb); cGVHD mice were administered isotype control at the same dosing schedule. RNA sequencing data from flow sorted CD4+ CXCR5+ ICOS+ GITR- TFH cells was compared against a gene set specific for PD-1 signaling. (A-B) TFH from the negative disease control group were not found to be enriched for genes associated with PD-1 signaling, as compared to cGVHD TFH, while both anti-PD-1 mAb treated and ITIM mutant TFH demonstrated significant upregulation of PD-1 pathway associated genes.

Supplementary Figure 7. Therapeutically administered PD-1 blockade and ITIM mutant T cell graft do not reshape TFH to TH17 phenotype in cGVHD

B10.BR mice were conditioned with cyclophosphamide (120 mg/kg/day, days -3 and -2) and total body irradiation (8.3Gy, day-1), and given bone marrow transplant on day 0. Recipient mice were given $1.0x10^6$ T-cell depleted bone marrow cells alone (BM only), with $7.0x10^4$ purified T cells from C57/BL6 mice (cGVHD) or ITIM mutant mice (ITIM mutant T). Blocking anti-PD-1 monoclonal antibody was administered therapeutically after day 28, at a dosing schedule of 250 μg 2x/week (anti-PD1 mAb); cGVHD mice were administered isotype control at the same dosing schedule. RNA sequencing data from flow sorted CD4+ CXCR5+ ICOS+ GITR- TFH cells was compared against a list of genes specific for TH17 enriched versus TH17 negative CD4+ T cells. (A) Anti-PD-1 mAb treated TFH and ITIM mutant TFH were more enriched for the TH17 negative phenotype, while negative disease control TFH appeared more TH17-like, as compared to cGVHD TFH. (B) Flow cytometry phenotyping demonstrated reduced expression of IL-6 signal transducer in TFH from anti-PD-1 mAb and ITIM mutant T groups. Flow cytometry data are representative of two experiments, shown with mean ± SEM. * $p < 0.05$, ** $p < 0.01$, *** $p < 0.001$, **** $p < 0.0001$

Supplementary Figure 8. ITSM mutant donor T cells phenocopies PD-1 KO donor T cells and accelerates lethality in cGVHD

B10.BR mice were conditioned with cyclophosphamide (120 mg/kg/day, days -3 and -2) and total body irradiation (8.3Gy, day-1), and given bone marrow transplant on day 0. Recipient mice were given $1.0x10^6$ T-cell depleted bone marrow cells alone (BM only), with $7.0x10^4$ purified T cells from C57/BL6 mice (cGVHD), ITIM mutant mice (ITIM mutant T), ITSM mutant mice (ITSM mutant T) or *Pdcd1-/-* mice (PD-1KO T). (A-C) Mass was not shown to change with either ITSM mutant or PD-1 KO T cells, but survival

was significantly diminished. Due to low survival rates, further analyses of remaining subjects were not conducted. Data are representative of three experiments, shown with mean ± SEM. * $p < 0.05$, ** $p < 0.01$, *** $p < 0.001$, **** $p < 0.0001$

Figures

Figure 1

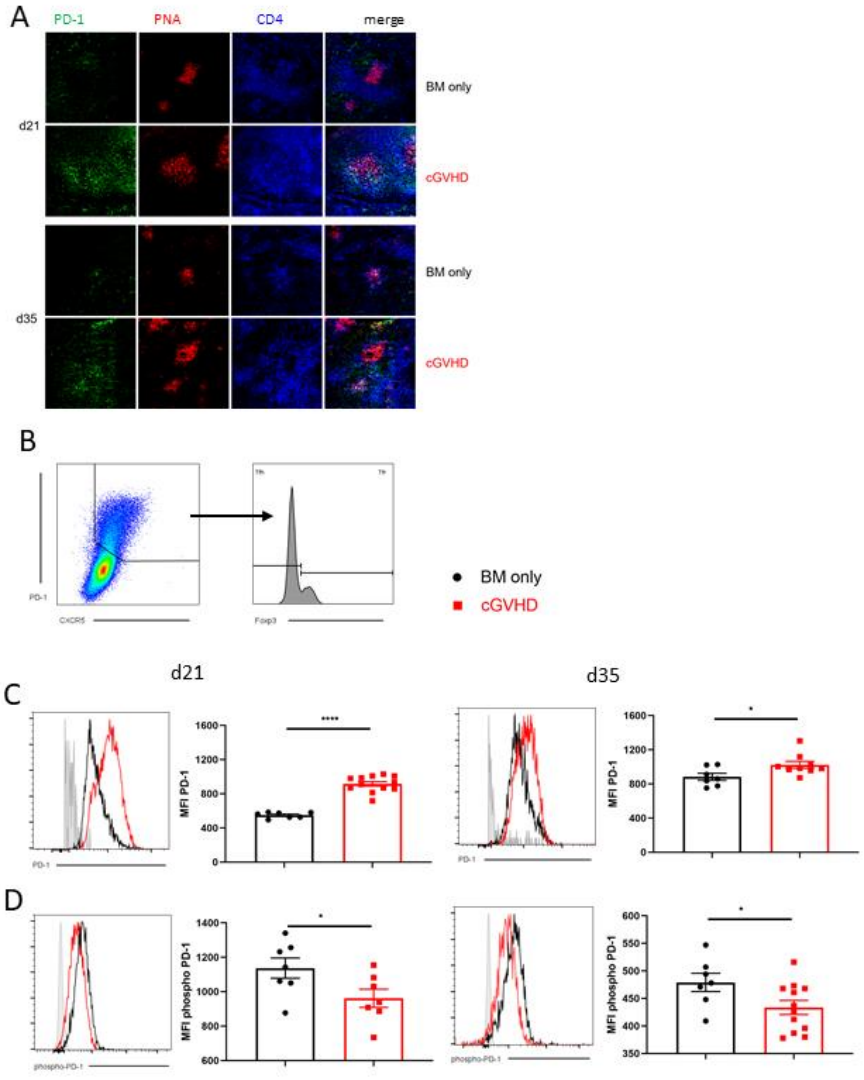

Figure 2

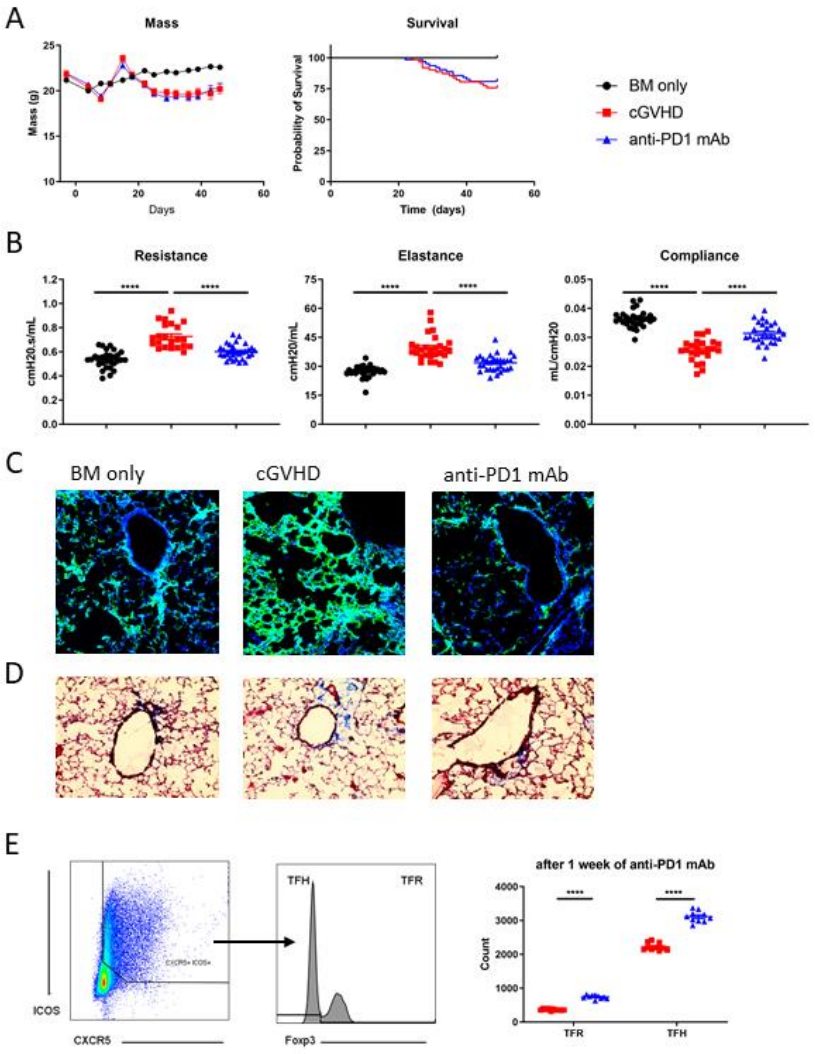
A
Mass
Mass (g)
Days
Survival
Probability of Survival
Time (days)
BM only
cGVHD
anti-PD1 mAb
B
Resistance
cmH20.s/mL
Elastance
cmH20/mL
Compliance
mL/cmH20
****
C
BM only
cGVHD
anti-PD1 mAb
D
E
ICOS
CXCR5
TFH
TFR
Foxp3
after 1 week of anti-PD1 mAb
Count
TFR
TFH

Figure 3

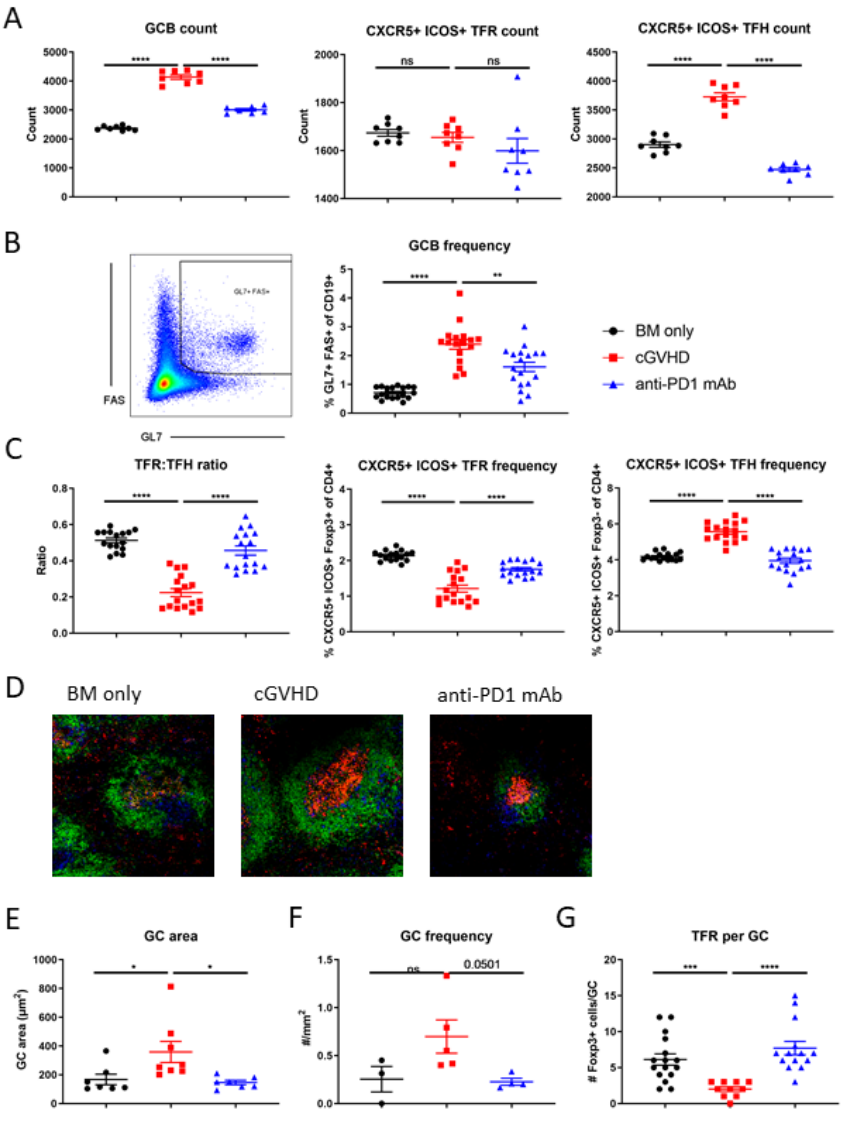
A
GCB count
CXCR5+ ICOS+ TFR count
CXCR5+ ICOS+ TFH count
Count
ns
****
B
GCB frequency
% GL7+ FAS+ of CD19+
FAS
GL7
BM only
cGVHD
anti-PD1 mAb
C
TFR:TFH ratio
Ratio
CXCR5+ ICOS+ TFR frequency
% CXCR5+ ICOS+ Foxp3+ of CD4+
CXCR5+ ICOS+ TFH frequency
% CXCR5+ ICOS+ Foxp3- of CD4+
D
BM only
cGVHD
anti-PD1 mAb
E
GC area
GC area (μm²)
F
GC frequency
0.0501
#/mm²
G
TFR per GC
Foxp3+ cells/GC

Figure 4

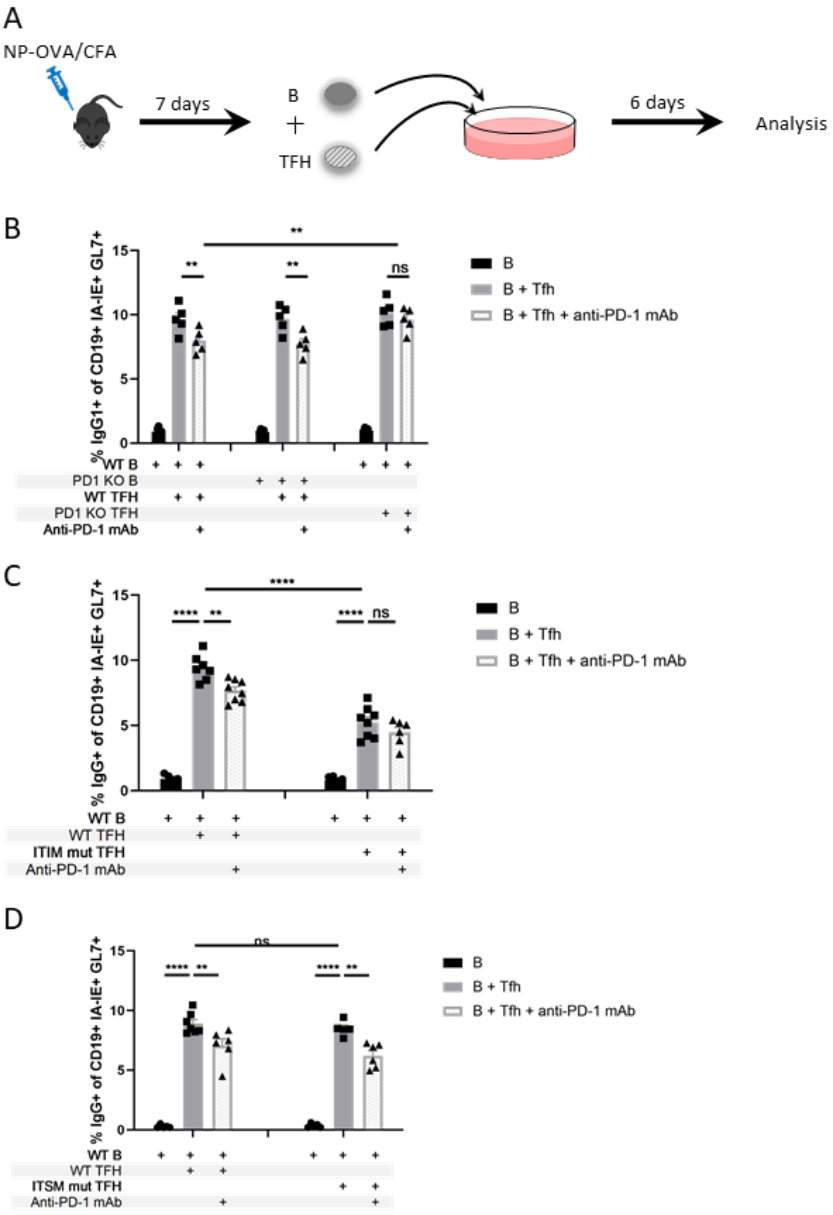
A
NP-OVA/CFA
7 days
B
+
TFH
6 days
Analysis
B
% IgG1+ of CD19+ IA-IE+ GL7+
**
**
**
ns
WT B
PD1 KO B
WT TFH
PD1 KO TFH
Anti-PD-1 mAb
B
B + Tfh
B + Tfh + anti-PD-1 mAb
C
% IgG+ of CD19+ IA-IE+ GL7+
****
****
**
****
ns
WT B
WT TFH
ITIM mut TFH
Anti-PD-1 mAb
B
B + Tfh
B + Tfh + anti-PD-1 mAb
D
% IgG+ of CD19+ IA-IE+ GL7+
ns
****
**
****
**
WT B
WT TFH
ITSM mut TFH
Anti-PD-1 mAb
B
B + Tfh
B + Tfh + anti-PD-1 mAb

Figure 5

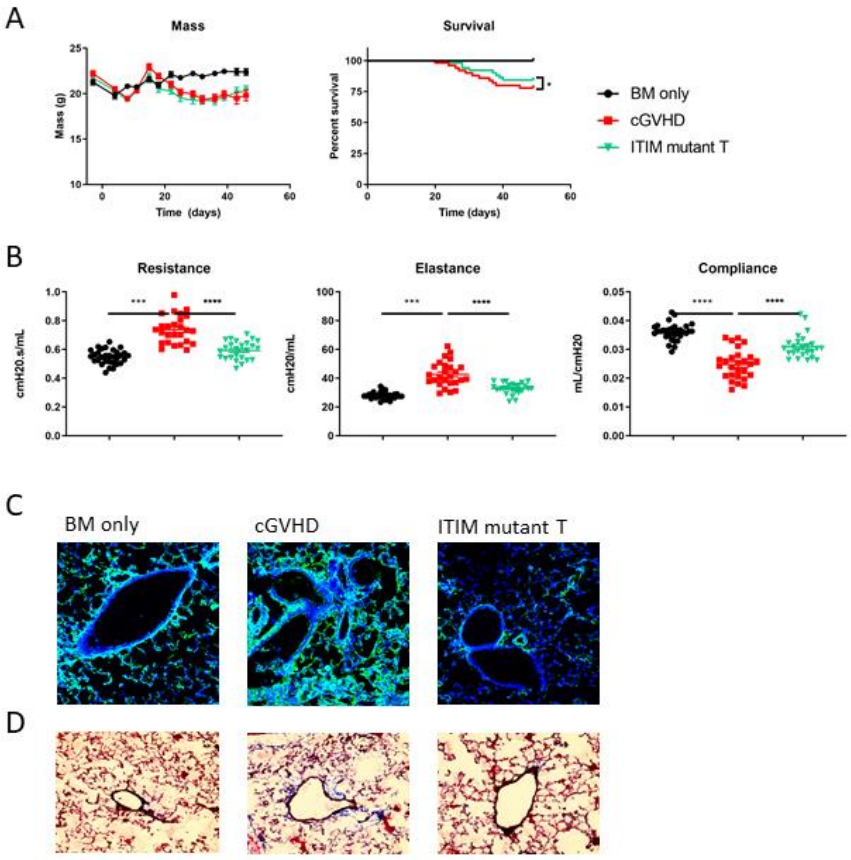
A
Mass
Mass (g)
Time (days)
Survival
Percent survival
Time (days)
BM only
cGVHD
ITIM mutant T
B
Resistance
cmH20.s/mL
Elastance
cmH20/mL
Compliance
mL/cmH20
C
BM only
cGVHD
ITIM mutant T
D

Figure 6

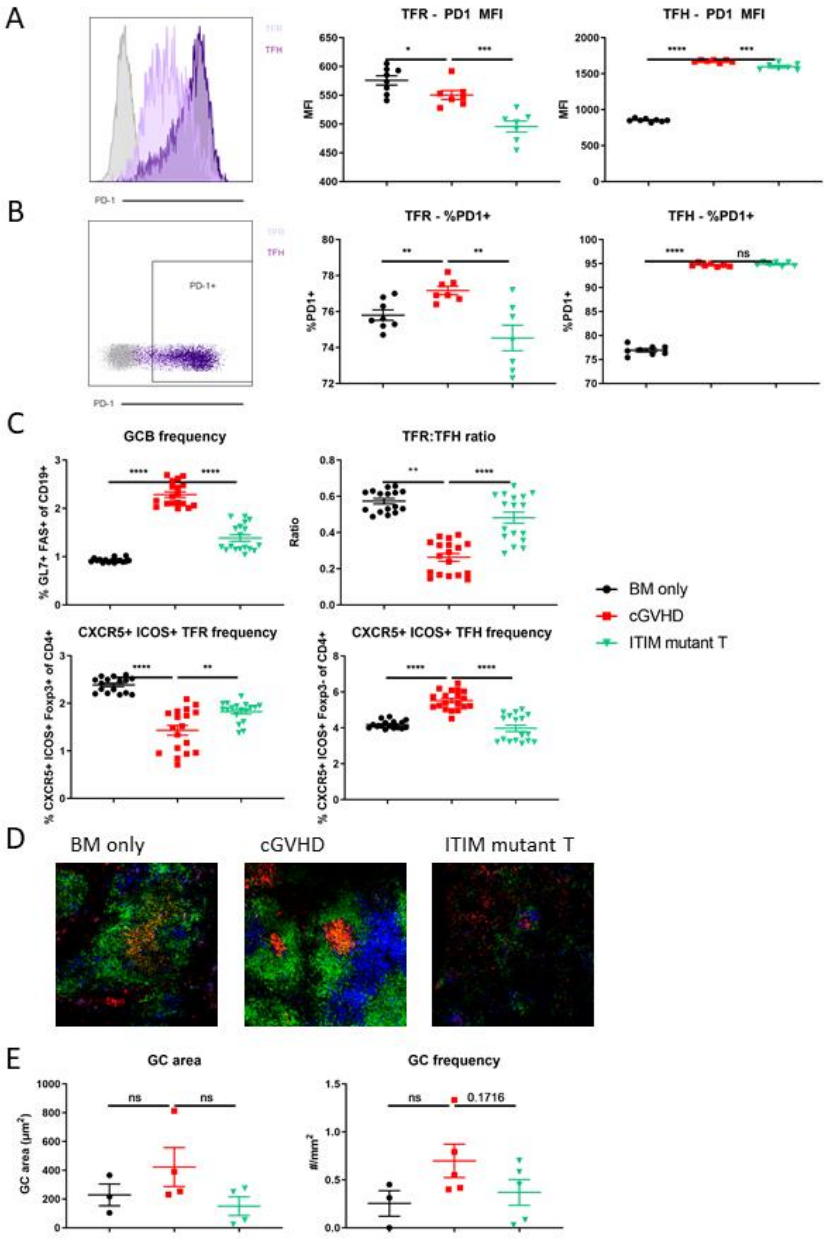
A
TFR - PD1 MFI
TFH - PD1 MFI
MFI
TFR
TFH
PD-1
B
TFR - %PD1+
TFH - %PD1+
%PD1+
PD-1+
C
GCB frequency
TFR:TFH ratio
% GL7+ FAS+ of CD19+
Ratio
CXCR5+ ICOS+ TFR frequency
CXCR5+ ICOS+ TFH frequency
% CXCR5+ ICOS+ Foxp3+ of CD4+
% CXCR5+ ICOS+ Foxp3- of CD4+
BM only
cGVHD
ITIM mutant T
D
BM only
cGVHD
ITIM mutant T
E
GC area
GC frequency
GC area (μm²)
#/mm²
ns
0.1716

Figure 7

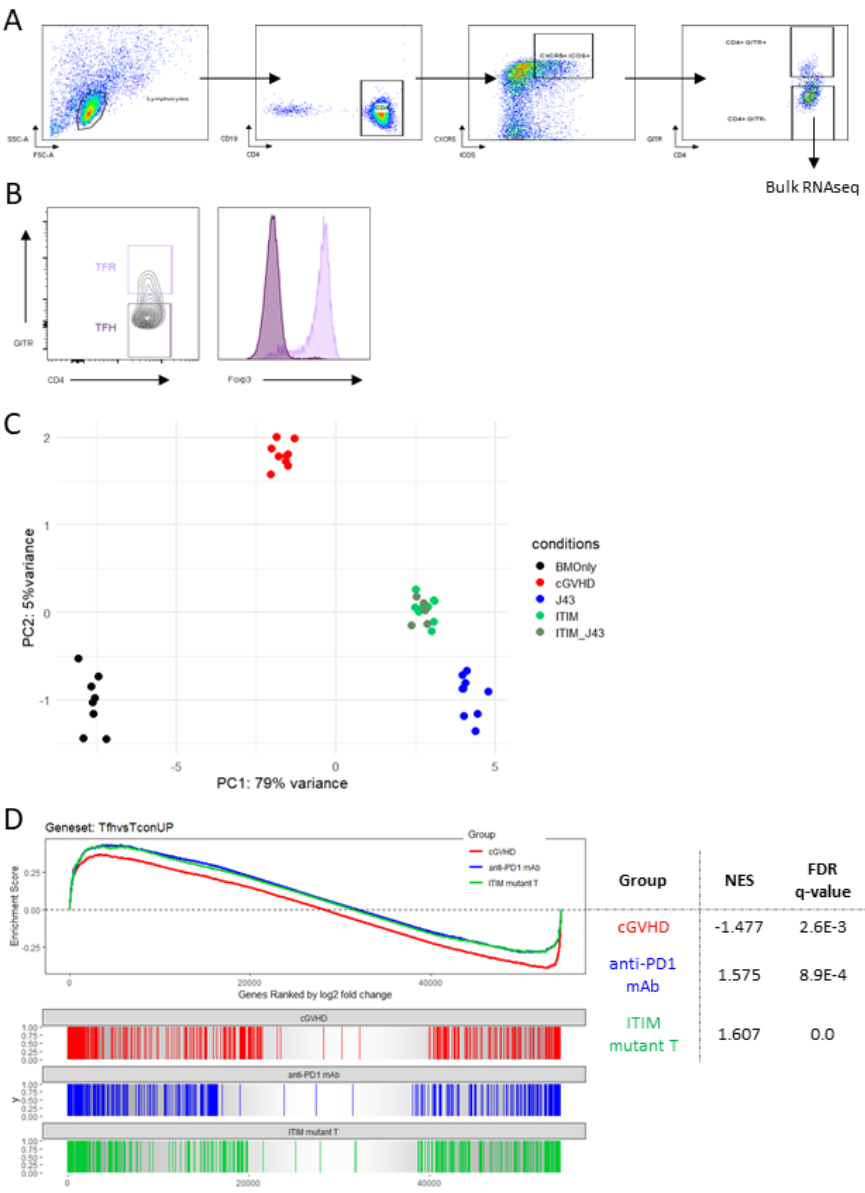

Group	NES	FDR q-value
cGVHD	-1.477	2.6E-3
anti-PD1 mAb	1.575	8.9E-4
ITIM mutant T	1.607	0.0

Figure 8

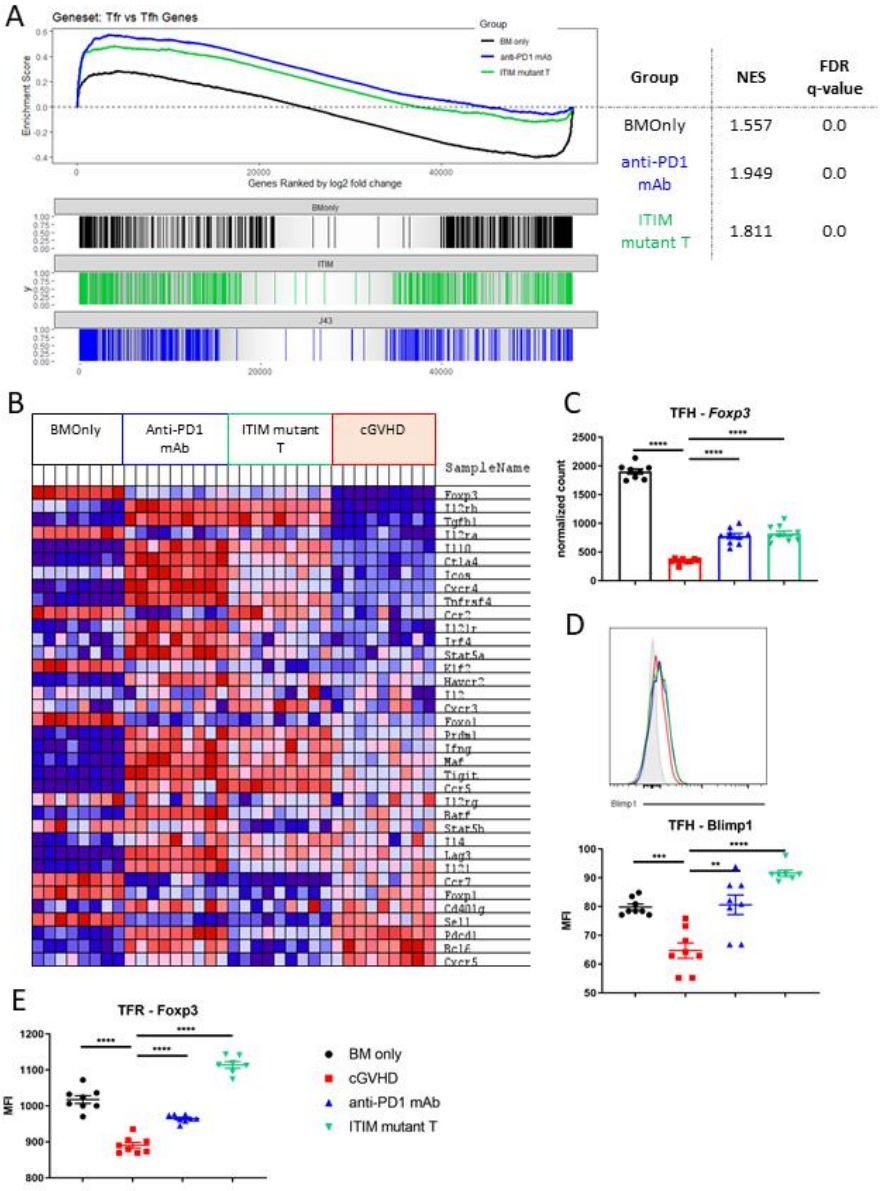
A
Geneset: Tfr vs Tfh Genes
Group
BM only
anti-PD1 mAb
ITIM mutant T
Enrichment Score
Genes Ranked by log2 fold change
Group
NES
FDR q-value
BMOnly
1.557
0.0
anti-PD1 mAb
1.949
0.0
ITIM mutant T
1.811
0.0
B
BMOnly
Anti-PD1 mAb
ITIM mutant T
cGVHD
SampleName
C
TFH - Foxp3
normalized count
D
Blimp1
TFH - Blimp1
MFI
E
TFR - Foxp3
MFI
BM only
cGVHD
anti-PD1 mAb
ITIM mutant T

Figure 9

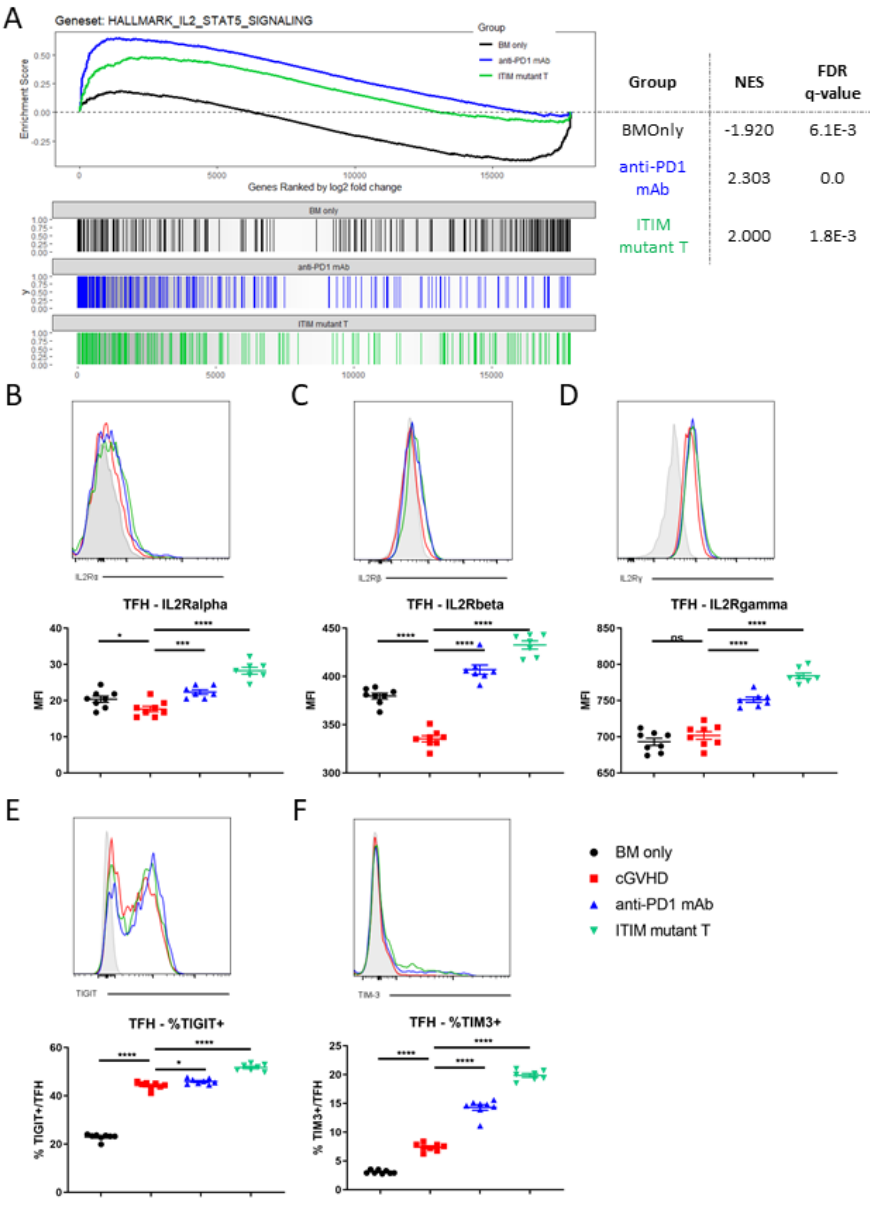
A
Geneset: HALLMARK_IL2_STAT5_SIGNALING
Group
BM only
anti-PD1 mAb
ITIM mutant T
Enrichment Score
Genes Ranked by log2 fold change
Group
NES
FDR q-value
BMOnly
-1.920
6.1E-3
anti-PD1 mAb
2.303
0.0
ITIM mutant T
2.000
1.8E-3
B
C
D
TFH - IL2Ralpha
TFH - IL2Rbeta
TFH - IL2Rgamma
MFI
E
F
TFH - %TIGIT+
TFH - %TIM3+
% TIGIT+/TFH
% TIM3+/TFH
BM only
cGVHD
anti-PD1 mAb
ITIM mutant T

Figure 10

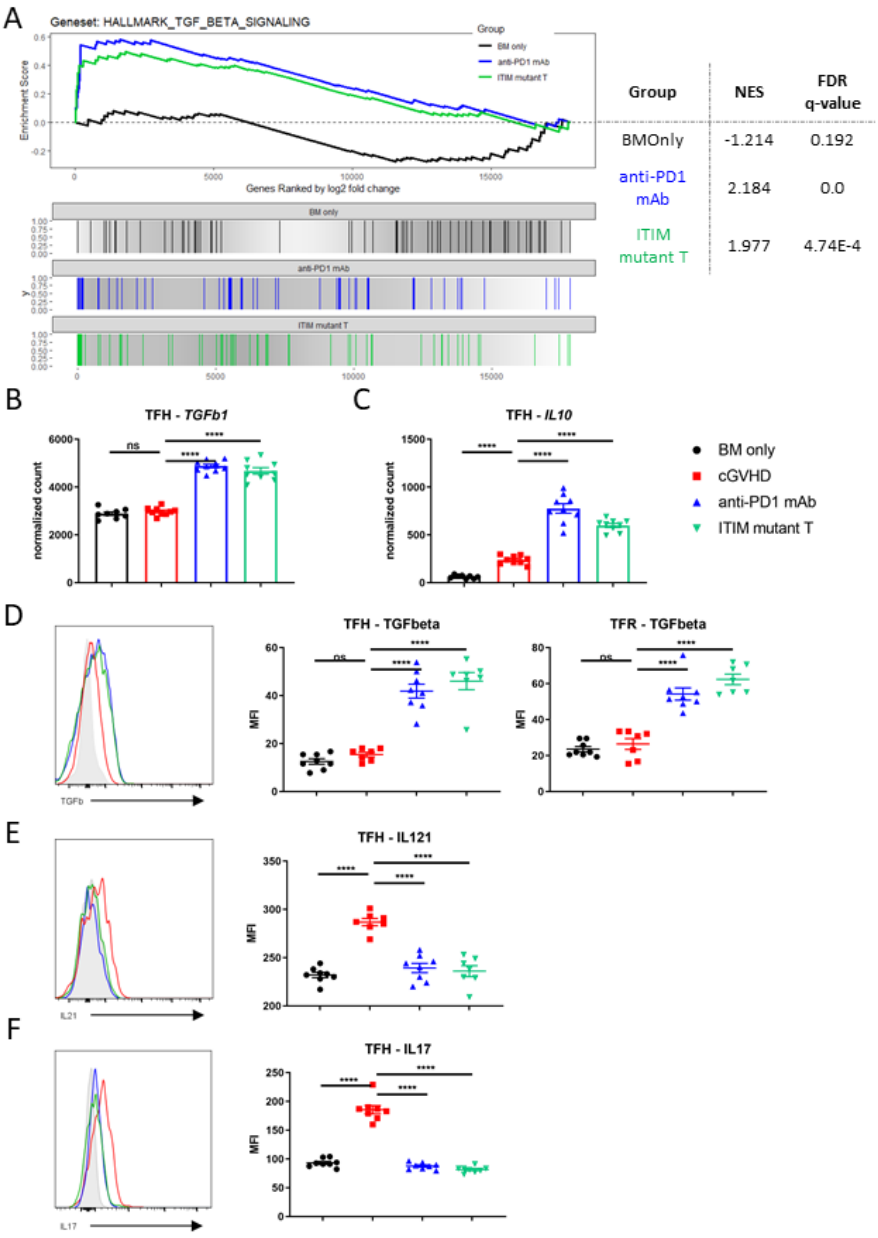
A
Geneset: HALLMARK_TGF_BETA_SIGNALING
Group
BM only
anti-PD1 mAb
ITIM mutant T
Enrichment Score
Genes Ranked by log2 fold change
Group
NES
FDR q-value
BMOnly
-1.214
0.192
anti-PD1 mAb
2.184
0.0
ITIM mutant T
1.977
4.74E-4
B
TFH - TGFb1
normalized count
C
TFH - IL10
normalized count
BM only
cGVHD
anti-PD1 mAb
ITIM mutant T
D
TFH - TGFbeta
TFR - TGFbeta
MFI
TGFb
E
TFH - IL121
MFI
IL21
F
TFH - IL17
MFI
IL17

Supplementary Figure 1

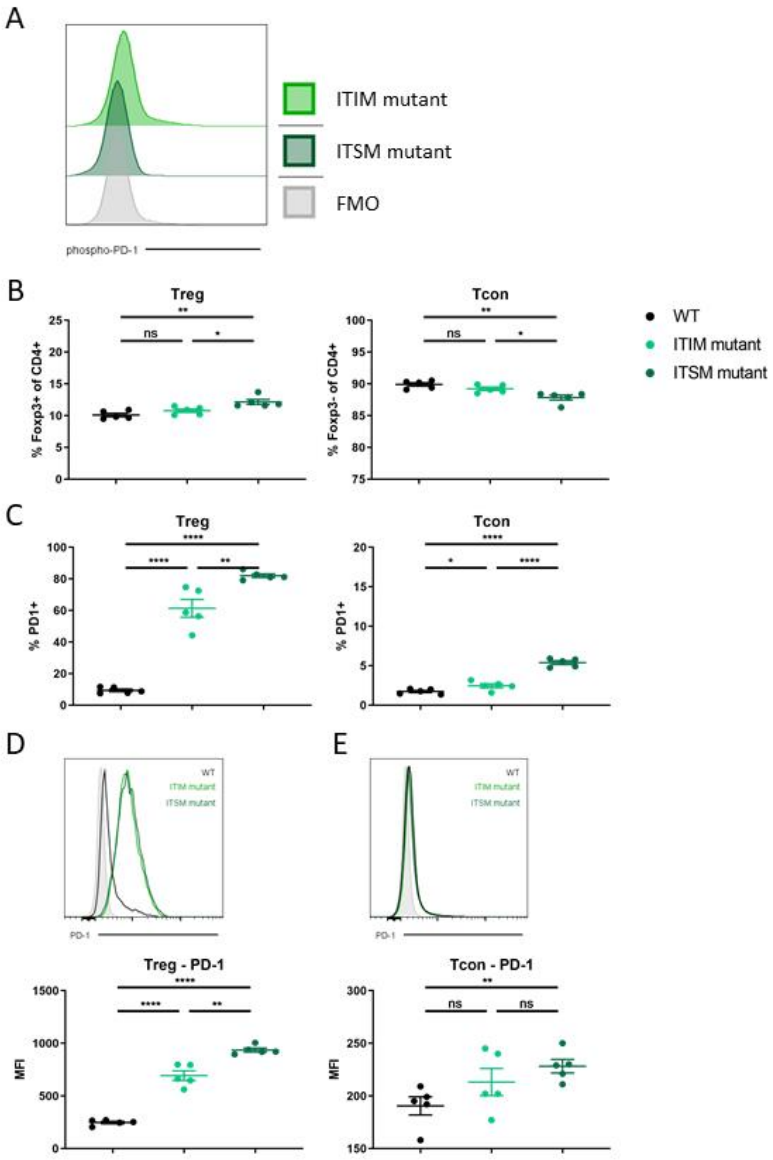

Supplementary Figure 2

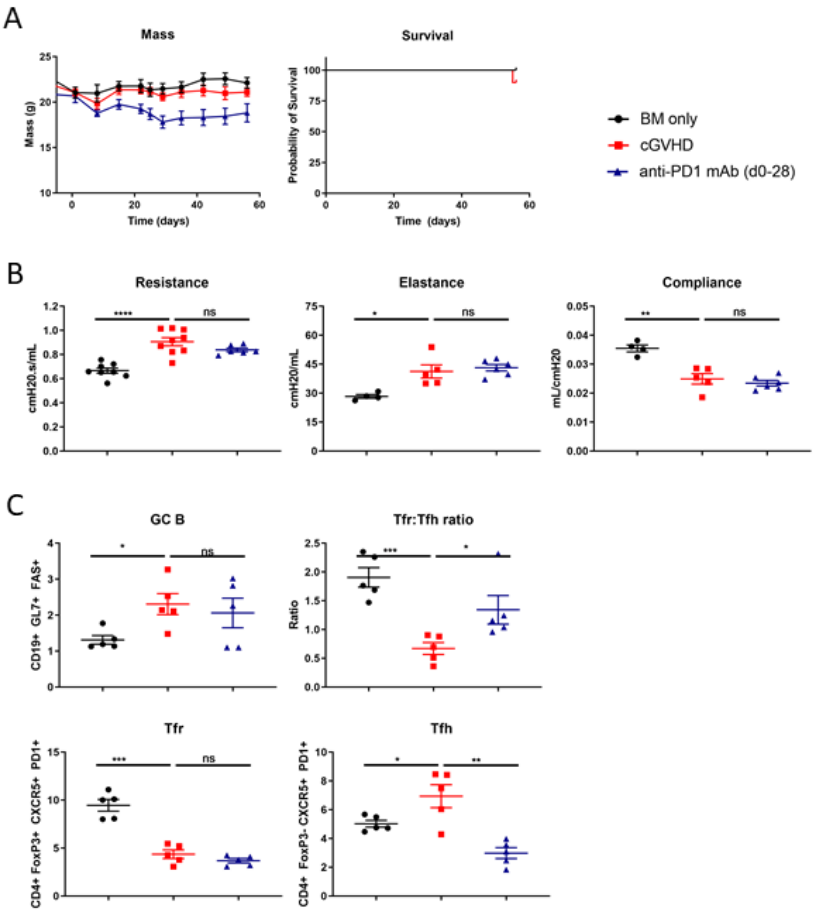

Supplementary Figure 3

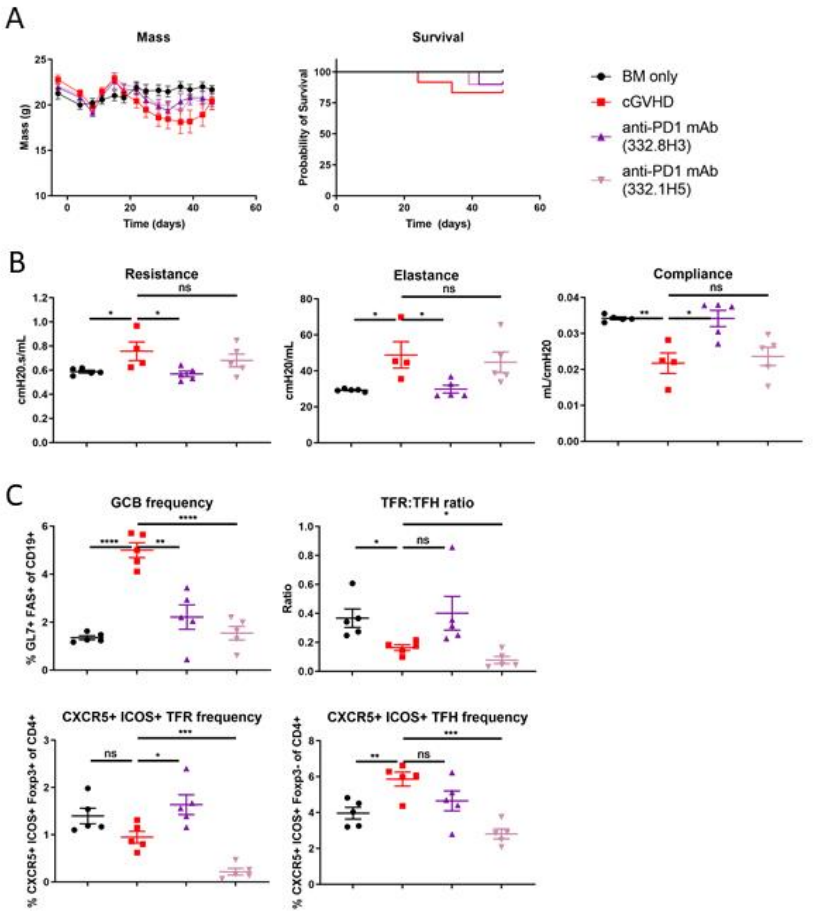

Supplementary Figure 4

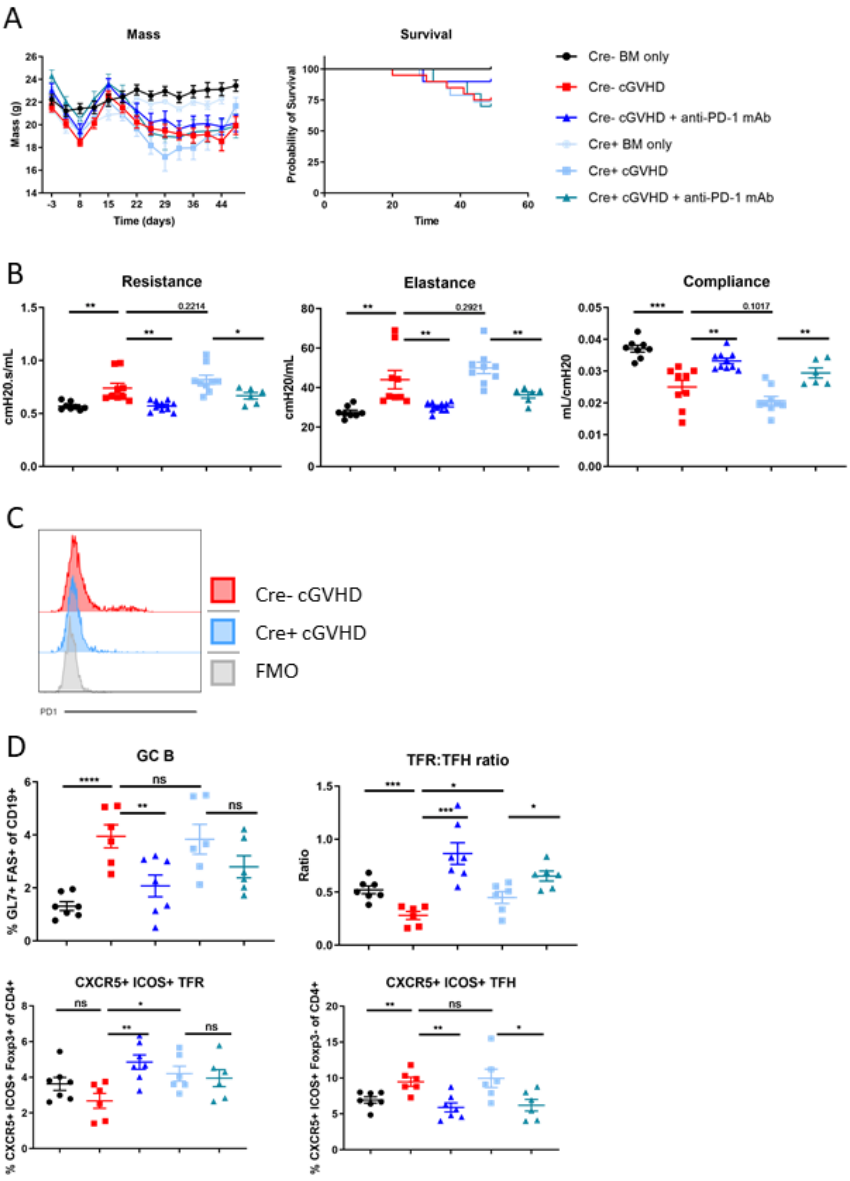

Supplementary Figure 5

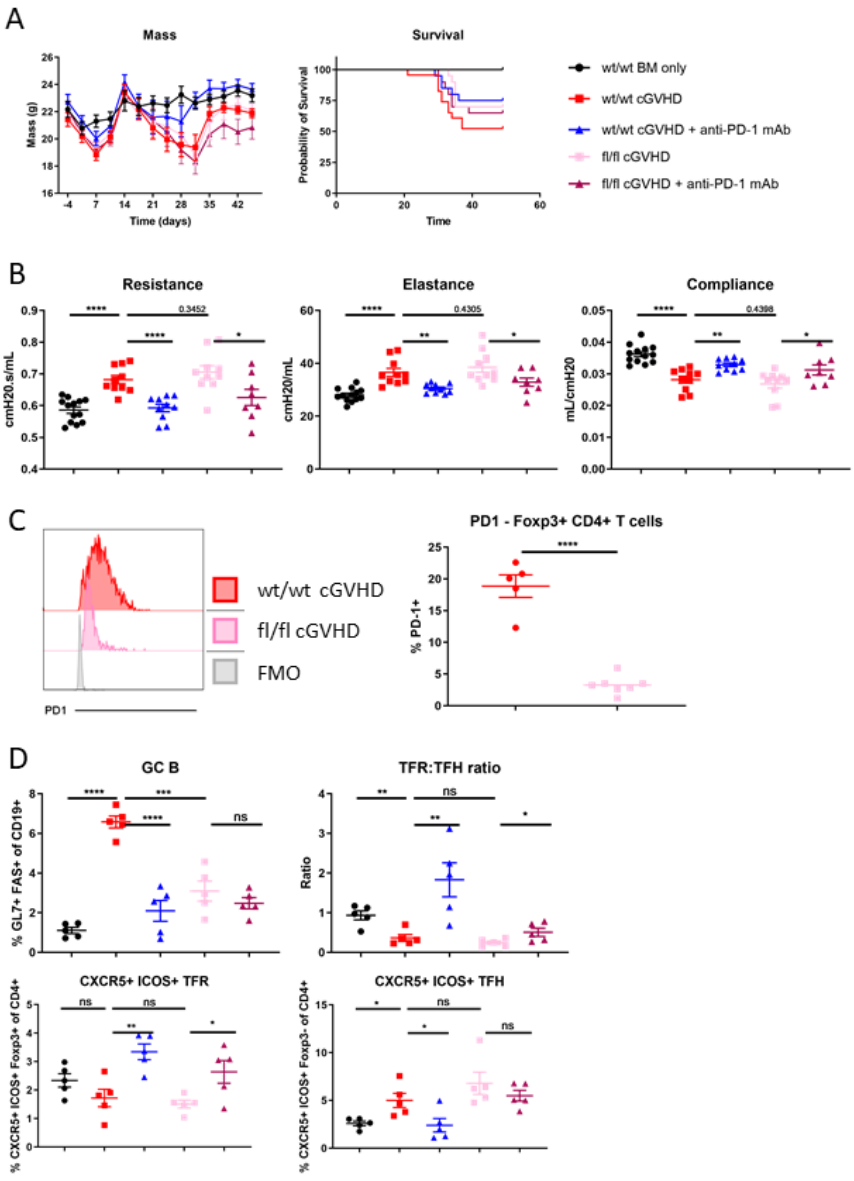

Supplementary Figure 6

A

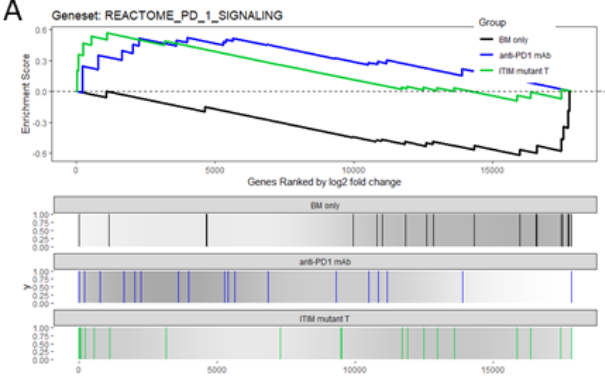

Group	NES	FDR q-value
BMOnly	-1.59	0.263
anti-PD1 mAb	1.47	0.110
ITIM mutant T	1.57	0.105

B

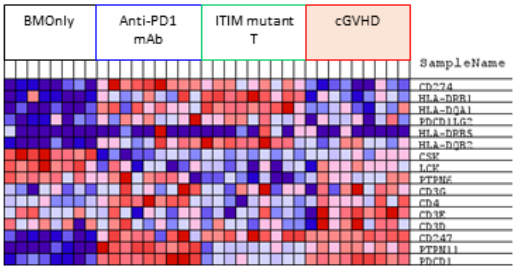

Supplementary Figure 7

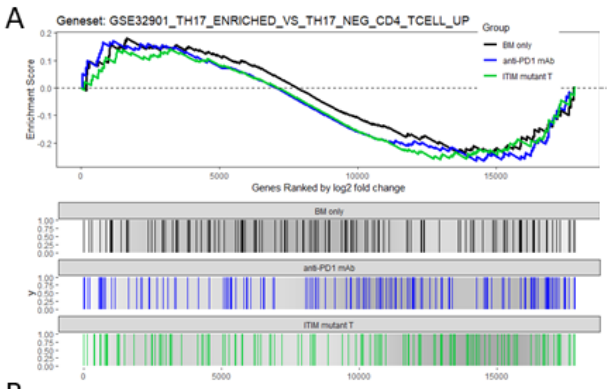

Group	NES	FDR q-value
BMOnly	-0.93	0.615
anti-PD1 mAb	-0.27	0.311
ITIM mutant T	-0.99	0.508

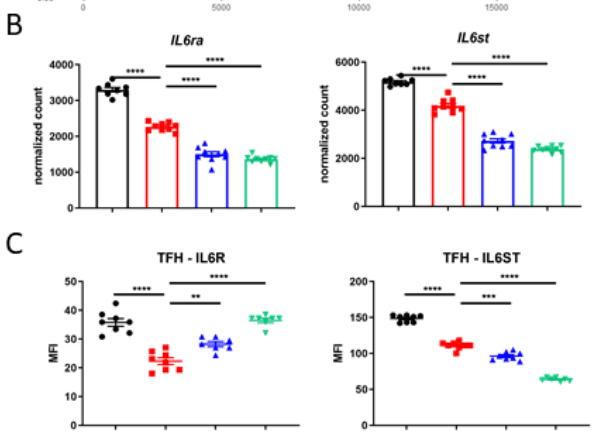

Supplementary Figure 8

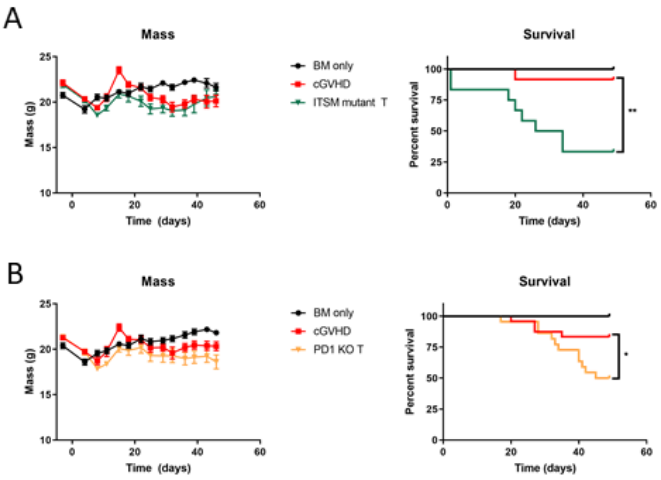

Supplementary Tables

Supplementary Table 1. Extended list of TFH vs Tcon genes

Gcnt1, Hmmr, Neil3, B4galnt4, Clspn, Abhd4, Ryr1, Melk, Cdc6, Cenph, Hk2, Bub1, Mcm10, 2610318N02Rik, Cpe, Padi4, Klrc1, Esco2, Foxm1, Jdp2, Hap1, H2-DMb2, Cep55, Rap1gap2, Tgfbi, Spdl1, Ccdc28b, Gm17586, Trip13, Il17f, Tnfsf11, Pbk, Abcc3, Dnase1l3, Pou2af1, Epdr1, Alcam, Ptpn5, Lgalsl, Parpbp, Plek, Tmem176a, Adam23, Spi1, Pxdc1, Mrgpre, Gm13704, Naprt1, Tnfsf14, Tiam1, Setbp1, A930002I21Rik, Rtn1, Wnt10a, Ptpn3, Depdc1a, Txlnb, Mtmr7, Syne3, Ffar2, Aif1, Ticrr, Fam20a, Pdzk1ip1, Exo1, Uevld, Myo1e, Gzmb, Itgae, Plcl1, Pdcd1lg2, 2010007H06Rik, Emp1, Sirpb1c, Cdca8, Gm14005, Naip2, Fgd2, Il4i1, Ankle1, Ifitm1, Bcl2a1a, Plxdc1, Chtf18, Troap, Nuf2, Acot7, Tcrg-C1, C030034L19Rik, Il22, Mfsd2a, Atp1a3, Stxbp1, Ms4a6d, Pdgfb, Tuft1, Rgs16, Ccdc109b, AA386476, Blk, Ska1, Olfm1, Lyz1, Cenpn, Ptpro, Xkr6, Klra4, Hist1h3c, 4930503L19Rik, Cd83, Adam12, Zbtb42, Klhl4, 4632434I11Rik, Gpt2, Cdkn1a, Asns, Wfdc17, Tbc1d9, Rapsn, Mmp14, Ncf2, Glycam1, Apol7c, Ptrh1, Klrb1c, Cd38, Kctd17, Hes1, Ncr1, Ppfibp1, Ska3, Ggh, BC035044, Repin1, Ercc6l, Aurkb, Prr11, Fhl2, Kcnq5, Slc9a7, Soat2, 2810417H13Rik, Pbx1, Il1b, Tnp2, Arnt2, Derl3, Ascl2, Ifitm2, Klra8, Cd300a, Sytl3, BC030867, Zfp316, Cyp27a1, Mmp25, Fbxl19, Lrr1, Lamc1, Ccr4, Eqtn, Lgr4, Metrnl, 4930430F08Rik, Gm26798, Casz1, 1600002H07Rik, Plekha8, Thnsl1, 6330403K07Rik, Zfp704, Six5, Cit, Mtfr2, Ppp1r13l, H2-Q2, Anxa4, Atrnl1, Sec16b, Cd244, Gas2l1, Ptafr, Gm9885, Mtus2, Klri2, Orc1, Sema7a, Vipr2, Igfbp7, Prr5l, Tspan17, Fkbpl, Mpp2, 2410018L13Rik, Rasgef1b, Lrrc20, Akap6, Slc15a3, Ctla2b, Ear2, Nek2, Scamp1, Myadm, Stom, Hfe, Chrm4, Cd24a, Zbtb32, Il4, Deptor, Slc43a3, St14, Gm11674, Ern1, Havcr2, Ufsp1, Zfp41, Itgb8, Ildr1, Sptb, Cd79b, Srxn1, Xylb, Dpep2, Klk1b9, Zbtbd6, Zfp385a, Penk, Hoxa7, Rapgef5, Cacna1g, H2-Eb2, Bcl2l15, Nek4, Dhrs3, Gm684, Gm12305, Rbm4, Ube2e2, Hist1h3d, Arhgap33, Batf3, Fam83d, E2f8, Hist1h2ai, Plekhf1, Oaf, 5830411N06Rik, Crat, Stil, Kdelc1, Pcyt1b, C1qc, Mical2, 1110019D14Rik,

Ccdc102a, Ctnnd2, Zc2hc1a, Il17re, Anxa3, Etv5, Rab31, Klrb1b, C1qtnf4, Lekr1, Tdrd7, 2810025M15Rik, Clec4a3, Tubb6, Dlg5, AF251705, Atp6v1g3, Zfp459, Actg2, Cebpd, Abcd2, Clec4a2, Fam89a, Kif2c, Kdelc2, Cnih2, Aunip, Dsn1, Tnfrsf19, Map3k8, Gpr55, Prnp, Cst6, Serpinb1a, Morn2, Rnf208, Prdm5, Tubg2, Dmwd, Traip, E230016M11Rik, Ttc30a1, Rbks, Trav10d, Cttn, St6galnac1, Cd209b, Hist1h3i, Hebp1, Stard9, Cd33, Maats1, Emr4, St6galnac3, Ttc8, Pon3, Ifng, Klre1, Trip10, Rpusd2, Dusp16, 5730409E04Rik, Amigo1, Pip5k1b, 4933406C10Rik, A430010J10Rik, Eid2, Mfsd9, Zfp473, Zfp563, Fut7, Hist1h1b, Fam72a, 2-Sep, Dab2ip, Il21, Mcm8, Adamtsl2, Hes5, Dtl, Aplp1, Map6, Mybl1, Stau2, Slfn4, 3110070M22Rik, Fabp4, Srgap3, Spc24, C430042M11Rik, Hspa2, 2210408F21Rik, Klra9, Xcr1, Gpr179, Gm14455, Spag5, Lacc1, Extl1, Cebpa, B430212C06Rik, Cenpf, Gpr141, Sema6c, Zfand4, Tnfrsf8, Chaf1a, Gm26965, Nr4a2, Gfra2, Cd8a, Rin2, Wwc1, Pif1, Dab2_1, Spint1, Hmox1, Zfp248, Otub2, Ebi3, Ell2, Mthfsd, Tlr2, Naip5, Ltb4r1, Marco, Trav13-4-dv7, Mcf2l, Popdc2, Cadm3, Cela1, Areg, Smpdl3b, 2700099C18Rik, Il13ra1, Cpd, Bag2, Upk1a, Zeb2, Trav9-4, Kcnk1, Slco4a1

Supplementary Table 2. Extended list of TFR vs TFH genes

Ccnd2, Rpl37a, Lgals1, 2810474O19Rik, Casp8, Folr4, Eif4a1, Tubb5, Itm2c, Crip1, Rps26, Rexo2, Mcm6, Cd2, Emp3, Sell, Clic1, Smc4, Picalm, H2-Q6, Hnrnpa1, Gm20521, Tagln2, Samhd1, Ahnak, Ptma, Sp110, Hsp90aa1, Hsp90b1, Inpp4b, Hmgb2, Fam169b, Junb, Lbh, E2f2, Pla2g16, Atxn7l3, S100a10, Gbp6, Gata3, D17H6S56E-5, Pa2g4, Sesn1, Hdac7, Glrx, Gm16039, Ergic1, Tfrc, Anxa2, Anxa6, Kdelr2, Bysl, Snrpg, Sdf4, Il4ra, Slc14a1, Fam3c, N4bp1, Il2rb, Mthfd1l, Nr4a1, Atic, Vim, Iigp1, Gm14085, Wdr89, Hivep3_1, Serinc3, Lfng, Hmgn5, Prc1, Sh3bp5, Ttc28, Itga6, Il21r, Lrba, Fam129a, Cldn25, Ighm, Csrp1, Rara, Lcor, Atp1a1, Slfn10-ps, Lpcat4, Acads, D16Ertd472e, Gadl1, Ly9, Il10ra, Snx18, Oaz2, Slc2a3, Pim1, Zc3h12d, Slc17a9, Urb1, Ube2c, Chchd10, Tuba1c, Irf5, Eml2, Gm5559, Kif20b, Spag7, Dst, Ppm1j, Mbnl3, Gvin1, Arl5a, Rpl10-ps3, Ift80, H2afz, Depdc1a, Gm11808, Gm20721, Vav2, Cd55, Sytl2, Gm10132, Fabp5, Atp5s, Tgfbr1, Igf2r, Ecm1, Gm10175, Cst7, Lmnb1, Gm26870, Ramp2, Ass1, Dclk2, Gm10335, Gm10288, Gm26951, Swap70, Dennd5a, Rgs1, Cebpb, Rras2, Rcn1, Gm8203, Spock2, Il1r2, Crim1, Adora2a, Axl, Rpp25l, Xrcc6bp1, Tprgl, Crem, Gm7808, Ndrg1, Phlpp1, Pard6g, Tmem254c, Gbp7, Rpl7a-ps10, Dusp5, Nrn1, Ccr2, Twsg1, Cerk, Havcr2, Prr11, Gbp5, Myo1e, Gm10123, Gm17275, Colq, Gm2000, Gm6472, Psme2b, Rps10-ps2, Gm26819, Gm10221, Cd81, Dedd, Gm17104, Ulk4, Ikzf2, Tmem254a, Ap1g1_2, Gm10774, Tnfrsf4, Rpl18-ps2, Lclat1, Pmepa1, Capg, Tmem254b, Gm11537, Tango6, Gm6395, Gm7589, Ebi3, Gpr83, Gm12250, Sp6, Gm10053, Myd88, Mxd1, Gm4631, Rps23-ps, Gm10094, Ncmap, Kif18b, Rpl7a-ps5, Prg4, Coro2a, Gm20529, Rhoc, Socs2, Gm9846, Hey1, Gm20463, Ebf1_2, Gm5619, Nucb1, Hist3h2ba, Abcg2, Trim14, Amd2, Rec8, Gzmb, Tanc2, Gm26770, Tnfrsf18, Serp2, Slc16a3, Itgb8, Med20, Ccr8, Celsr2, Mt2, Mtif3, Gm17178, Ppap2a, Lamc1, Doc2a, Pop7, Sdc4, Gm11532, Tmem158, Gm11362, Glcci1, Vsig10, 10-Sep, Ctla4, Ppm1l, Ndnl2, Npas4, Dpm1, Lsr, Ier5l, Il1rn, Gm16894, G530011O06Rik, Tomt, Sigmar1, Rangrf, Lmna, Pik3r3, Tnfrsf8, Gm6169, Grb7, Tyk2, Vill, Zbed6,

Lztfl1, Adnp, Serpinf1, Gm10722, C1qtnf6, Src, Tnfrsf1b, Gm9803, Itgae, Pvrl1, Hopx, Gsta4, Rhob, Lancl2, Gm10146, 4632428N05Rik, Ank3, RPL24, Neurl1b, Penk, Gm13166, Eme2, Wdr19, Gm7901, Stk32c, Foxj1, Csrnp1, Gjb2, Ccr10, Klrg1, Entpd1, Gm10717, Il2ra, 4930524J08Rik, Ikzf4, B020018G12Rik, 4930539E08Rik, Gm26675, Ccdc38, Atp5l-ps1, Tdgf1, 9630013D21Rik, Synj2bp, RP23-100J17.7, Rtkn2, Tlr7, Camk2n1, Prdm1, Il10, Tceal3, Gm17354, Gbp3, Gm5918, Rps4y2, Trex1, Acot10, Wdr66, Pld1, Il1rl1, Rpl7a-ps3, Gpr160, Hist1h4a, Hist1h3g, Gm4956, Atp6v0d2, Ctif, Gm10499, Pros1, Gpr68, Gm20663, Rpl14-ps1, Ankrd55, Fgl2, Srgap1, Tmod1, Kifap3, Zhx1, Nup43, Klhl32, Cnrip1, Cntd1, Plcd1, Gorasp1, Grin3b, Tnfrsf9, Pla2g4f, 0610040B10Rik, Eml1, Ccr3, Ptar1, 2200002D01Rik, Gm5422, R74862, Tln2, Slc6a13, Cacna1s, Hist1h4j, Gata1, Fam114a1, B3gnt8, Igsf9, Tnip3, Nup62, Prox2, 5-Sep, Medag, Rgag4, 2210417A02Rik, Xlr, Gm20621, Cspg5, Dgat2, A630081J09Rik, Hdac9, Cxcl2, Eaf2, Rpl21-ps4, Cish, Gbp2b, Hist1h2bb, Tmem184a, Piwil2, AI838599, Tmem30b, Neb, AA543186, Cdcp1, Gstm5, 6330549D23Rik, Nphp4, Crb3, Efcab12, Pnoc, Syce1, Disc1, Il11, Pm20d1, Cep112, Aifm2, Armcx1, Mcam, Gja1, Csrp2, Spats2l, Fam167a, Foxp3, Gm14290, Drc1, Cdhr3, Gm16157, Adssl1, Hsbp1l1, A630091E08Rik, Cybrd1, Trp73, C2cd4b, Ltf, RP24-308I2.1, Capsl, Gm15270, Dyrk3, Dclk1, Hist1h2ah, Tff1, Dlk1, Boc, Tubal3, Cc2d2a, Hist1h2bc, Btnl2, Ticam2, Zfp26, Rgs9, Nos1, Gucy1a3, Apol10b, Fbxo48, Nsun7, Lmo7, Magi1, Scin, Mmp11, Bicd1, Slc22a2, Faim3, Slc7a10, Ermn, Nid2, Bcam, Gm26771, Ky, Slc24a3, Gucy2e, Gm4841, Mmp9, Fam81a, Lrrc32

Supplementary Table 3. Extended list of IL-2/STAT5 signaling genes

SOCS2, CISH, PIM1, IL2RA, SOCS1, TNFRSF9, XBP1, RRAGD, HK2, PHLDA1, IL2RB, CTLA4, NFIL3, CD83, IKZF2, IL10, TNFRSF18, DHRS3, ECM1, ADAM19, SLC2A3, HIPK2, BATF3, BHLHE40, PTGER2, DENND5A, ITIH5, PHTF2, GADD45B, NRP1, NCOA3, CD79B, AHR, TNFRSF1B, NDRG1, BCL2L1, GABARAPL1, LIF, TIAM1, BMPR2, MAP3K8, RHOB, MYC, S100A1, ETFBKMT, CAPG, ST3GAL4, PENK, IRF4, CST7, WLS, TLR7, IKZF4, GBP4, RGS16, SPP1, IL13, SLC29A2, NFKBIZ, IL4R, MXD1, CSF2, FAH, CTSZ, ITGAE, MUC1, MAPKAPK2, TNFRSF21, NT5E, FLT3LG, CCND2, TRAF1, LCLAT1, IL3RA, CYFIP1, BCL2, FGL2, PRNP, EEF1AKMT1, PUS1, ITGAV, NCS1, DCPS, AMACR, FAM126B, PTH1R, ODC1, IGF1R, PTCH1, ENO3, CD81, MAFF, EMP1, CDKN1C, CAPN3, IL1R2, SYT11, TTC39B, ANXA4, BATF, P4HA1, GPR65, SLC1A5, IGF2R, CKAP4, CCR4, CD44, P2RX4, GATA1, KLF6, ARL4A, HOPX, GPR83, ITGA6, CD48, DRC1, SELP, GLIPR2, SMPDL3A, PLSCR1, FURIN, SERPINB6, TNFSF11, GPX4, LRRC8C, CCNE1, CASP3, SH3BGRL2, SNX9, PLEC, BMP2, ICOS, ALCAM, LTB, ENPP1, IL1RL1, MYO1C, IFNGR1, PLIN2, IL18R1, AHNAK, PRKCH, TNFRSF8, SYNGR2, GALM, POU2F1, EOMES, NOP2, PTRH2, RHOH, CDC6, MYO1E, CXCL10, SNX14, IRF6, IL10RA, MAP6, TNFSF10, SPRED2, SELL, SERPINC1, CDCP1, RORA, COCH, CSF1, F2RL2, UCK2, CA2, IFITM3, UMPS, HUWE1, COL6A1, ABCB1, RNH1, IRF8, GUCY1B1, AHCY, PRAF2, GSTO1, TWSG1, CDC42SE2, PLAGL1, APLP1, PLPP1, SPRY4, SCN9A, SHE, PDCD2L, CCND3, LRIG1, SWAP70, SLC39A8, RABGAP1L, TGM2, PNP, AGER, ETV4, CD86

Supplementary Table 4. Extended list of TGF-β signaling genes

TGFBR1, SMAD7, TGFB1, SMURF2, SMURF1, BMPR2, SKIL, SKI, ACVR1, PMEPA1, NCOR2, SERPINE1, JUNB, SMAD1, SMAD6, PPP1R15A, TGIF1, FURIN, SMAD3, FKBP1A, MAP3K7, BMPR1A, CTNNB1, HIPK2, KLF10, BMP2, ENG, APC, PPM1A, XIAP, CDH1, ID1, LEFTY2, CDKN1C, TRIM33, RAB31, TJP1, SLC20A1, CDK9, ID3, NOG, ARID4B, IFNGR2, ID2, PPP1CA, SPTBN1, WWTR1, BCAR3, THBS1, FNTA, HDAC1, UBE2D3, LTBP2, RHOA

Supplementary Table 5. Extended list of PD-1 signaling genes

CD4, CSK, PTPN6, CD274, CD3G, CD3D, PTPN11, LCK, PDCD1, HLA-DRB1, HLA-DQB2, HLA-DQA1, PDCD1LG2, HLA-DRB5, CD247, CD3E

Supplementary Table 6. Extended list of TH17 enriched genes

ACE, ACOT6, ACTRT1, ADRB2, AIPL1, AMOT, ARFRP1, AXIN2, BAHCC1, C16orf54, CBLN3, CBX8, CCDC73, CCS, CD302, CLEC4G, CNDP1, CNKSR2, CNMD, CNP, CRCT1, CXXC4, CYP26B1, CYP4B1, DNAJB2, DNAJC19, DNAJC22, DOK2, DRD5, DYNLT5, EIF2B4, EIF3K, EPM2AIP1, ETV2, EXOC8, FAM168B, FAM83E, FBXO33, FGF17, FOXP2, GHR, GHSR, GLS2, GNA14, GPR137B, GPR173, GRM2, GSTP1, H2AB1, HAPLN3, HCST, HSD11B1, HSD17B7, HSD3B1, KCNMB3, KIF26A, KLHL21, KYAT3, L2HGDH, LIPT1, LMLN, LPO, LRRC56, MAGEL2, MAP3K21, METTL13, MIR150, MIR16-1, MIR187, MIR485, MIR495, MSRB2, MYH8, MYOZ1, NDUFA12, NOM1, NUDT8, NXF3, NXPE3, NXT1, OPRPN, OSBPL5, OTP, PADI6, PANX2, PKD2, PLA2G12A, PRRG3, PRSS51, RHOU, RHOV, RPL8, RPS13, RPS8, SBK2, SCN3B, SDSL, SEC61G, SH2B2, SLC17A8, SLC26A3, SLC38A8, SLC5A3, SLC66A2, SLC9A3, SVIP, TACR2, TENT5C, TGFBI, TLR3, TMEM121B, TMEM200B, TMEM220, TMEM26, TRA2A, TRIB2, TRMT12, TSC22D3, TSSC4, UFSP1, UGGT2, UNC13B, UPP1, VEGFD, VTN, WASHC3, ZFP57

Chapter IV: Concluding statements

General Discussion

The therapeutic benefits of allogeneic hematopoietic stem cell transplantation are severely curtailed by the occurrence of graft-versus-host disease (GVHD), a major complication that leads to long-term morbidity, mortality, and reduced quality of life. Though improvements in transplantation practices have reduced the incidence of acute GVHD, the incidence of chronic GVHD (cGVHD) has not experienced the same relief. A more thorough comprehension of cGVHD pathophysiology is necessary to empower scientists and physicians to develop and offer improved targeted treatment options for cGVHD patients

A distinctive feature of cGVHD versus aGVHD pathology is the presence of poorly controlled B cell-mediated immune responses[235]. During cGVHD, coordinated action by dysregulated donor T and B cells leads to their expansion and activation against both allogeneic recipient antigens and autologous donor antigens. T cells directly cause destruction of recipient tissues and indirectly fuel a positive feedback cycle of tissue injury, leading to the release of cytokines and other soluble factors that further activate antigen-presenting cells and maintain an inflammatory state. With help from expanded T cell populations, hyperreactive B cells engage in the germinal center reaction to produce allo- and auto-antibodies that distribute systemically and contribute to peripheral tissue damage, sclerosis, and fibrosis.

Despite the existence of numerous preclinical models that are used to identify and validate novel targets for cGVHD, no one individual model is able to fully reproduce the heterogeneous spectrum of clinical presentation. Yet, the bronchiolitis obliterans murine model does recapitulate the multi-organ tissue damage that is driven by pathogenic germinal center responses. The data presented in this work examines the mechanisms of the germinal center reaction and explores new means of regulating T cell-mediated humoral immunity within the context of this model. We specifically focus

on the biology of T follicular helper (TFH) cells, which provide co-stimulatory contact-dependent and secreted signals to germinal center B (GC B) cells, enabling their differentiation into antibody-producing plasma cells.

During activation, immune cells undergo metabolic changes to fuel their increase in cellular activity, and different T cell subsets preferentially utilize different metabolic pathways. Our work investigating the metabolic profile of TFH finds their metabolic requirements to change over the course of the germinal center response, from an initial reliance on glycolysis to later predilection for oxidative phosphorylation. We demonstrate that this temporal shift in metabolic dependencies allows the inhibition of glycolysis to prevent, but not treat, cGVHD, and we further identify the use of a pharmaceutical agent inhibiting mitochondrial pyruvate transport as an effective means of treating established cGVHD. Our data additionally illustrate that this therapeutic regulation of TFH mitochondrial respiration results in the loss of the TFH lineage-defining transcription factor and therefore the loss of the TFH phenotype. These data highlight the importance of understanding the temporal activity of cells to best regulate pathogenic functions and suggest another potential target in the continued search for cGVHD therapies.

However, though heartened by these results, we acknowledge the limitations of our findings. Our studies with the mitochondrial pyruvate transport inhibitor have only been extended within the bronchiolitis obliterans cGVHD model. Appropriate testing in other models will be necessary in order to extrapolate our results. We also do not know if pathogenic cells will be able to use compensatory metabolic pathways to circumvent this therapeutic strategy, or even what effects prolonged administration of the mitochondrial pyruvate transport inhibitor will have on other cell types. For example, regulatory T cells that suppress inflammatory immune cell activity have been shown to be dependent on oxidative phosphorylation. Within the timeframe of our transplantation experiments, the activity of these pathogenic cells did not appear to sidestep metabolic inhibition, and

regulatory cells did not appear to be negatively influenced, but additional studies will be required to answer these questions.

Upon activation, T cells also upregulate expression of the co-inhibitory receptor programmed cell death protein 1 (PD-1). PD-1 is a defining surface marker for follicular T cells, both germinal center-supporting TFH and germinal center-suppressing T follicular regulatory (TFR) cells. Our work provides evidence that the TFH require the PD-1 pathway to support the germinal center reaction, and that administration of blocking anti-PD-1 monoclonal antibody targets TFH PD-1 activity, reducing the severity of cGVHD driven by the germinal center reaction. We also specifically identify the necessity of the PD-1 immunoreceptor tyrosine-based inhibitory motif (ITIM), but not the immunoreceptor tyrosine-based switch motif (ITSM), in supporting PD-1 signaling in TFH, as nonfunctional mutation of ITIM fails to sustain a functional TFH phenotype and the development of cGVHD. Furthermore, our studies most surprisingly find that PD-1 blockade and ITIM mutation in donor T cells lead to the expansion of the TFR population and reshape TFH toward adopting suppressive TFR-like characteristics in our cGVHD model.

These results were especially exciting, as they suggest fluidity between the follicular T cell populations in the germinal center. Moreover, our findings immediately solicited a number of additional questions. Though the vast majority of TFR are believed to arise from Foxp3+ precursors, and therefore in our bronchiolitis obliterans model of cGVHD, arise from the bone marrow, is it possible that PD-1 blockade and ITIM mutation in donor T cells lead to the proliferation of natural Treg-derived TFR? Or does the increase in TFR come from the adoption of a TFR phenotype by TFH with anti-PD-1 monoclonal antibody treatment and ITIM mutation? Does the post-transplantation environment, where engraftment of hematopoietic cells is ongoing, or the cGVHD environment, where the germinal center reaction is unregulated, enable TFH to take on

TFR traits with PD-1 blockade and ITIM mutation? Or is this plasticity inherent in germinal centers within other contexts? If there is indeed flexibility between the TFH and TFR phenotypes, what are the mechanisms involved and can other signaling pathways be manipulated to produce similar results?

The research presented in this thesis illuminates our understanding of the germinal center reaction in cGVHD, but also, both frustratingly and exhilaratingly, pose more questions for the future. The potential therapeutic approaches for cGVHD identified here are promising, but this author cannot wait to see what novel targets will be discovered through deeper investigations into the immunobiology offered here.

REFERENCES

1. Hill, G. R., Betts, B. C., Tkachev, V., Kean, L. S. & Blazar, B. R. Current Concepts and Advances in Graft-Versus-Host Disease Immunology. *Annu. Rev. Immunol.* **39**, 19–49 (2021).

2. Pidala, J. *et al.* The global severity of chronic graft-versus-host disease, determined by National Institutes of Health consensus criteria, is associated with overall survival and non-relapse mortality. *Haematologica* **96**, 1678–1684 (2011).

3. Arora, M. *et al.* Late Acute and Chronic Graft-versus-Host Disease after Allogeneic Hematopoietic Cell Transplantation. *Biol. Blood Marrow Transplant.* **22**, 449–455 (2016).

4. Flowers, M. E. D. *et al.* Comparative analysis of risk factors for acute graft-versus-host disease and for chronic graft-versus-host disease according to National Institutes of Health consensus criteria. *Blood* **117**, 3214–3219 (2011).

5. Shlomchik, W. D. *et al.* Prevention of graft versus host disease by inactivation of host antigen-presenting cells. *Science* **285**, 412–415 (1999).

6. Zhang, Y. *et al.* APCs in the liver and spleen recruit activated allogeneic CD8+ T cells to elicit hepatic graft-versus-host disease. *J. Immunol. Baltim. Md 1950* **169**, 7111–7118 (2002).

7. Benichou, G., Takizawa, P. A., Olson, C. A., McMillan, M. & Sercarz, E. E. Donor major histocompatibility complex (MHC) peptides are presented by recipient MHC molecules during graft rejection. *J. Exp. Med.* **175**, 305–308 (1992).

8. Liu, Z., Braunstein, N. S. & Suciu-Foca, N. T cell recognition of allopeptides in context of syngeneic MHC. *J. Immunol. Baltim. Md 1950* **148**, 35–40 (1992).

9. Tivol, E., Komorowski, R. & Drobyski, W. R. Emergent autoimmunity in graft-versus-host disease. *Blood* **105**, 4885–4891 (2005).

10. Blazar, B., White, E. S. & Couriel, D. Understanding Chronic GVHD from Different Angles. *Biol. Blood Marrow Transplant. J. Am. Soc. Blood Marrow Transplant.* **18**, S184–S188 (2012).

11. Arai, S. *et al.* Increasing Incidence of Chronic Graft-versus-Host Disease in Allogeneic Transplantation: A Report from the Center for International Blood and Marrow Transplant Research. *Biol. Blood Marrow Transplant.* **21**, 266–274 (2015).

12. Zeiser, R. & Blazar, B. R. Pathophysiology of Chronic Graft-versus-Host Disease and Therapeutic Targets. *N. Engl. J. Med.* **377**, 2565–2579 (2017).

13. Sarantopoulos, S. & Ritz, J. Aberrant B-cell homeostasis in chronic GVHD. *Blood* **125**, 1703–1707 (2015).

14. Sarantopoulos, S. *et al.* Altered B-cell homeostasis and excess BAFF in human chronic graft-versus-host disease. *Blood* **113**, 3865–3874 (2009).

15. Jia, W. *et al.* BAFF promotes heightened BCR responsiveness and manifestations of chronic GVHD after allogeneic stem cell transplantation. *Blood* **137**, 2544–2557 (2021).

16. Allen, J. L. *et al.* B cells from patients with chronic GVHD are activated and primed for survival via BAFF-mediated pathways. *Blood* **120**, 2529–2536 (2012).

17. Allen, J. L. *et al.* BCR Hyper-Responsiveness In B Cells From Patients With Chronic Gvhd Is Blocked With The Syk Inhibitor R406. *Blood* **122**, 910–910 (2013).

18. Allen, J. L. *et al.* Increased BCR responsiveness in B cells from patients with chronic GVHD. *Blood* **123**, 2108–2115 (2014).

19. Young, J. S. *et al.* Donor B Cells in Transplants Augment Clonal Expansion and Survival of Pathogenic CD4+ T Cells That Mediate Autoimmune-like Chronic Graft-versus-Host Disease. *J. Immunol.* **189**, 222–233 (2012).

20. Srinivasan, M. *et al.* Donor B-cell alloantibody deposition and germinal center formation are required for the development of murine chronic GVHD and bronchiolitis obliterans. *Blood* **119**, 1570–1580 (2012).

21. Flynn, R. *et al.* Increased T follicular helper cells and germinal center B cells are required for cGVHD and bronchiolitis obliterans. *Blood* **123**, 3988–3998 (2014).

22. Jin, H. *et al.* Antibodies from donor B cells perpetuate cutaneous chronic graft-versus-host disease in mice. *Blood* **127**, 2249–2260 (2016).

23. Wu, T. *et al.* Thymic damage, impaired negative selection, and development of chronic graft-versus-host disease caused by donor CD4+ and CD8+ T cells. *J. Immunol. Baltim. Md 1950* **191**, 488–499 (2013).

24. Dertschnig, S., Hauri-Hohl, M. M., Vollmer, M., Holländer, G. A. & Krenger, W. Impaired thymic expression of tissue-restricted antigens licenses the de novo generation of autoreactive CD4+ T cells in acute GVHD. *Blood* **125**, 2720–2723 (2015).

25. Dertschnig, S. *et al.* Graft-versus-host disease reduces lymph node display of tissue-restricted self-antigens and promotes autoimmunity. *J. Clin. Invest.* **130**, 1896–1911 (2020).

26. Carrington, L. J. & Maillard, I. One-two punch injury to tolerance mechanisms in graft-versus-host disease. *J. Clin. Invest.* **130**, 1625–1628 (2020).

27. Zorn, E. *et al.* Reduced frequency of FOXP3+ CD4+CD25+ regulatory T cells in patients with chronic graft-versus-host disease. *Blood* **106**, 2903–2911 (2005).

28. Weinberg, K. *et al.* Factors affecting thymic function after allogeneic hematopoietic stem cell transplantation. *Blood* **97**, 1458–1466 (2001).

29. Alho, A. C. *et al.* Unbalanced recovery of regulatory and effector T cells after allogeneic stem cell transplantation contributes to chronic GVHD. *Blood* **127**, 646–657 (2016).

30. Le Huu, D. *et al.* Donor-derived regulatory B cells are important for suppression of murine sclerodermatous chronic graft-versus-host disease. *Blood* **121**, 3274–3283 (2013).

31. Khoder, A. *et al.* Regulatory B cells are enriched within the IgM memory and transitional subsets in healthy donors but are deficient in chronic GVHD. *Blood* **124**, 2034–2045 (2014).

32. de Masson, A. *et al.* CD24hiCD27+ and plasmablast-like regulatory B cells in human chronic graft-versus-host disease. *Blood* **125**, 1830–1839 (2015).

33. Forcade, E. *et al.* An activated Th17-prone T cell subset involved in chronic graft-versus-host disease sensitive to pharmacological inhibition. *JCI Insight* **2**, 92111 (2017).

34. Wynn, T. Cellular and molecular mechanisms of fibrosis. *J. Pathol.* **214**, 199–210 (2008).

35. Svegliati, S. *et al.* Stimulatory autoantibodies to PDGF receptor in patients with extensive chronic graft-versus-host disease. *Blood* **110**, 237–241 (2007).

36. Claman, H. N., Jaffee, B. D., Huff, J. C. & Clark, R. A. F. Chronic graft-versus-host disease as a model for scleroderma: II. Mast cell depletion with deposition of immunoglobulins in the skin and fibrosis. *Cell. Immunol.* **94**, 73–84 (1985).

37. Jagasia, M. H. *et al.* National Institutes of Health Consensus Development Project on Criteria for Clinical Trials in Chronic Graft-versus-Host Disease: I. The 2014 Diagnosis and Staging Working Group Report. *Biol. Blood Marrow Transplant. J. Am. Soc. Blood Marrow Transplant.* **21**, 389-401.e1 (2015).

38. Miklos, D. *et al.* Ibrutinib for chronic graft-versus-host disease after failure of prior therapy. *Blood* **130**, 2243–2250 (2017).

39. Jagasia, M. *et al.* ROCK2 Inhibition With Belumosudil (KD025) for the Treatment of Chronic Graft-Versus-Host Disease. *J. Clin. Oncol.* **39**, 1888–1898 (2021).

40. Zeiser, R. *et al.* Ruxolitinib for Glucocorticoid-Refractory Chronic Graft-versus-Host Disease. *N. Engl. J. Med.* **385**, 228–238 (2021).

41. Song, Q., Kong, X., Martin, P. J. & Zeng, D. Murine Models Provide New Insights Into Pathogenesis of Chronic Graft-Versus-Host Disease in Humans. *Front. Immunol.* **12**, (2021).

42. Skert, C. *et al.* Sclerodermatous chronic graft-versus-host disease after allogeneic hematopoietic stem cell transplantation: incidence, predictors and outcome. *Haematologica* **91**, 258–261 (2006).

43. Salhotra, A. *et al.* Sclerodermatous chronic graft-versus-host disease in patients receiving tyrosine kinase inhibitors after allogeneic hematopoietic cell transplantation. *Bone Marrow Transplant.* **50**, 139–141 (2015).

44. Inamoto, Y. *et al.* Incidence, risk factors, and outcomes of sclerosis in patients with chronic graft-versus-host disease. *Blood* **121**, 5098–5103 (2013).

45. Panoskaltsis-Mortari, A., Tram, K. V., Price, A. P., Wendt, C. H. & Blazar, B. R. A New Murine Model for Bronchiolitis Obliterans Post–Bone Marrow Transplant. *Am. J. Respir. Crit. Care Med.* **176**, 713–723 (2007).

46. Dubovsky, J. A. *et al.* Ibrutinib treatment ameliorates murine chronic graft-versus-host disease. https://www.jci.org/articles/view/75328/pdf (2014) doi:10.1172/JCI75328.

47. Flynn, R. *et al.* Targeted Rho-associated kinase 2 inhibition suppresses murine and human chronic GVHD through a Stat3-dependent mechanism. *Blood* **127**, 2144–2154 (2016).

48. Victora, G. D. *et al.* Germinal Center Dynamics Revealed by Multiphoton Microscopy Using a Photoactivatable Fluorescent Reporter. *Cell* **143**, 592–605 (2010).

49. Gitlin, A. D., Shulman, Z. & Nussenzweig, M. C. Clonal selection in the germinal center by regulated proliferation and hypermutation. *Nature* **509**, 637–640 (2014).

50. Crotty, S. T follicular helper cell biology: A decade of discovery and diseases. *Immunity* **50**, 1132–1148 (2019).

51. Weinstein, J. S. *et al.* Follicular helper T cells progressively differentiate to regulate the germinal center response. *Nat. Immunol.* **17**, 1197–1205 (2016).

52. Langenkamp, A. *et al.* Kinetics and expression patterns of chemokine receptors in human CD4+ T lymphocytes primed by myeloid or plasmacytoid dendritic cells. *Eur. J. Immunol.* **33**, 474–482 (2003).

53. Baumjohann, D., Okada, T. & Ansel, K. M. Cutting Edge: Distinct Waves of BCL6 Expression during T Follicular Helper Cell Development. *J. Immunol.* **187**, 2089–2092 (2011).

54. Bauquet, A. T. *et al.* Costimulatory molecule ICOS plays a critical role in the development of TH-17 and follicular T-helper cells by regulating c-Maf expression and IL-21 production. *Nat. Immunol.* **10**, 167–175 (2009).

55. Choi, Y. S. *et al.* Bcl6 dependent T follicular helper cell differentiation diverges from effector cell differentiation during priming and depends on the gene Icos. *Immunity* **34**, 932–946 (2011).

56. Xu, H. *et al.* Follicular T-helper cell recruitment governed by bystander B cells and ICOS-driven motility. *Nature* **496**, 523–527 (2013).

57. Stone, E. L. *et al.* ICOS Coreceptor Signaling Inactivates the Transcription Factor FOXO1 to Promote Tfh Cell Differentiation. *Immunity* **42**, 239–251 (2015).

58. Baumjohann, D. *et al.* Persistent Antigen and Germinal Center B Cells Sustain T Follicular Helper Cell Responses and Phenotype. *Immunity* **38**, 596–605 (2013).

59. Choi, Y. S. *et al.* Bcl6 Expressing Follicular Helper CD4 T Cells Are Fate Committed Early and Have the Capacity To Form Memory. *J. Immunol.* **190**, 4014–4026 (2013).

60. Leavenworth, J. W., Verbinnen, B., Yin, J., Huang, H. & Cantor, H. A p85α-osteopontin axis couples the receptor ICOS to sustained Bcl-6 expression by follicular helper and regulatory T cells. *Nat. Immunol.* **16**, 96–106 (2015).

61. Johnston, R. J. *et al.* Bcl6 and Blimp-1 are reciprocal and antagonistic regulators of T follicular helper cell differentiation. *Science* **325**, 1006–1010 (2009).

62. DiToro, D. *et al.* Differential IL-2 Expression Defines Developmental Fates of Follicular versus Non-follicular Helper T cells. *Science* **361**, eaao2933 (2018).

63. Weber, J. P. *et al.* ICOS maintains the T follicular helper cell phenotype by down-regulating Krüppel-like factor 2. *J. Exp. Med.* **212**, 217–233 (2015).

64. Lee, J.-Y. *et al.* The Transcription Factor KLF2 Restrains CD4 + T Follicular Helper Cell Differentiation. *Immunity* **42**, 252–264 (2015).

65. Haynes, N. M. *et al.* Role of CXCR5 and CCR7 in Follicular Th Cell Positioning and Appearance of a Programmed Cell Death Gene-1High Germinal Center-Associated Subpopulation. *J. Immunol.* **179**, 5099–5108 (2007).

66. Hatzi, K. *et al.* BCL6 orchestrates Tfh cell differentiation via multiple distinct mechanisms. *J. Exp. Med.* **212**, 539–553 (2015).

67. Choi, J. & Crotty, S. Bcl6-Mediated Transcriptional Regulation of Follicular Helper T cells (TFH). *Trends Immunol.* **42**, 336–349 (2021).

68. Lu, K. T. *et al.* Functional and Epigenetic Studies Reveal Multistep Differentiation and Plasticity of In Vitro-Generated and In Vivo-Derived Follicular T Helper Cells. *Immunity* **35**, 622–632 (2011).

69. Olatunde, A. C., Hale, J. S. & Lamb, T. J. Cytokine-skewed Tfh cells: functional consequences for B cell help. *Trends Immunol.* **42**, 536–550 (2021).

70. Chung, Y. *et al.* Follicular regulatory T cells expressing Foxp3 and Bcl-6 suppress germinal center reactions. *Nat. Med.* **17**, 983–988 (2011).

71. Wu, H. *et al.* Follicular regulatory T cells repress cytokine production by follicular helper T cells and optimize IgG responses in mice. *Eur. J. Immunol.* **46**, 1152–1161 (2016).

72. Lu, Y. & Craft, J. T Follicular Regulatory Cells: Choreographers of Productive Germinal Center Responses. *Front. Immunol.* **12**, 679909 (2021).

73. Tsuji, M. *et al.* Preferential Generation of Follicular B Helper T Cells from Foxp3+ T Cells in Gut Peyer's Patches. *Science* **323**, 1488–1492 (2009).

74. Linterman, M. A. *et al.* Foxp3+ follicular regulatory T cells control T follicular helper cells and the germinal center response. *Nat. Med.* **17**, 975–982 (2011).

75. Aloulou, M. *et al.* Follicular regulatory T cells can be specific for the immunizing antigen and derive from naive T cells. *Nat. Commun.* **7**, 10579 (2016).

76. Maceiras, A. R. *et al.* T follicular helper and T follicular regulatory cells have different TCR specificity. *Nat. Commun.* **8**, 15067 (2017).

77. Fonseca, V. R., Ribeiro, F. & Graca, L. T follicular regulatory (Tfr) cells: Dissecting the complexity of Tfr-cell compartments. *Immunol. Rev.* **288**, 112–127 (2019).

78. Linterman, M. A. *et al.* CD28 expression is required after T cell priming for helper T cell responses and protective immunity to infection. *eLife* **3**, e03180 (2014).

79. Sage, P. T., Francisco, L. M., Carman, C. V. & Sharpe, A. H. The receptor PD-1 controls follicular regulatory T cells in the lymph nodes and blood. *Nat. Immunol.* **14**, 152–161 (2013).

80. Pratama, A. *et al.* MicroRNA-146a regulates ICOS–ICOSL signalling to limit accumulation of T follicular helper cells and germinal centres. *Nat. Commun.* **6**, 6436 (2015).

81. Nurieva, R. I. *et al.* Bcl6 mediates the development of T follicular helper cells. *Science* **325**, 1001–1005 (2009).

82. Yang, G. *et al.* Transcriptional repressor Blimp1 regulates follicular regulatory T-cell homeostasis and function. *Immunology* **153**, 105–117 (2018).

83. Sage, P. T. *et al.* Suppression by T_{FR} cells leads to durable and selective inhibition of B cell effector function. *Nat. Immunol.* **17**, 1436–1446 (2016).

84. Sage, P. T., Paterson, A. M., Lovitch, S. B. & Sharpe, A. H. The Coinhibitory Receptor CTLA-4 Controls B Cell Responses by Modulating T Follicular Helper, T Follicular Regulatory, and T Regulatory Cells. *Immunity* **41**, 1026–1039 (2014).

85. Wing, J. B., Ise, W., Kurosaki, T. & Sakaguchi, S. Regulatory T Cells Control Antigen-Specific Expansion of Tfh Cell Number and Humoral Immune Responses via the Coreceptor CTLA-4. *Immunity* **41**, 1013–1025 (2014).

86. McCarron, M. J. & Marie, J. C. TGF-β prevents T follicular helper cell accumulation and B cell autoreactivity. *J. Clin. Invest.* **124**, 4375–4386 (2014).

87. Sage, P. T., Alvarez, D., Godec, J., von Andrian, U. H. & Sharpe, A. H. Circulating T follicular regulatory and helper cells have memory-like properties. *J. Clin. Invest.* **124**, 5191–5204 (2014).

88. Clement, R. L. *et al.* Follicular regulatory T cells control humoral and allergic immunity by restraining early B cell responses. *Nat. Immunol.* **20**, 1360–1371 (2019).

89. Ishida, Y., Agata, Y., Shibahara, K. & Honjo, T. Induced expression of PD-1, a novel member of the immunoglobulin gene superfamily, upon programmed cell death. *EMBO J.* **11**, 3887–3895 (1992).

90. Francisco, L. M., Sage, P. T. & Sharpe, A. H. The PD-1 Pathway in Tolerance and Autoimmunity. *Immunol. Rev.* **236**, 219–242 (2010).

91. Sharpe, A. H. & Pauken, K. E. The diverse functions of the PD1 inhibitory pathway. *Nat. Rev. Immunol.* **18**, 153–167 (2018).

92. Freeman, G. J. Structures of PD-1 with its ligands: Sideways and dancing cheek to cheek. *Proc. Natl. Acad. Sci.* **105**, 10275–10276 (2008).

93. Fife, B. T. *et al.* Interactions between programmed death-1 and programmed death ligand-1 promote tolerance by blocking the T cell receptor-induced stop signal. *Nat. Immunol.* **10**, 1185–1192 (2009).

94. Lin, D. Y. *et al.* The PD-1/PD-L1 complex resembles the antigen-binding Fv domains of antibodies and T cell receptors. *Proc. Natl. Acad. Sci. U. S. A.* **105**, 3011–3016 (2008).

95. Lázár-Molnár, E. *et al.* Crystal structure of the complex between programmed death-1 (PD-1) and its ligand PD-L2. *Proc. Natl. Acad. Sci. U. S. A.* **105**, 10483–10488 (2008).

96. Shinohara, T., Taniwaki, M., Ishida, Y., Kawaichi, M. & Honjo, T. Structure and Chromosomal Localization of the Human PD-1 Gene (PDCD1). *Genomics* **23**, 704–706 (1994).

97. Chemnitz, J. M., Parry, R. V., Nichols, K. E., June, C. H. & Riley, J. L. SHP-1 and SHP-2 Associate with Immunoreceptor Tyrosine-Based Switch Motif of Programmed Death 1 upon Primary Human T Cell Stimulation, but Only Receptor Ligation Prevents T Cell Activation. *J. Immunol.* **173**, 945–954 (2004).

98. Riley, J. L. PD-1 signaling in primary T cells. *Immunol. Rev.* **229**, 114–125 (2009).

99. Hui, E. *et al.* T cell costimulatory receptor CD28 is a primary target for PD-1–mediated inhibition. *Science* **355**, 1428–1433 (2017).

100. Chatterjee, P., Patsoukis, N., Freeman, G. J. & Boussiotis, V. A. Distinct Roles Of PD-1 Itsm and ITIM In Regulating Interactions With SHP-2, ZAP-70 and Lck, and PD-1-Mediated Inhibitory Function. *Blood* **122**, 191–191 (2013).

101. Boussiotis, V. A., Chatterjee, P. & Li, L. Biochemical Signaling of PD-1 on T Cells and Its Functional Implications. *Cancer J. Sudbury Mass* **20**, 265–271 (2014).

102. Patsoukis, N., Wang, Q., Strauss, L. & Boussiotis, V. A. Revisiting the PD-1 pathway. *Sci. Adv.* **6**, eabd2712.

103. Peled, M. *et al.* Affinity purification mass spectrometry analysis of PD-1 uncovers SAP as a new checkpoint inhibitor. *Proc. Natl. Acad. Sci.* **115**, E468–E477 (2018).

104. Marasco, M. *et al.* Molecular mechanism of SHP2 activation by PD-1 stimulation. *Sci. Adv.* **6**, eaay4458 (2020).

105. Patsoukis, N. *et al.* Interaction of SHP-2 SH2 domains with PD-1 ITSM induces PD-1 dimerization and SHP-2 activation. *Commun. Biol.* **3**, 128 (2020).

106. Bardhan, K. *et al.* Phosphorylation of PD-1-Y248 is a marker of PD-1-mediated inhibitory function in human T cells. *Sci. Rep.* **9**, 17252 (2019).

107. Parry, R. V. *et al.* CTLA-4 and PD-1 Receptors Inhibit T-Cell Activation by Distinct Mechanisms. *Mol. Cell. Biol.* **25**, 9543–9553 (2005).

108. Okazaki, T., Maeda, A., Nishimura, H., Kurosaki, T. & Honjo, T. PD-1 immunoreceptor inhibits B cell receptor-mediated signaling by recruiting src homology 2-domain-containing tyrosine phosphatase 2 to phosphotyrosine. *Proc. Natl. Acad. Sci.* **98**, 13866–13871 (2001).

109. Yokosuka, T. *et al.* Programmed cell death 1 forms negative costimulatory microclusters that directly inhibit T cell receptor signaling by recruiting phosphatase SHP2. *J. Exp. Med.* **209**, 1201–1217 (2012).

110. Rota, G. *et al.* Shp-2 Is Dispensable for Establishing T Cell Exhaustion and for PD-1 Signaling In Vivo. *Cell Rep.* **23**, 39–49 (2018).

111. Celis-Gutierrez, J. *et al.* Quantitative Interactomics in Primary T Cells Provides a Rationale for Concomitant PD-1 and BTLA Coinhibitor Blockade in Cancer Immunotherapy. *Cell Rep.* **27**, 3315-3330.e7 (2019).

112. Sheppard, K.-A. *et al.* PD-1 inhibits T-cell receptor induced phosphorylation of the ZAP70/CD3ζ signalosome and downstream signaling to PKCθ. *FEBS Lett.* **574**, 37–41 (2004).

113. Hukelmann, J. L. *et al.* The cytotoxic T cell proteome and its shaping by mammalian Target of Rapamycin. *Nat. Immunol.* **17**, 104–112 (2016).

114. Rieckmann, J. C. *et al.* Social network architecture of human immune cells unveiled by quantitative proteomics. *Nat. Immunol.* **18**, 583–593 (2017).

115. Frearson, J. A. & Alexander, D. R. The Phosphotyrosine Phosphatase SHP-2 Participates in a Multimeric Signaling Complex and Regulates T Cell Receptor (TCR) coupling to the Ras/Mitogen-activated Protein Kinase (MAPK) Pathway in Jurkat T Cells. *J. Exp. Med.* **187**, 1417–1426 (1998).

116. Tailor, P. *et al.* Involvement of Src-homology-2-domain-containing Protein-tyrosine Phosphatase 2 in T Cell Activation. *Eur. J. Biochem.* **237**, 736–742 (1996).

117. Nguyen, T. V., Ke, Y., Zhang, E. E. & Feng, G.-S. Conditional Deletion of Shp2 Tyrosine Phosphatase in Thymocytes Suppresses Both Pre-TCR and TCR Signals. *J. Immunol.* **177**, 5990–5996 (2006).

118. Bardhan, K. *et al.* PD-1 inhibits the TCR signaling cascade by sequestering SHP-2 phosphatase, preventing its translocation to lipid rafts and facilitating Csk-mediated inhibitory phosphorylation of Lck. *J. Immunol.* **196**, 128.15-128.15 (2016).

119. Salmond, R. J., Huyer, G., Kotsoni, A., Clements, L. & Alexander, D. R. The src Homology 2 Domain-Containing Tyrosine Phosphatase 2 Regulates Primary T-Dependent Immune Responses and Th Cell Differentiation. *J. Immunol.* **175**, 6498–6508 (2005).

120. Plas, D. R. *et al.* Direct regulation of ZAP-70 by SHP-1 in T cell antigen receptor signaling. *Science* **272**, 1173–1176 (1996).

121. Zhang, J., Somani, A.-K. & Siminovitch, K. A. Roles of the SHP-1 tyrosine phosphatase in the negative regulation of cell signalling. *Semin. Immunol.* **12**, 361–378 (2000).

122. Hebeisen, M. *et al.* SHP-1 phosphatase activity counteracts increased T cell receptor affinity. *J. Clin. Invest.* **123**, 1044–1056 (2013).

123. Mercadante, E. R. & Lorenz, U. M. T Cells Deficient in the Tyrosine Phosphatase SHP-1 Resist Suppression by Regulatory T Cells. *J. Immunol.* **199**, 129–137 (2017).

124. Lorenz, U. SHP-1 and SHP-2 in T cells: two phosphatases functioning at many levels. *Immunol. Rev.* **228**, 342–359 (2009).

125. Pearce, E. L. & Pearce, E. J. Metabolic Pathways In Immune Cell Activation And Quiescence. *Immunity* **38**, 633–643 (2013).

126. Caputa, G., Castoldi, A. & Pearce, E. J. Metabolic adaptations of tissue-resident immune cells. *Nat. Immunol.* **20**, 793–801 (2019).

127. Frauwirth, K. A. *et al.* The CD28 Signaling Pathway Regulates Glucose Metabolism. *Immunity* **16**, 769–777 (2002).

128. MacIver, N. J., Michalek, R. D. & Rathmell, J. C. Metabolic Regulation of T Lymphocytes. *Annu. Rev. Immunol.* **31**, 259–283 (2013).

129. Dumitru, C., Kabat, A. M. & Maloy, K. J. Metabolic Adaptations of CD4+ T Cells in Inflammatory Disease. *Front. Immunol.* **9**, (2018).

130. Almeida, L., Lochner, M., Berod, L. & Sparwasser, T. Metabolic pathways in T cell activation and lineage differentiation. *Semin. Immunol.* **28**, 514–524 (2016).

131. Greiner, E. F., Guppy, M. & Brand, K. Glucose is essential for proliferation and the glycolytic enzyme induction that provokes a transition to glycolytic energy production. *J. Biol. Chem.* **269**, 31484–31490 (1994).

132. Carr, E. L. *et al.* Glutamine Uptake and Metabolism Are Coordinately Regulated by ERK/MAPK During T Lymphocyte Activation. *J. Immunol. Baltim. Md 1950* **185**, 1037–1044 (2010).

133. O'Neill, L. A. J. & Hardie, D. G. Metabolism of inflammation limited by AMPK and pseudo-starvation. *Nature* **493**, 346–355 (2013).

134. Peng, M. *et al.* Aerobic glycolysis promotes T helper 1 cell differentiation through an epigenetic mechanism. *Science* **354**, 481–484 (2016).

135. Lochner, M., Berod, L. & Sparwasser, T. Fatty acid metabolism in the regulation of T cell function. *Trends Immunol.* **36**, 81–91 (2015).

136. Macintyre, A. N. *et al.* The glucose transporter Glut1 is selectively essential for CD4 T cell activation and effector function. *Cell Metab.* **20**, 61–72 (2014).

137. Heintzman, D. R., Fisher, E. L. & Rathmell, J. C. Microenvironmental influences on T cell immunity in cancer and inflammation. *Cell. Mol. Immunol.* **19**, 316–326 (2022).

138. Michalek, R. D. *et al.* Cutting Edge: Distinct Glycolytic and Lipid Oxidative Metabolic Programs Are Essential for Effector and Regulatory CD4+ T Cell Subsets. *J. Immunol.* **186**, 3299–3303 (2011).

139. Klysz, D. *et al.* Glutamine-dependent α-ketoglutarate production regulates the balance between T helper 1 cell and regulatory T cell generation. *Sci. Signal.* **8**, ra97–ra97 (2015).

140. Johnson, M. O. *et al.* Distinct Regulation of Th17 and Th1 Cell Differentiation by Glutaminase-Dependent Metabolism. *Cell* **175**, 1780-1795.e19 (2018).

141. Young, K. E., Flaherty, S., Woodman, K. M., Sharma-Walia, N. & Reynolds, J. M. Fatty acid synthase regulates the pathogenicity of Th17 cells. *J. Leukoc. Biol.* **102**, 1229–1235 (2017).

142. Geiger, R. *et al.* L-Arginine Modulates T Cell Metabolism and Enhances Survival and Anti-tumor Activity. *Cell* **167**, 829-842.e13 (2016).

143. Ma, E. H. *et al.* Serine Is an Essential Metabolite for Effector T Cell Expansion. *Cell Metab.* **25**, 345–357 (2017).

144. Liu, H. *et al.* Increased expression of IDO associates with poor postoperative clinical outcome of patients with gastric adenocarcinoma. *Sci. Rep.* **6**, 21319 (2016).

145. Munn, D. H. & Mellor, A. L. IDO in the Tumor Microenvironment: Inflammation, Counter-Regulation, and Tolerance. *Trends Immunol.* **37**, 193–207 (2016).

146. Liu, M. *et al.* Targeting the IDO1 pathway in cancer: from bench to bedside. *J. Hematol. Oncol.J Hematol Oncol* **11**, 100 (2018).

147. Wen, T. *et al.* Single-cell RNA sequencing identifies inflammatory tissue T cells in eosinophilic esophagitis. *J. Clin. Invest.* **129**, 2014–2028 (2019).

148. Tibbitt, C. A. *et al.* Single-Cell RNA Sequencing of the T Helper Cell Response to House Dust Mites Defines a Distinct Gene Expression Signature in Airway Th2 Cells. *Immunity* **51**, 169-184.e5 (2019).

149. Crotty, S. Follicular helper CD4 T cells (TFH). *Annu. Rev. Immunol.* **29**, 621–663 (2011).

150. Cho, S. H. *et al.* Hypoxia-inducible factors in CD4+ T cells promote metabolism, switch cytokine secretion, and T cell help in humoral immunity. *Proc. Natl. Acad. Sci. U. S. A.* **116**, 8975–8984 (2019).

151. Abboud, G. *et al.* Inhibition of Glycolysis Reduces Disease Severity in an Autoimmune Model of Rheumatoid Arthritis. *Front. Immunol.* **9**, 1973 (2018).

152. Choi, S.-C. *et al.* Inhibition of glucose metabolism selectively targets autoreactive follicular helper T cells. *Nat. Commun.* **9**, 4369 (2018).

153. Dong, L. *et al.* HIF1α-Dependent Metabolic Signals Control the Differentiation of Follicular Helper T Cells. *Cells* **8**, 1450 (2019).

154. Som, P. *et al.* A FluorinatedGlucose Analog, 2-fluoro-2-deoxy-D-glucose(F-18): Nontoxic Tracer for RapidTumor Detection. **21**, 6.

155. Corbet, C. *et al.* Interruption of lactate uptake by inhibiting mitochondrial pyruvate transport unravels direct antitumor and radiosensitizing effects. *Nat. Commun.* **9**, 1–11 (2018).

156. Gerriets, V. A. *et al.* Foxp3 and Toll-like receptor signaling balance Treg cell anabolic metabolism for suppression. *Nat. Immunol.* **17**, 1459–1466 (2016).

157. Procaccini, C. *et al.* An oscillatory switch in mTOR kinase activity sets regulatory T cell responsiveness. *Immunity* **33**, 929–941 (2010).

158. Cho, S. H. *et al.* Germinal centre hypoxia and regulation of antibody qualities by a hypoxia response system. *Nature* **537**, 234–238 (2016).

159. Abbott, R. K. *et al.* Germinal Center Hypoxia Potentiates Immunoglobulin Class Switch Recombination. *J. Immunol.* **197**, 4014–4020 (2016).

160. Jacobs, S. R. *et al.* Glucose Uptake Is Limiting in T Cell Activation and Requires CD28-Mediated Akt-Dependent and Independent Pathways. *J. Immunol.* **180**, 4476–4486 (2008).

161. Weisel, F. J. *et al.* Germinal center B cells selectively oxidize fatty acids for energy while conducting minimal glycolysis. *Nat. Immunol.* 1–12 (2020) doi:10.1038/s41590-020-0598-4.

162. He, N. *et al.* Metabolic control of regulatory T cell (Treg) survival and function by Lkb1. *Proc. Natl. Acad. Sci.* **114**, 12542–12547 (2017).

163. Howie, D. *et al.* Foxp3 drives oxidative phosphorylation and protection from lipotoxicity. *JCI Insight* **2**, e89160.

164. Clambey, E. T. *et al.* Hypoxia-inducible factor-1 alpha-dependent induction of FoxP3 drives regulatory T-cell abundance and function during inflammatory hypoxia of the mucosa. *Proc. Natl. Acad. Sci. U. S. A.* **109**, E2784-2793 (2012).

165. Paz, K. *et al.* Small-molecule BCL6 inhibitor effectively treats mice with nonsclerodermatous chronic graft-versus-host disease. *Blood* **133**, 94–99 (2019).

166. Jones, R. G. & Thompson, C. B. Revving the Engine: Signal Transduction Fuels T Cell Activation. *Immunity* **27**, 173–178 (2007).

167. Gerriets, V. A. *et al.* Metabolic programming and PDHK1 control CD4+ T cell subsets and inflammation. *J. Clin. Invest.* **125**, 194–207 (2015).

168. Angelin, A. *et al.* Foxp3 Reprograms T Cell Metabolism to Function in Low-Glucose, High-Lactate Environments. *Cell Metab.* **25**, 1282-1293.e7 (2017).

169. Pearce, E. L., Poffenberger, M. C., Chang, C.-H. & Jones, R. G. Fueling immunity: insights into metabolism and lymphocyte function. *Science* **342**, 1242454 (2013).

170. Zeng, H. *et al.* mTORC1 couples immune signals and metabolic programming to establish Treg cell function. *Nature* **499**, 485–490 (2013).

171. Gong, M., Cornaby, C., Michailidis, G. & Morel, L. Follicular helper T cells express a metabolic and cell signaling gene signature in a lupus-prone murine model. *J. Immunol.* **204**, 142.19-142.19 (2020).

172. Hsu, W.-C. *et al.* DUSP6 mediates T cell receptor-engaged glycolysis and restrains TFH cell differentiation. *Proc. Natl. Acad. Sci. U. S. A.* **115**, E8027–E8036 (2018).

173. Ray, J. P. *et al.* The Interleukin-2-mTORc1 Kinase Axis Defines the Signaling, Differentiation, and Metabolism of T Helper 1 and Follicular B Helper T Cells. *Immunity* **43**, 690–702 (2015).

174. Yin, Y. *et al.* Normalization of CD4 $^{+}$ T cell metabolism reverses lupus. *Sci. Transl. Med.* **7**, 274ra18-274ra18 (2015).

175. McDonald-Hyman, C. *et al.* Therapeutic regulatory T-cell adoptive transfer ameliorates established murine chronic GVHD in a CXCR5-dependent manner. *Blood* **128**, 1013–1017 (2016).

176. Chen, Y. *et al.* CXCR5+PD-1+ follicular helper CD8 T cells control B cell tolerance. *Nat. Commun.* **10**, 4415 (2019).

177. Fu, G. *et al.* Metabolic control of TFH cells and humoral immunity by phosphatidylethanolamine. *Nature* **595**, 724–729 (2021).

178. Ralser, M. *et al.* A catabolic block does not sufficiently explain how 2-deoxy-d-glucose inhibits cell growth. *Proc. Natl. Acad. Sci.* **105**, 17807–17811 (2008).

179. Xie, M. M., Amet, T., Liu, H., Yu, Q. & Dent, A. L. AMP Kinase Promotes Bcl6 Expression in both Mouse and Human T cells. *Mol. Immunol.* **81**, 67–75 (2017).

180. Oestreich, K. J. *et al.* Bcl-6 directly represses the gene program of the glycolysis pathway. *Nat. Immunol.* **15**, 957–964 (2014).

181. Rashida Gnanaprakasam, J. N., Wu, R. & Wang, R. Metabolic Reprogramming in Modulating T Cell Reactive Oxygen Species Generation and Antioxidant Capacity. *Front. Immunol.* **9**, (2018).

182. Kono, M., Yoshida, N., Maeda, K. & Tsokos, G. C. Transcriptional factor ICER promotes glutaminolysis and the generation of Th17 cells. *Proc. Natl. Acad. Sci.* **115**, 2478–2483 (2018).

183. Leone, R. D. *et al.* Glutamine blockade induces divergent metabolic programs to overcome tumor immune evasion. *Science* **366**, 1013–1021 (2019).

184. Schulte, M. L. *et al.* Pharmacological blockade of ASCT2-dependent glutamine transport leads to antitumor efficacy in preclinical models. *Nat. Med.* **24**, 194–202 (2018).

185. Pearce, E. J. & Pearce, E. L. Driving immunity: all roads lead to metabolism. *Nat. Rev. Immunol.* **18**, 81–82 (2018).

186. Haniuda, K., Fukao, S. & Kitamura, D. Metabolic Reprogramming Induces Germinal Center B Cell Differentiation through Bcl6 Locus Remodeling. *Cell Rep.* **33**, 108333 (2020).

187. Patsoukis, N. *et al.* PD-1 alters T-cell metabolic reprogramming by inhibiting glycolysis and promoting lipolysis and fatty acid oxidation. *Nat. Commun.* **6**, 1–13 (2015).

188. Glancy, B. *et al.* Mitochondrial lactate metabolism: history and implications for exercise and disease. *J. Physiol.* **599**, 863–888 (2021).

189. Watson, M. J. *et al.* Metabolic support of tumour-infiltrating regulatory T cells by lactic acid. *Nature* (2021) doi:10.1038/s41586-020-03045-2.

190. Renner, K. *et al.* Restricting Glycolysis Preserves T Cell Effector Functions and Augments Checkpoint Therapy. *Cell Rep.* **29**, 135-150.e9 (2019).

191. Bennett, F. *et al.* Program Death-1 Engagement Upon TCR Activation Has Distinct Effects on Costimulation and Cytokine-Driven Proliferation: Attenuation of ICOS, IL-4, and IL-21, But Not CD28, IL-7, and IL-15 Responses. *J. Immunol.* **170**, 711–718 (2003).

192. Velu, V. *et al.* Enhancing SIV-Specific Immunity In Vivo by PD-1 Blockade. *Nature* **458**, 206–210 (2009).

193. Hams, E. *et al.* Blockade of B7-H1 (Programmed Death Ligand 1) Enhances Humoral Immunity by Positively Regulating the Generation of T Follicular Helper Cells. *J. Immunol.* **186**, 5648–5655 (2011).

194. Mizuno, R. *et al.* PD-1 Primarily Targets TCR Signal in the Inhibition of Functional T Cell Activation. *Front. Immunol.* **10**, (2019).

195. Peng, C. *et al.* BCL6-Mediated Silencing of PD-1 Ligands in Germinal Center B Cells Maintains Follicular T Cell Population. *J. Immunol.* **202**, 704–713 (2019).

196. Good-Jacobson, K. L. *et al.* PD-1 regulates germinal center B cell survival and the formation and affinity of long-lived plasma cells. *Nat. Immunol.* **11**, 535–542 (2010).

197. Hamel, K. M. *et al.* B7-H1 Promotes Germinal Center B cell Survival and Inhibits T cell Activation. *Eur. J. Immunol.* **40**, 3117–3127 (2010).

198. Kawamoto, S. *et al.* The inhibitory receptor PD-1 regulates IgA selection and bacterial composition in the gut. *Science* **336**, 485–489 (2012).

199. Xu, H., Wang, X., Lackner, A. & Veazey, R. PD-1HIGH Follicular CD4 T Helper Cell Subsets Residing in Lymph Node Germinal Centers Correlate with B Cell Maturation and IgG Production in Rhesus Macaques. *Front. Immunol.* **5**, (2014).

200. Shi, J. *et al.* PD-1 Controls Follicular T Helper Cell Positioning and Function. *Immunity* **49**, 264-274.e4 (2018).

201. Shulman, Z. *et al.* T Follicular Helper Cell Dynamics in Germinal Centers. *Science* **341**, 673–677 (2013).

202. Nakajima, C. *et al.* Induction of the chemokine receptor CXCR3 on TCR-stimulated T cells: dependence on the release from persistent TCR-triggering and requirement for IFN-γ stimulation. *Eur. J. Immunol.* **32**, 1792–1801 (2002).

203. Groom, J. R. *et al.* CXCR3 chemokine receptor-ligand interactions in the lymph node optimize CD4+ T helper 1 cell differentiation. *Immunity* **37**, 1091–1103 (2012).

204. Campbell, D. J., Kim, C. H. & Butcher, E. C. Separable effector T cell populations specialized for B cell help or tissue inflammation. *Nat. Immunol.* **2**, 876–881 (2001).

205. Patsoukis, N. *et al.* Selective Effects of PD-1 on Akt and Ras Pathways Regulate Molecular Components of the Cell Cycle and Inhibit T Cell Proliferation. *Sci. Signal.* **5**, ra46–ra46 (2012).

206. Gigoux, M. *et al.* Inducible costimulator promotes helper T-cell differentiation through phosphoinositide 3-kinase. *Proc. Natl. Acad. Sci.* **106**, 20371–20376 (2009).

207. Preite, S., Huang, B., Cannons, J. L., McGavern, D. B. & Schwartzberg, P. L. PI3K Orchestrates T Follicular Helper Cell Differentiation in a Context Dependent Manner: Implications for Autoimmunity. *Front. Immunol.* **9**, (2019).

208. Preite, S. *et al.* Hyperactivated PI3Kδ promotes self and commensal reactivity at the expense of optimal humoral immunity. *Nat. Immunol.* **19**, 986–1000 (2018).

209. Franko, J. L. & Levine, A. D. Antigen-independent adhesion and cell spreading by inducible costimulator engagement inhibits T cell migration in a PI-3K-dependent manner. *J. Leukoc. Biol.* **85**, 526–538 (2009).

210. Pedros, C. *et al.* A TRAF-like motif of the inducible costimulator ICOS controls development of germinal center TFH cells via the kinase TBK1. *Nat. Immunol.* **17**, 825–833 (2016).

211. Akiba, H. *et al.* The Role of ICOS in the CXCR5 $^{+}$ Follicular B Helper T Cell Maintenance In Vivo. *J. Immunol.* **175**, 2340–2348 (2005).

212. Tafuri, A. *et al.* ICOS is essential for effective T-helper-cell responses. *Nature* **409**, 105–109 (2001).

213. Mak, T. W. *et al.* Costimulation through the inducible costimulator ligand is essential for both T helper and B cell functions in T cell–dependent B cell responses. *Nat. Immunol.* **4**, 765–772 (2003).

214. Dong, C., Temann, U.-A. & Flavell, R. A. Cutting Edge: Critical Role of Inducible Costimulator in Germinal Center Reactions. *J. Immunol.* **166**, 3659–3662 (2001).

215. McAdam, A. J. *et al.* ICOS is critical for CD40-mediated antibody class switching. *Nature* **409**, 102–105 (2001).

216. Keir, M. E., Butte, M. J., Freeman, G. J. & Sharpe, A. H. PD-1 and Its Ligands in Tolerance and Immunity. *Annu. Rev. Immunol.* **26**, 677–704 (2008).

217. Nurieva, R. I. *et al.* Generation of follicular helper T cells is mediated by IL-21 but independent of TH1, TH2 or TH17 lineages. *Immunity* **29**, 138–149 (2008).

218. Vogelzang, A. *et al.* A Fundamental Role for Interleukin-21 in the Generation of T Follicular Helper Cells. *Immunity* **29**, 127–137 (2008).

219. Yu, D. *et al.* The Transcriptional Repressor Bcl-6 Directs T Follicular Helper Cell Lineage Commitment. *Immunity* **31**, 457–468 (2009).

220. Ettinger, R. *et al.* IL-21 Induces Differentiation of Human Naive and Memory B Cells into Antibody-Secreting Plasma Cells. *J. Immunol.* **175**, 7867–7879 (2005).

221. Kuchen, S. *et al.* Essential Role of IL-21 in B Cell Activation, Expansion, and Plasma Cell Generation during CD4+ T Cell-B Cell Collaboration. *J. Immunol.* **179**, 5886–5896 (2007).

222. Avery, D. T., Bryant, V. L., Ma, C. S., Malefyt, R. de W. & Tangye, S. G. IL-21-Induced Isotype Switching to IgG and IgA by Human Naive B Cells Is Differentially Regulated by IL-4. *J. Immunol.* **181**, 1767–1779 (2008).

223. Linterman, M. A. *et al.* IL-21 acts directly on B cells to regulate Bcl-6 expression and germinal center responses. *J. Exp. Med.* **207**, 353–363 (2010).

224. Zotos, D. *et al.* IL-21 regulates germinal center B cell differentiation and proliferation through a B cell–intrinsic mechanism. *J. Exp. Med.* **207**, 365–378 (2010).

225. Tangye, S. G. & Ma, C. S. Regulation of the germinal center and humoral immunity by interleukin-21. *J. Exp. Med.* **217**, e20191638 (2019).

226. Wang, P., Shih, C., Qi, H. & Lan, Y. A Stochastic Model of the Germinal Center Integrating Local Antigen Competition, Individualistic T–B Interactions, and B Cell Receptor Signaling. *J. Immunol.* **197**, 1169–1182 (2016).

227. Shimizu, K. *et al.* PD-1 preferentially inhibits the activation of low-affinity T cells. *Proc. Natl. Acad. Sci.* **118**, e2107141118 (2021).

228. Agata, Y. *et al.* Expression of the PD-1 antigen on the surface of stimulated mouse T and B lymphocytes. *Int. Immunol.* **8**, 765–772 (1996).

229. Bu, X. *et al.* Monitoring PD-1 phosphorylation to evaluate PD-1 signaling during anti-tumor immune responses. *Cancer Immunol. Res.* canimm.CIR-21-0493-E.2021 (2021) doi:10.1158/2326-6066.CIR-21-0493.

230. Love, M. I., Huber, W. & Anders, S. Moderated estimation of fold change and dispersion for RNA-seq data with DESeq2. *Genome Biol.* **15**, 550 (2014).

231. Wu, T. *et al.* clusterProfiler 4.0: A universal enrichment tool for interpreting omics data. *The Innovation* **2**, (2021).

232. Yu, G., Wang, L.-G., Han, Y. & He, Q.-Y. clusterProfiler: an R Package for Comparing Biological Themes Among Gene Clusters. *https://home.liebertpub.com/omi* https://www.liebertpub.com/doi/abs/10.1089/omi.2011.0118 (2012) doi:10.1089/omi.2011.0118.

233. Zhang, W. *et al.* Effector CD4+ T Cell Expression Signatures and Immune-Mediated Disease Associated Genes. *PLoS ONE* **7**, e38510 (2012).

234. Blazar, B. R. *et al.* Blockade of Programmed Death-1 Engagement Accelerates Graft-Versus-Host Disease Lethality by an IFN-γ-Dependent Mechanism. *J. Immunol.* **171**, 1272–1277 (2003).

235. Zeiser, R., Sarantopoulos, S. & Blazar, B. R. B-cell targeting in chronic graft-versus-host disease. *Blood* **131**, 1399–1405 (2018).

236. Fujiwara, H. *et al.* Programmed Death-1 Pathway in Host Tissues Ameliorates Th17/Th1-Mediated Experimental Chronic Graft-versus-Host Disease. *J. Immunol.* **193**, 2565–2573 (2014).

237. Tan, C. L. *et al.* PD-1 restraint of regulatory T cell suppressive activity is critical for immune tolerance. *22*.

238. Vick, S. C., Kolupaev, O. V., Perou, C. M. & Serody, J. S. Anti–PD-1 Checkpoint Therapy Can Promote the Function and Survival of Regulatory T Cells. *J. Immunol.* **207**, 2598–2607 (2021).

239. Sage, P. T. & Sharpe, A. H. The multifaceted functions of follicular regulatory T cells. *Curr. Opin. Immunol.* **67**, 68–74 (2020).

240. Wollenberg, I. *et al.* Regulation of the Germinal Center Reaction by Foxp3+ Follicular Regulatory T Cells. *J. Immunol.* **187**, 4553–4560 (2011).

241. Sage, P. T. & Sharpe, A. H. T follicular regulatory cells. *Immunol. Rev.* **271**, 246–259 (2016).

242. Hori, S., Nomura, T. & Sakaguchi, S. Control of Regulatory T Cell Development by the Transcription Factor Foxp3. *Science* **299**, 1057–1061 (2003).

243. Rudra, D. *et al.* Transcription factor Foxp3 and its protein partners form a complex regulatory network. *Nat. Immunol.* **13**, 1010–1019 (2012).

244. Ohkura, N. & Sakaguchi, S. Transcriptional and epigenetic basis of Treg cell development and function: its genetic anomalies or variations in autoimmune diseases. *Cell Res.* **30**, 465–474 (2020).

245. Hou, S. *et al.* FoxP3 and Ezh2 regulate Tfr cell suppressive function and transcriptional program. *J. Exp. Med.* **216**, 605–620 (2019).

246. Fontenot, J. D., Gavin, M. A. & Rudensky, A. Y. Foxp3 programs the development and function of CD4+CD25+ regulatory T cells. *Nat. Immunol.* **4**, 330–336 (2003).

247. Gavin, M. A. *et al.* Foxp3-dependent programme of regulatory T-cell differentiation. *Nature* **445**, 771–775 (2007).

248. Allan, S. E. *et al.* Generation of Potent and Stable Human CD4+ T Regulatory Cells by Activation-independent Expression of FOXP3. *Mol. Ther.* **16**, 194–202 (2008).

249. Setoguchi, R., Hori, S., Takahashi, T. & Sakaguchi, S. Homeostatic maintenance of natural Foxp3 + CD25+ CD4+ regulatory T cells by interleukin (IL)-2 and induction of autoimmune disease by IL-2 neutralization. *J. Exp. Med.* **201**, 723–735 (2005).

250. Burchill, M. A., Yang, J., Vogtenhuber, C., Blazar, B. R. & Farrar, M. A. IL-2 Receptor β-Dependent STAT5 Activation Is Required for the Development of Foxp3+ Regulatory T Cells. *J. Immunol.* **178**, 280–290 (2007).

251. Zheng, S. G., Wang, J., Wang, P., Gray, J. D. & Horwitz, D. A. IL-2 Is Essential for TGF-β to Convert Naive CD4+CD25− Cells to CD25+Foxp3+ Regulatory T Cells and for Expansion of These Cells. *J. Immunol.* **178**, 2018–2027 (2007).

252. Chen, Q., Kim, Y. C., Laurence, A., Punkosdy, G. A. & Shevach, E. M. IL-2 Controls the Stability of Foxp3 expression in TGF-β-induced Foxp3+ T cells in vivo. *J. Immunol. Baltim. Md 1950* **186**, 6329–6337 (2011).

253. Chinen, T. *et al.* An essential role for IL-2 receptor in regulatory T cell function. *Nat. Immunol.* **17**, 1322–1333 (2016).

254. Freudenberg, K. *et al.* Critical Role of TGF-β and IL-2 Receptor Signaling in Foxp3 Induction by an Inhibitor of DNA Methylation. *Front. Immunol.* **9**, (2018).

255. Ghelani, A. *et al.* Defining the Threshold IL-2 Signal Required for Induction of Selective Treg Cell Responses Using Engineered IL-2 Muteins. *Front. Immunol.* **11**, (2020).

256. Chen, W. *et al.* Conversion of Peripheral CD4+CD25− Naive T Cells to CD4+CD25+ Regulatory T Cells by TGF-β Induction of Transcription Factor Foxp3. *J. Exp. Med.* **198**, 1875–1886 (2003).

257. Huber, S. *et al.* Cutting Edge: TGF-β Signaling Is Required for the In Vivo Expansion and Immunosuppressive Capacity of Regulatory CD4+CD25+ T Cells. *J. Immunol.* **173**, 6526–6531 (2004).

258. Takimoto, T. *et al.* Smad2 and Smad3 Are Redundantly Essential for the TGF-β–Mediated Regulation of Regulatory T Plasticity and Th1 Development. *J. Immunol.* **185**, 842–855 (2010).

259. Liberzon, A. *et al.* The Molecular Signatures Database (MSigDB) hallmark gene set collection. *Cell Syst.* **1**, 417–425 (2015).

260. Garg, G. *et al.* Blimp1 Prevents Methylation of Foxp3 and Loss of Regulatory T Cell Identity at Sites of Inflammation. *Cell Rep.* **26**, 1854-1868.e5 (2019).

261. Nurieva, R. I. *et al.* STAT5 Protein Negatively Regulates T Follicular Helper (Tfh) Cell Generation and Function. *J. Biol. Chem.* **287**, 11234–11239 (2012).

262. Johnston, R. J., Choi, Y. S., Diamond, J. A., Yang, J. A. & Crotty, S. STAT5 is a potent negative regulator of TFH cell differentiation. *J. Exp. Med.* **209**, 243–250 (2012).

263. Oestreich, K. J., Mohn, S. E. & Weinmann, A. S. Molecular mechanisms that control the expression and activity of Bcl-6 in TH1 cells to regulate flexibility with a TFH-like gene profile. *Nat. Immunol.* **13**, 405–411 (2012).

264. Botta, D. *et al.* Dynamic regulation of T Follicular Regulatory cell responses by interleukin 2 during influenza infection. *Nat. Immunol.* **18**, 1249–1260 (2017).

265. Mahmud, S. A., Manlove, L. S. & Farrar, M. A. Interleukin-2 and STAT5 in regulatory T cell development and function. *JAK-STAT* **2**, e23154 (2013).

266. Betts, B. C., Veerapathran, A., Pidala, J., Yu, X.-Z. & Anasetti, C. STAT5 polarization promotes iTregs and suppresses human T-cell alloresponses while preserving CTL capacity. *J. Leukoc. Biol.* **95**, 205–213 (2014).

267. Mikami, N. *et al.* Epigenetic conversion of conventional T cells into regulatory T cells by CD28 signal deprivation. *Proc. Natl. Acad. Sci.* **117**, 12258–12268 (2020).

268. Cretney, E. *et al.* The transcription factors Blimp-1 and IRF4 jointly control the differentiation and function of effector regulatory T cells. *Nat. Immunol.* **12**, 304–311 (2011).

269. Alvisi, G. *et al.* IRF4 instructs effector Treg differentiation and immune suppression in human cancer. *J. Clin. Invest.* **130**, 3137–3150.

270. Bankoti, R. *et al.* Differential regulation of Effector and Regulatory T cell function by Blimp1. *Sci. Rep.* **7**, 12078 (2017).

271. Hayatsu, N. *et al.* Analyses of a Mutant Foxp3 Allele Reveal BATF as a Critical Transcription Factor in the Differentiation and Accumulation of Tissue Regulatory T Cells. *Immunity* **47**, 268-283.e9 (2017).

272. Delacher, M. *et al.* Genome-wide DNA methylation landscape defines specialization of regulatory T cells in tissues. *Nat. Immunol.* **18**, 1160–1172 (2017).

273. Klunker, S. *et al.* Transcription factors RUNX1 and RUNX3 in the induction and suppressive function of Foxp3+ inducible regulatory T cells. *J. Exp. Med.* **206**, 2701–2715 (2009).

274. Kitoh, A. *et al.* Indispensable Role of the Runx1-Cbfβ Transcription Complex for In Vivo-Suppressive Function of FoxP3+ Regulatory T Cells. *Immunity* **31**, 609–620 (2009).

275. Kakugawa, K. *et al.* Essential Roles of SATB1 in Specifying T Lymphocyte Subsets. *Cell Rep.* **19**, 1176–1188 (2017).

276. Kitagawa, Y. *et al.* Guidance of regulatory T cell development by Satb1-dependent super-enhancer establishment. *Nat. Immunol.* **18**, 173–183 (2017).

277. Beyer, M. *et al.* Repression of SATB1 in regulatory T cells is required for suppressive function and inhibition of effector differentiation. *Nat. Immunol.* **12**, 898–907 (2011).

278. Sekiya, T. *et al.* The nuclear orphan receptor Nr4a2 induces Foxp3 and regulates differentiation of CD4+ T cells. *Nat. Commun.* **2**, 269 (2011).

279. Liu, X. *et al.* Genome-wide analysis identifies NR4A1 as a key mediator of T cell dysfunction. *Nature* **567**, 525–529 (2019).

280. Sekiya, T. *et al.* Regulation of peripheral Th/Treg differentiation and suppression of airway inflammation by Nr4a transcription factors. *iScience* **24**, 102166 (2021).

281. Sekiya, T. *et al.* Nr4a Receptors Regulate Development and Death of Labile Treg Precursors to Prevent Generation of Pathogenic Self-Reactive Cells. *Cell Rep.* **24**, 1627-1638.e6 (2018).

282. Fu, W. *et al.* A multiple redundant genetic switch locks in the transcriptional signature of T regulatory cells. *Nat. Immunol.* **13**, 972–980 (2012).

283. Brunet, J.-F. *et al.* A new member of the immunoglobulin superfamily—CTLA-4. *Nature* **328**, 267–270 (1987).

284. Walunas, T. L. *et al.* CTLA-4 can function as a negative regulator of T cell activation. *Immunity* **1**, 405–413 (1994).

285. Wing, K. *et al.* CTLA-4 control over Foxp3+ regulatory T cell function. *Science* **322**, 271–275 (2008).

286. Scalapino, K. J. & Daikh, D. I. CTLA-4: a key regulatory point in the control of autoimmune disease. *Immunol. Rev.* **223**, 143–155 (2008).

287. Joller, N. *et al.* Treg cells expressing the co-inhibitory molecule TIGIT selectively inhibit pro-inflammatory Th1 and Th17 cell responses. *Immunity* **40**, 569–581 (2014).

288. Levin, S. D. *et al.* Vstm3 is a Member of the CD28 Family and an Important Modulator of T Cell Function. *Eur. J. Immunol.* **41**, 902–915 (2011).

289. Lozano, E., Dominguez-Villar, M., Kuchroo, V. & Hafler, D. A. The TIGIT/CD226 Axis Regulates Human T Cell Function. *J. Immunol.* **188**, 3869–3875 (2012).

290. Sakuishi, K. *et al.* TIM3+FOXP3+ regulatory T cells are tissue-specific promoters of T-cell dysfunction in cancer. *Oncoimmunology* **2**, e23849 (2013).

291. Wolf, Y., Anderson, A. C. & Kuchroo, V. K. TIM3 comes of age as an inhibitory receptor. *Nat. Rev. Immunol.* **20**, 173–185 (2020).

292. Banerjee, H. *et al.* Expression of Tim-3 drives phenotypic and functional changes in Treg cells in secondary lymphoid organs and the tumor microenvironment. *Cell Rep.* **36**, 109699 (2021).

293. Thaker, Y. R., Andrews, L. P., Workman, C. J., Vignali, D. A. A. & Sharpe, A. H. Treg-specific LAG3 deletion reveals a key role for LAG3 in regulatory T cells to inhibit CNS autoimmunity. *J. Immunol.* **200**, 101.7-101.7 (2018).

294. Workman, C. J. & Vignali, D. A. A. Negative Regulation of T Cell Homeostasis by Lymphocyte Activation Gene-3 (CD223). *J. Immunol.* **174**, 688–695 (2005).

295. Linsley, P. S. *et al.* Coexpression and functional cooperation of CTLA-4 and CD28 on activated T lymphocytes. *J. Exp. Med.* **176**, 1595–1604 (1992).

296. Qureshi, O. S. *et al.* Trans-endocytosis of CD80 and CD86: a molecular basis for the cell extrinsic function of CTLA-4. *Science* **332**, 600–603 (2011).

297. Yu, X. *et al.* The surface protein TIGIT suppresses T cell activation by promoting the generation of mature immunoregulatory dendritic cells. *Nat. Immunol.* **10**, 48–57 (2009).

298. Anderson, A. C., Joller, N. & Kuchroo, V. K. Lag-3, Tim-3, and TIGIT: Co-inhibitory Receptors with Specialized Functions in Immune Regulation. *Immunity* **44**, 989–1004 (2016).

299. Kurtulus, S. *et al.* TIGIT predominantly regulates the immune response via regulatory T cells. *J. Clin. Invest.* **125**, 4053–4062.

300. Gupta, S. *et al.* Allograft rejection is restrained by short-lived TIM-3+PD-1+Foxp3+ Tregs. *J. Clin. Invest.* **122**, 2395–2404 (2012).

301. Gautron, A.-S., Dominguez-Villar, M., de Marcken, M. & Hafler, D. A. Enhanced suppressor function of TIM-3+FoxP3+ regulatory T cells. *Eur. J. Immunol.* **44**, 2703–2711 (2014).

302. Tahiliani, V., Hutchinson, T. E., Abboud, G., Croft, M. & Salek-Ardakani, S. OX40 Co-operates with ICOS to Amplify Follicular T Helper Cell Development and Germinal Center Reactions During Infection. *J. Immunol. Baltim. Md 1950* **198**, 218–228 (2017).

303. Landuyt, A. E., Klocke, B. J., Colvin, T. B., Schoeb, T. R. & Maynard, C. L. Cutting Edge: ICOS-Deficient Regulatory T Cells Display Normal Induction of Il10 but Readily Downregulate Expression of Foxp3. *J. Immunol.* **202**, 1039–1044 (2019).

304. Burmeister, Y. *et al.* ICOS Controls the Pool Size of Effector-Memory and Regulatory T Cells. *J. Immunol.* **180**, 774–782 (2008).

305. Chen, Y., Shen, S., Gorentla, B., Gao, J. & Zhong, X.-P. Murine regulatory T cells contain hyper-proliferative and death-prone subsets with differential ICOS expression. *J. Immunol. Baltim. Md 1950* **188**, 1698–1707 (2012).

306. Löhning, M. *et al.* Expression of ICOS In Vivo Defines CD4+ Effector T Cells with High Inflammatory Potential and a Strong Bias for Secretion of Interleukin 10. *J. Exp. Med.* **197**, 181–193 (2003).

307. Ito, T. *et al.* Two Functional Subsets of FOXP3+ Regulatory T Cells in Human Thymus and Periphery. *Immunity* **28**, 870–880 (2008).

308. Saraiva, M., Vieira, P. & O'Garra, A. Biology and therapeutic potential of interleukin-10. *J. Exp. Med.* **217**, e20190418 (2019).

309. Batlle, E. & Massagué, J. Transforming Growth Factor-β Signaling in Immunity and Cancer. *Immunity* **50**, 924–940 (2019).

310. Jandl, C. *et al.* IL-21 restricts T follicular regulatory T cell proliferation through Bcl-6 mediated inhibition of responsiveness to IL-2. *Nat. Commun.* **8**, 14647 (2017).

311. Ding, Y. *et al.* Interleukin-21 Promotes Germinal Center Reaction by Skewing the Follicular Regulatory T Cell to Follicular Helper T Cell Balance in Autoimmune BXD2 Mice. *Arthritis Rheumatol. Hoboken NJ* **66**, 2601–2612 (2014).

312. Nian, Y. *et al.* IL-21 Receptor Blockade Shifts the Follicular T Cell Balance and Reduces De Novo Donor-Specific Antibody Generation. *Front. Immunol.* **12**, (2021).

313. Ding, Y. *et al.* IL-17RA is essential for optimal localization of follicular Th cells in the germinal center light zone to promote autoantibody-producing B cells. *J. Immunol. Baltim. Md 1950* **191**, 1614–1624 (2013).

314. Harbour, S. N. *et al.* Th17 Cells Require Ongoing Classic IL-6 Receptor Signaling to Retain Transcriptional and Functional Identity. *Sci. Immunol.* **5**, eaaw2262 (2020).

315. Spender, L. C. *et al.* TGF-β induces apoptosis in human B cells by transcriptional regulation of BIK and BCL-XL. *Cell Death Differ.* **16**, 593–602 (2009).

316. Cañete, P. F. *et al.* Regulatory roles of IL-10–producing human follicular T cells. *J. Exp. Med.* **216**, 1843–1856 (2019).

317. Almanan, M. *et al.* IL-10–producing Tfh cells accumulate with age and link inflammation with age-related immune suppression. *Sci. Adv.* **6**, eabb0806.

318. Cazac, B. B. & Roes, J. TGF-β Receptor Controls B Cell Responsiveness and Induction of IgA In Vivo. *Immunity* **13**, 443–451 (2000).

319. Albright, A. R. *et al.* TGFβ signaling in germinal center B cells promotes the transition from light zone to dark zone. *J. Exp. Med.* **216**, 2531–2545 (2019).

320. Laidlaw, B. J. *et al.* Interleukin-10 from CD4+ follicular regulatory T cells promotes the germinal center response. *Sci. Immunol.* **2**, eaan4767 (2017).

321. Guthmiller, J. J., Graham, A. C., Zander, R. A., Pope, R. L. & Butler, N. S. IL-10 is essential for the generation of germinal center B cell responses and anti-Plasmodium humoral immunity. *J. Immunol. Baltim. Md 1950* **198**, 617–622 (2017).

322. Xin, G. *et al.* Single-cell RNA sequencing unveils an IL-10-producing helper subset that sustains humoral immunity during persistent infection. *Nat. Commun.* **9**, 5037 (2018).